5-2015

Alternative Method for Determining Plutonium-240 Content

Tracey-Ann Althea Wellington
University of Tennessee, Knoxville, twelling@vols.utk.edu

To the Graduate Council:

I am submitting herewith a dissertation written by Tracey-Ann Althea Wellington entitled "Alternative Method for Determining Plutonium-240 Content." I have examined the final electronic copy of this dissertation for form and content and recommend that it be accepted in partial fulfillment of the requirements for the degree of Doctor of Philosophy, with a major in Energy Science and Engineering.

Jason P. Hayward, Major Professor

We have read this dissertation and recommend its acceptance:

John T. Mihalczo, Howard L. Hall, Lawrence H. Heilbronn

Accepted for the Council:

Carolyn R. Hodges

Vice Provost and Dean of the Graduate School

(Original signatures are on file with official student records.)

Alternative Method for Determining Plutonium-240 Content

A Dissertation Presented for the
Doctor of Philosophy
Degree
The University of Tennessee, Knoxville

Tracey-Ann Althea Wellington
May 2015

ACKNOWLEDGEMENTS

I would like to thank my dissertation committee, which includes Dr. Jason Hayward, Dr. John Mihalczo, Dr. Howard Hall and Dr. Lawrence Heilbronn for all the support they have provided me during my dissertation research. I am especially indebted to my mentor, Dr. Mihalczo, for his support and patience as I tried to learn a new field. I would also like to thank Dr. Seth McConchie, Christopher Poe and Steve Kyle who made sure that I never said anything I wasn't supposed to, and Dr. James Henkel who taught me as much as I could possibly learn about MCNP. A special thanks to James Mullens, whose conversations always got me thinking and questioning ideas and concepts that I thought I knew.

Blake Palles has been a great friend and the best research partner a person could ask for, and I appreciate all the work you have done to help me make this research successful. Bonnie Canion has been my proof reader, a person I can bounce my ideas off, and a great friend and colleague. I am indebted to my ORNL family, including Deb Austin, Marc Hampton and Gomez Wright, who made sure I had anything I needed, kept me fed and kept me laughing. You guys made it feel like home.

My Bredesen Center family, Dr. Lee Riedinger, Wanda Davis and Dr. Mike Simpson, has made this graduate school experience the best I could ever ask for. Somehow anything I wanted to do, you found a way for me to do it, and I couldn't ask for a better program to be a part of.

To my parents, Albert and Erica, and my brother and sister, Andrew and Terry, thank you for all the support and the prayers. And all my relatives and friends, since I could never have done this alone, I can never repay all that you have done, but I am extremely grateful.

Finally, I would like to thank the U.S. Department of Energy National Nuclear Security Administration Office of Nonproliferation and Verification Research and Development for sponsoring this research.

ABSTRACT

The ability to detect the presence of Pu and identify the material as weapons-grade plutonium (WGPu) has a number of applications in the field of nuclear nonproliferation. This is particularly important in counterterrorism applications where the goal is to detect Pu that might be heavily shielded. Once WGPu has been identified, characterization of the material can provide valuable information such as mass, dimensions, and isotopic content. Aiming to enhance the capability of the Nuclear Materials Identification System (NMIS) at Oak Ridge National Laboratory, the objective of this project is to develop a proof-of-concept method to identify the presence of WGPu by determining the ^{240}Pu [plutonium-240] content in bare Pu metal assemblies of spherical or shell type configuration, or assemblies surrounded by neutron or gamma shielding. WGPu has a ^{240}Pu/^{239}Pu [plutonium-239] ratio below 0.10, or below ~7% ^{240}Pu content. The method is based solely on a NMIS passive time correlation signature and the dimensions of the Pu assembly (obtained from NMIS imaging data or external sources).

The method was built using MCNP simulations to predict the effects of certain Pu assembly parameters on the observed time distribution of correlated events from passive measurements. Analysis of the simulations resulted in a series of equations that account for these parameters when calculating the ^{240}Pu content. These equations were compiled in an algorithm that provides the ^{240}Pu content in percent, the uncertainty of this result, and a statement declaring whether or not the sample contains WGPu. The accuracy of the algorithm was verified using NMIS simulated and measured data, and the algorithm was able to determine the ^{240}Pu content of the spherical or shell type Pu assembly and identify the presence of WGPu in nine out of ten cases.

The algorithm is suitable for a number of applications, such as treaty verification and materials accounting, perhaps even with a different measurement setup, provided that a rough estimate of the ^{240}Pu isotopic content is sufficient. Furthermore, the method outlined in this work may be used to expand the developed algorithm to include other types of Pu assemblies and different reflector or shielding materials.

TABLE OF CONTENTS

LIST OF TABLES

LIST OF FIGURES

CHAPTER 1

INTRODUCTION

Plutonium-239 is produced when uranium-238 absorbs a neutron and decays to Pu. As the Pu absorbs additional neutrons, other isotopes are created, including ^{240}Pu, which has a high spontaneous fission rate (~416 fissions/g/s) [1]. This high spontaneous fission rate results in a constant production of neutrons by the Pu, and can potentially reduce the weapon yield [2]. Hence, a high ^{239}Pu content is preferred for nuclear weapons, and weapons grade plutonium (WGPu) is defined as having an isotopic ratio of ^{240}Pu/^{239}Pu of no more than 0.10 [3], which is ~7% ^{240}Pu content [2]. Only the even isotopes of Pu (^{238}Pu, ^{240}Pu, ^{242}Pu) provide significant spontaneous fission yields, and ^{240}Pu is usually the dominant isotope during the emission of spontaneous fission neutrons [4]. In the case of WGPu, we can assume that approximately 99% of the plutonium sample is composed of ^{239}Pu and ^{240}Pu [5], while all other plutonium isotopes are considered negligible. A number of allotropes of Pu exist, with densities ranging from ~16.0-20.0 g/cm^3. When alloyed with a small percentage of materials such as gallium and aluminum, delta-phase is the most stable allotrope of Pu at room temperature [6]. Alpha-phase Pu is another allotrope of Pu used in WGPu assemblies, but it is less stable than delta-phase.

1.1 Nuclear Materials Identification System (NMIS/FNMIS)

The Nuclear Materials Identification System (NMIS) is a time-coincidence system [7], [8], that includes tomographic imaging [9] (with fission site mapping [10],[11]), and gamma spectrometry. In addition to passive counting, the system detects transmitted 14.1 MeV neutrons as well as fission neutrons and gamma rays that may be emitted from an

interrogated target. NMIS employs an associated particle deuterium-tritium (D-T) neutron generator that contains an embedded pixelated alpha detector. The alpha detector electronically tags the emission time and direction of the emitted neutrons resulting from the D-T reaction. On the opposite side of a target object are the transmission imaging detectors, a row of thirty-two 2.5 × 2.5 × 10 cm plastic scintillators that records neutrons and gamma rays, as shown in Figure 1-1 [12]. The system also contains eight 25 × 25 × 10 cm fission radiation detectors that detect radiation from induced fission. NMIS uses a row of sixteen alpha pixels to define a neutron fan beam of sixteen beamlets, aimed towards the transmission imaging detectors. The fan beam and detectors can scan vertically in order to image an object, and the detectors can move laterally in small increments to increase resolution [13]. The fieldable version of NMIS (FNMIS) is shown in Figure 1-2.

The fast neutron imaging capabilities of NMIS can be leveraged to provide information on the characteristics of Pu assemblies, in order to determine the ^{240}Pu content. This is especially useful in situations where the assembly is unknown, and therefore there is no information on the materials present or their dimensions. The imaging system makes tomographic images, as shown in the example in Figure 1-3 [14]. The magnitude of the image at any pixel is the neutron cross section of the material at that pixel. A ray tracing algorithm can then be used to determine the material and dimensions of the assembly.

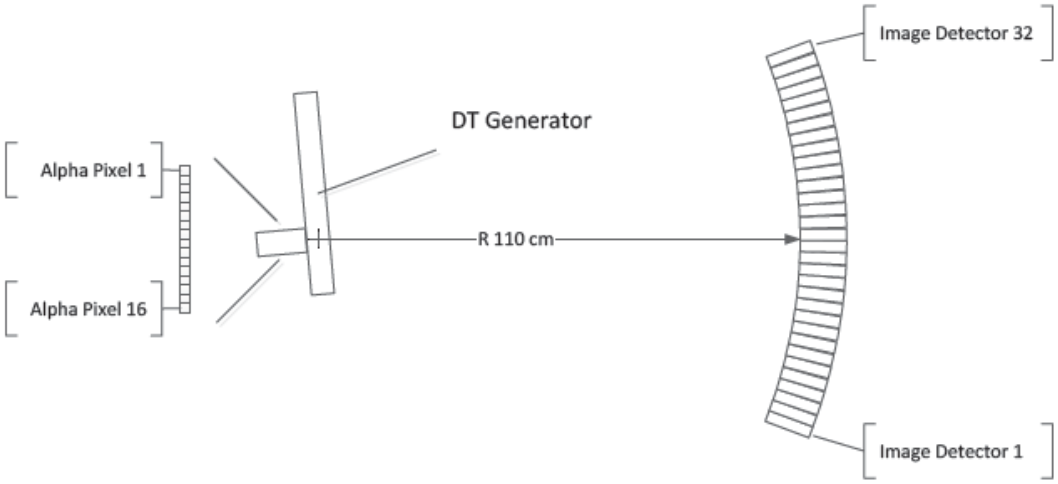

Figure 1-1. Schematic of NMIS set up with DT generator and imaging detectors.

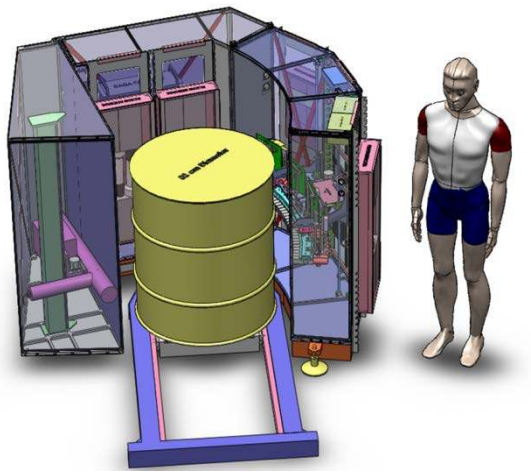

Figure 1-2. Fieldable Nuclear Materials Identification System (FNMIS), a fieldable version of NMIS.

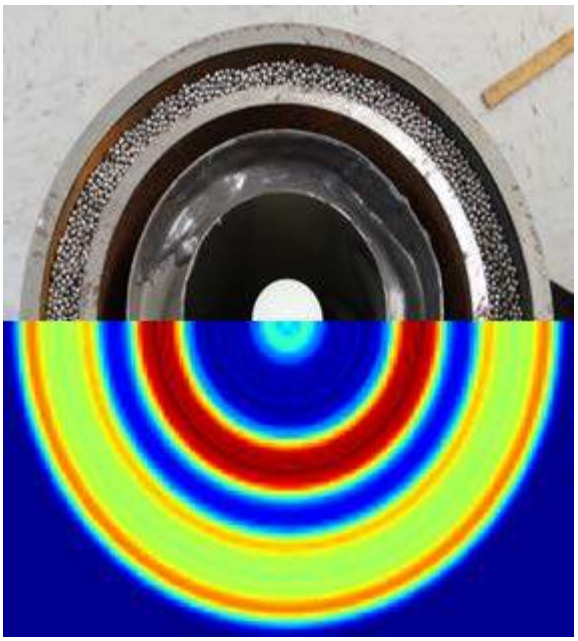

Figure 1-3. Comparison of photograph (top) and image reconstruction (bottom) of a composite assembly composed of, from inside to outside, of a polyethylene rod, a depleted uranium (DU) annular casting, a smaller diameter iron pipe, steel shot, and a larger diameter iron pipe. The image was made using filtered back projection.

1.2 Passive Neutron Detection

Passive neutron detection relies on measuring the spontaneous fission particles, and subsequent fission chain particles, emitted passively by the sample [15]. This process is especially useful in measuring bulk neutron-emitting materials, due to the greater penetration ability of the neutron compared with that of gamma rays. There are three types of neutron producing reactions that are encountered in passive neutron detection. These are spontaneous fission reactions, neutron multiplication and (α,n)-reactions [16].

During a spontaneous fission event the number of neutrons emitted and its probability distribution are referred to as the neutron multiplicity (ν) and the neutron multiplicity

distribution *P(ν)* respectively. The average number of neutrons emitted per spontaneous fission ($\bar{\nu}$) is [16]

$$\bar{\nu} = \sum_{\nu} \nu P(\nu) \tag{1-1}$$

The number of spontaneous fissions per gram of the isotope is referred to as the spontaneous fission yield of the isotope (*Y*). The spontaneous fission neutron yield is the product of the spontaneous fission yield and the average number of neutrons emitted per spontaneous fission for the different Pu isotopes [16].

Passive neutron coincidence counting detects the prompt neutrons from spontaneous fission in a sample and distinguishes them from other sources, by separating time correlated events, from those that are randomly distributed in time [17]. These correlated events are counted to provide information on the amount of fissionable isotopes in the sample. The measured neutron signal, as a result of decay by spontaneous fission, is represented as a ^{240}Pu effective mass ($^{240}Pu_{eff}$), since the ^{240}Pu isotope contributes the most spontaneous neutron signal [4]. The $^{240}Pu_{eff}$ mass is defined as the mass of ^{240}Pu that would give the same coincidence response as the amount obtained from all the even isotopes in the sample. The $^{240}Pu_{eff}$ mass is

$$^{240}Pu_{eff} = 2.52\,^{238}Pu + {}^{240}Pu + 1.68\,^{242}Pu \tag{1-2}$$

where ^{X}Pu is the mass of the plutonium isotope with mass number *X* [16]. The coefficients in Equation 1-2 are the spontaneous fission neutron yields of each Pu isotope. The total Pu mass can be determined from the $^{240}Pu_{eff}$ mass if the isotopic composition of the sample is known. The total Pu mass is

$$Pu_{total} = \frac{^{240}Pu_{eff}}{2.52 f_{238} + f_{240} + 1.68 f_{242}} \tag{1-3}$$

where f_X is the relative mass fractions for the Pu isotope with mass number X [16].

Multiplication in a sample is due to the presence of fissile material in the sample. If neutron multiplication occurs in the sample the proportionality between the neutron emitting mass and the number of spontaneous fission neutrons will change. Induced fissions increase the neutron emission of a sample by the neutron multiplication factor (m), which is the total number of neutrons created from a single neutron after all generations. The neutron multiplication factor is

$$m = \sum_{n=0}^{\infty} \left(p\bar{\nu}\right)^n = \frac{1}{1 - p\bar{\nu}} \tag{1-4}$$

where p is the probability of each neutron to induce a fission [16].

The (α,n)-reaction is observed in Pu compounds due to the presence of lighter elements such as oxygen. The neutrons originate as a result of the interaction between the lighter elements and the alpha particles emitted from the Pu. The (α,n)-reaction differs from spontaneous fission in both the energy spectrum and the neutron multiplicity distribution. In spontaneous fission emits groups of neutrons while the (α,n)-reaction always emits only one neutron at a time [16]. This research does not analyze Pu compounds, therefore discrimination of (α,n)-neutrons from spontaneous fission neutrons have not been studied.

1.3 Time Correlation Measurements

During passive neutron detection not all fission neutrons are detected, and the ones that are detected may not arrive at the same time, as they may not travel the same distance to reach the detector, and they may not travel at the same speed. Although the detection times for the fission neutrons are not the same, these detection times are correlated [12]. In time correlation measurements the detection time of the radiation is recorded and analyzed for possible correlations. These types of measurements are best suited for assemblies that include fissile or fissionable materials, since the fission process usually results in more than one prompt neutron being created [12].

In time correlation measurements the frequency distribution ($R_{k,g}$) is analyzed. This frequency distribution represents the frequency that a number of neutrons (k) falls into a gate of length (g) opened by a triggering signal, and is

$$R_{k,g} = \sum_{n=0}^{n\_max} \sum_{k'=0}^{n} M_{n'} U_{n,k',g} V_{k-k',g} \tag{1-5}$$

where $M_{n'}$ is the number of start neutrons per second correlated with *n* other subsequent neutrons, $U_{n,k',g}$ is the contribution of k′ correlated neutrons from the same fission event to the gate with gate length g, and $V_{k-k',g}$ is the contribution of k-k′ non-correlated neutrons to the gate with gate length g [16]. The equation takes into account all the different combinations of correlated and uncorrelated events falling into the gate [16].

Two types of frequency distributions obtained from time correlation measurements are called auto-correlations and cross-correlations. Auto-correlations are events between a source and a single detector (or a group of detectors summed and treated as a single

detector). The source and detector correlation is a function of the time delay between the source emission and the detector count [18]. The auto-correlation highlights how the detection time of the particle vary in relation to the time the interrogating particle was created [12]. In Figure 1-4, the major features of the time distribution of auto-correlated events are shown. The first peak is due to gammas transmitted from the active source, and the second, broader peak is due mainly due to neutrons transmitted from the active source. As a result, spontaneous fission events within the assembly do not contribute to this time distribution because they are statistically independent to active source emission events.

Cross-correlations are events between a pair of detectors as a function of the time delay between the detectors [19]. The time distribution of cross-correlated events show the detection time difference between all gamma and neutron pairs in a specified time window [12]. This time window is selected to include prompt neutrons, and is on the scale of nanoseconds (ns). The detector signals are synchronized at time=0 ns [19]. In a passive measurement, only the time distribution of cross-correlated events can be obtained, as there is no active source present. In this research it is the time distribution of cross-correlated events that is analyzed. An example of a time distribution of cross-correlated events for a spherical Pu shell is shown in Figure 1-5. The neutrons are time-tagged, and are distinguished from the gammas based only on time of flight. The gamma pairs ($\gamma\gamma$) are primarily a result of spontaneous fission within a nuclear material assembly, as are the neutron pairs, which are defined as either a gamma count coincident with a subsequent neutron count (γn), a neutron count coincident with a subsequent gamma count (nγ), or a neutron count coincident with a subsequent neutron count (nn). Therefore, as the number of spontaneous fissions increases, an increase in the number of gamma pairs and neutron pairs

is expected. A higher multiplicity means more induced fissions per spontaneous fission, which results in more pairs. The analysis conducted for this research looks at the total cross correlated events, which includes all types of pairs.

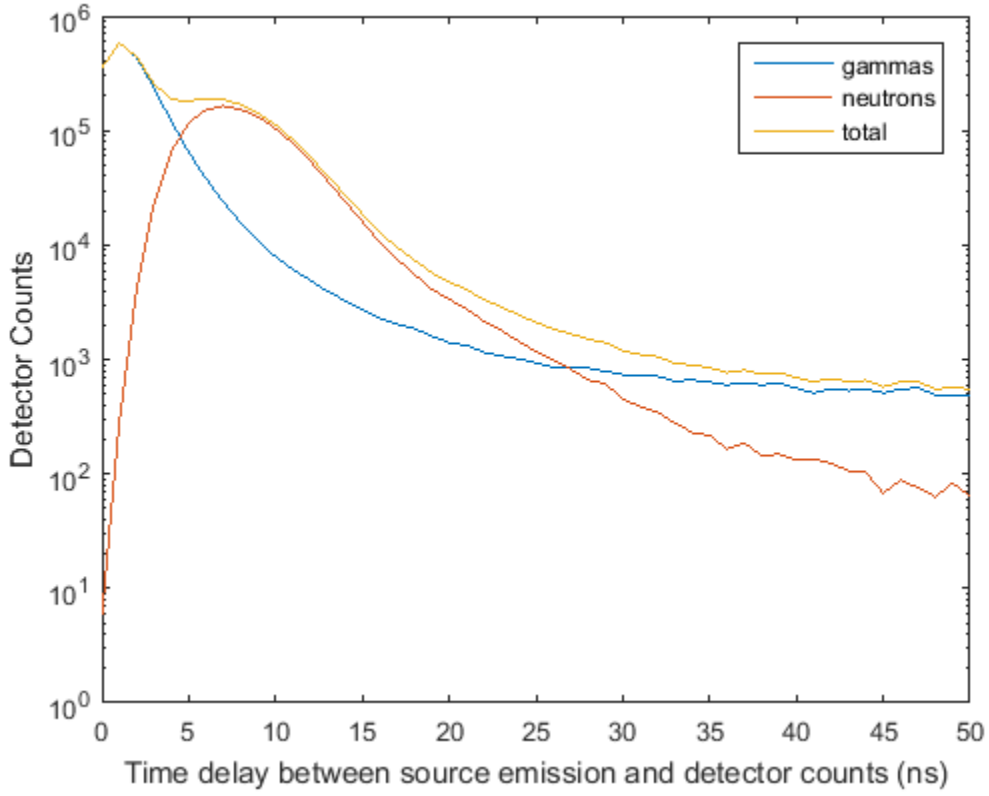

Figure 1-4. Example of time distribution of auto-correlated events for a spherical shell, including regions containing gammas and neutrons transmitted from an active source. In this system, gammas are distinguished from neutrons only based upon time of flight.

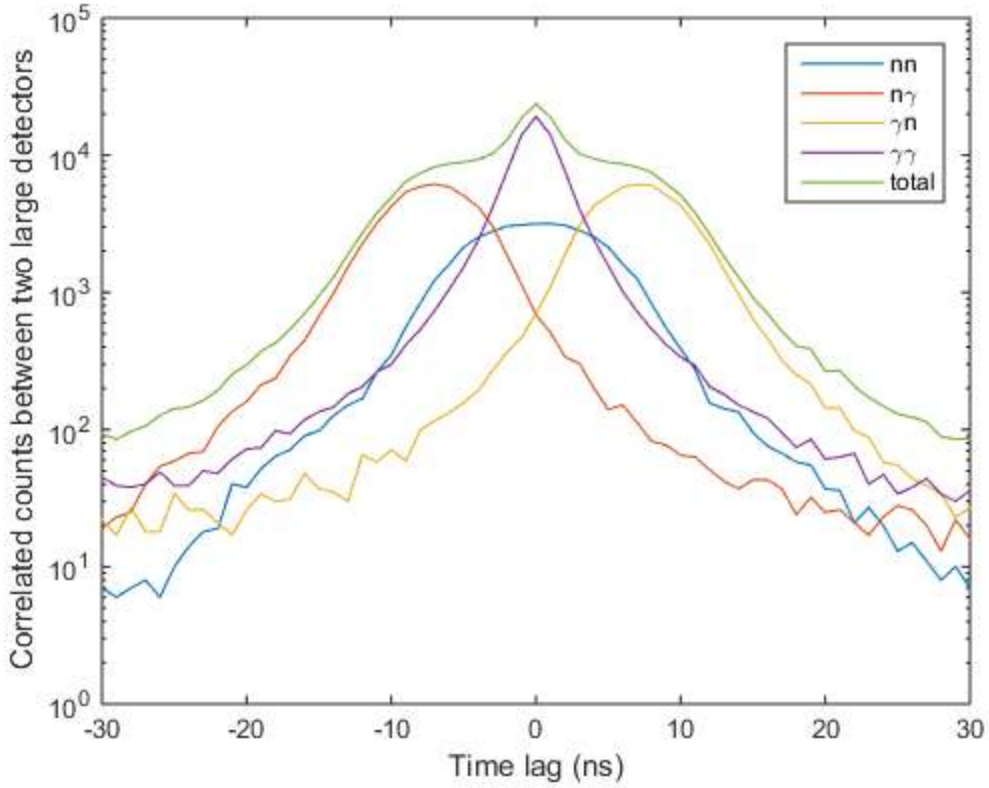

Figure 1-5. Example of time distribution of cross-correlated events for a spherical shell, including regions containing primary gamma pairs, neutron-neutron pairs, neutron-gamma pairs and gamma-neutron pairs. In this system, gammas are distinguished from neutrons only based upon time of flight.

1.4 Monte Carlo Simulations

The simulations used to develop the method were completed using the MCNP-PoliMi code version 2.0.0, which uses MCNP5. MCNP-PoliMi was developed to use neutron and gamma rays to simulate correlation measurements. The prompt neutrons and gamma rays that are associated with each event are explicitly modeled, and each collision in the detector is treated individually. The MCNP-PoliMi output file records all the relevant information about each interaction in specified cells. This information includes the reaction type, target

nucleus, position of collision, deposited energy and collision time [20]. This information is then post-processed to simulate the response of the detectors.

PoliMiPP is the post-processor used in this research, and it is a FORTRAN program developed by Grogan [21]. PoliMiPP computes the singles and doubles using the data MCNP-PoliMi output file. The post-processor allows users to specify the detector characteristics, such as dead time and neutron threshold, based on the properties of the detectors used experimentally. PoliMiPP determines the detector cells that had an interaction and the time between the collisions for each history [12]. Each interaction is assigned a scintillation light output based on the interaction type, target nucleus and the energy deposited. Once the light from the appropriate collisions has been combined, PoliMiPP determines if a pulse has occurred during the dead time. The pulse is not counted if it occurs within the dead time of a previous pulse. The post-processor also determines if the height of the pulse passes the energy threshold [21]. Once all the histories have been processed, PoliMiPP writes the resulting distributions to output files. Throughout the post-processing, the code simulates realistic precision by sampling Gaussian distributions with user defined variances.

1.5 Outline of Work

Chapter 2 provides details on the prior work related to concepts discussed in this research. Chapter 3 outlines the steps taken to develop the method, and provide information on the Pu assemblies and measurement configurations used for the simulations. Chapter 4 provides an analysis of the simulation results in order to develop the method to determine the ^{240}Pu content. The accuracy of the method is verified in Chapter 5, using simulated

measurement data and data from previous passive measurements of Pu samples. Chapter 6 discusses the conclusions and future work.

CHAPTER 2

PREVIOUS WORK

2.1 Plutonium Isotopic Analysis

There are several existing methods used to determine Pu isotopic content using gamma-ray spectroscopy. These methods analyze certain regions of interest of the Pu spectra. These Pu isotopic analyses can support other nondestructive assay (NDA) methods such as coincidence or multiplicity counting in order to provide information on the total Pu mass of the sample. The plutonium gamma ray spectrum varies greatly with plutonium isotopic content, and the lower energy gamma rays (up to 200 keV) tend to be more intense than the higher energy ones [22]. The lower energy gamma rays are sometimes impossible to analyze, especially in the presence of shielding material such as lead.

The first practical method, using gamma-ray spectrum analysis, for determining the isotopic composition of an arbitrary Pu sample used what is known as intrinsic self-calibration technique [23]. This self-calibration of the relative efficiency of a measurement is a key component of current gamma-ray isotopic analysis. The relative efficiency is a function of energy and any changes in the absorption or intensity of the gamma rays can affect the shape or the energy dependence of the relative efficiency curve [24]. This isotopic analysis technique uses energies from the measured gamma-ray spectrum of an unknown Pu sample to determine the ratio of the relative efficiency at specified energies from the measured gamma-ray spectrum of an unknown sample [24]. This technique forms the basis of a number of gamma-ray spectroscopy isotopic analysis applications that are used today. One such application is the PC/FRAM code.

PC/FRAM is a gamma-ray isotopic analysis software, developed at Los Alamos National Laboratory in 1988, for the nondestructive measurement of isotopic composition for safeguards applications. The PC/FRAM code can be applied in a number of different scenarios, including quantifying individual isotopes of Pu in bulk Pu measurements and verifying the isotopic composition and quantifying the concentration of fission products in mixed oxide (MOX) fuel [24]. PC/FRAM also supports the Segmented Gamma Scanner (SGS), which is a transmission-corrected passive assay technique used to quantify individual isotopes in scrap and waste items [24], [25].

PC/FRAM uses a single detector to acquire data making it easier to use, less expensive and more compact. It can use a single planar or coaxial high purity germanium (HPGe) detector or a cadmium telluride (CdTe) detector to perform the isotopic analysis in the 120-420 keV range. Results from PC/FRAM version 4, for plutonium spectral data obtained from coaxial HPGe detector measurements, show that the biases in measuring ^{238}Pu, ^{239}Pu, ^{240}Pu and ^{241}Pu are 0.9958, 1.0001, 1.0000 and 0.9999, respectively, in the region 120-450 keV [24]. The bias is determined by finding the difference between the measured value and the true value. PC/FRAM has also been tested in shielded configurations. It has been demonstrated that PC/FRAM can perform a complete Pu isotopic analysis through as much as 25 mm of lead [26], but requires modification to the parameter file in order to accomplish this, since the lower energy gamma rays tend to be harder to analyze as the thickness of the lead increases [24]. Three Pu sources, with ^{240}Pu content ranging from 6-17%, were measured with lead thicknesses ranging from 0-25.3 mm. As the shielding thickness increased toward 25 mm, the count time was increased in order to compensate for the reduced input rate, with count times as high as four hours. The results

show that the bias in the measurement of ^{240}Pu content, across all three samples shielded by a 25 mm lead thickness ranged from 0.9667-1.0128 [26].

Another gamma-ray spectroscopy isotopic analysis method, developed at Lawrence Livermore National Laboratory involves combination of three Fissile Material Transparency Technology Demonstration (FMTTD) codes, in order to determine attributes of Pu objects. These codes are Pu-300, Pu-600, and Pu-900, and the names refer to the corresponding region of interest in the Pu spectra [27], [28], [29]. Pu-300 determines the Pu age, which is the time that has elapsed since the chemical purification of the Pu object, by analyzing the resulting ^{241}Am and ^{237}U peaks from the decay of ^{241}Pu [27]. The Pu-600 method looks at gamma ray pulse height distributions in the region between 630 and 670 keV [28], [29]. The Pu-600 method measures the ^{240}Pu/^{239}Pu ratio by analyzing the areas of the ^{240}Pu peak at 642.5 keV and the ^{239}Pu peak at 646.0 keV [5], and a ratio of <0.1 indicates the presence of WGPu. The presence of Pu is determined by the sum of the net areas of three ^{239}Pu peaks, one in the 300 keV region and two in the 600 keV region. The Pu-900 method is used to determine the absence of PuO_2 by determining the absence of a 870.7 keV peak. This peak results from a de-excitation of the first excited state of ^{17}O [27]; therefore, an absence of this peak shows that no oxide is present in the sample.

Previous measurement results obtained using the Pu-600 method have validated its ability to identify the presence of WGPu in bare and containerized assemblies. In one measurement, the Pu objects were either bare or enclosed in AT400A or AL-R8 containers [27]. AT400A containers are 304L stainless steel containers forged into two half shells [30] and AL-R8 containers are light weight carbon steel drums [31]. The ^{240}Pu/^{239}Pu ratio was determined, using a data acquisition time of 15 minutes, and the measured ratio normalized

to actual values of the ratio was found to be 0.99±0.05. If the measurements were perfect, this value would have been 1 [27]. Pu-600 measurements on the Zero Power Physics Reactor (ZPPR) plates were performed to determine the $^{240}Pu/^{239}Pu$ ratio. The plutonium aluminum (PuAl) ZPPR plates also have a stainless steel cladding and are stored in clamshell containers [32]. The isotopic ratio of the ZPPR plates was found to be 0.134±0.014 for an average of 52 measurements, with an actual isotopic ratio of 0.136 [33].

2.2 Time Correlation Measurements

Time correlation measurements have been used to identify the presence of special nuclear materials in different types of samples, by analyzing the time distributions of gamma and neutron detection. Time correlation measurements were conducted on a 4.5 kg bare plutonium sphere, and the same spheres surrounded by various thicknesses of polyethylene and tungsten reflectors, to gain an understanding of the multiplication of the sample. The measurement results showed that the bare sample had the shortest fission chains while the polyethylene reflector had the longest, which is expected due to the ability of the polyethylene reflector to moderate the neutrons, resulting in more fission chains [34].

Measurements have also been conducted to determine the multiplication and fissile content in bare uranium metal assemblies using a ^{252}Cf source [35]. Due to the low spontaneous fission of uranium metal, a time tagged active source, such as a ^{252}Cf ionization chamber, is useful to determine the multiplication and fissile content of the assembly. Using this active source, time correlation measurements were performed to estimate the multiplicities of the uranium assemblies, in order to characterize the assembly. Active time correlation measurements, using a ^{252}Cf source, have also been investigated for use in cargo

container inspections for the detection of nuclear materials [36]. The presence of shielding materials such as iron and lead alter the observed time distributions, especially the gamma-gamma and neutron-neutron coincidences, and these changes can be used to detect the presence of shielded nuclear materials.

Time correlation measurements have also been used to estimate uranium metal enrichment when the sample is heavily shielded by high-Z material [37]. The measurement involves interrogating the item and shielding, with 14 MeV neutrons using a D-T neutron generator. During the interrogation the D-T generator measures the particle arrival time at the detectors in relation to the neutron creation time. The time distribution for auto-correlation and cross-correlation events from these measurements are used to generate Monte Carlo simulations in order to develop a method to estimate uranium metal enrichment [37].

Passive time correlation measurements were conducted to develop a model to determine Pu mass and multiplication [19], [38]. The Pu samples were delta-phase Pu shells with 1.77% ^{240}Pu content of various sizes and masses. Due to the constant ^{240}Pu content of the Pu samples, the total Pu mass, ^{239}Pu mass and ^{240}Pu mass are directly proportional to each other. The multiplication and mass of the assemblies were determined by analyzing the full-width at tenth-maximum (FWTM) of the time distribution of the cross-correlated events. The results show that the model is able to estimate the multiplication within 5% and the ^{240}Pu mass within 7%, in terms of the root-mean-square (RMS) [19], [38]. If the ^{240}Pu mass and total Pu mass is known, the ^{240}Pu content can be calculated, but this study was not expanded to determine the ^{240}Pu content in the shells as all the samples had the same ^{240}Pu content, and so it cannot be demonstrated solely from these measurements.

Time correlation measurements have also been conducted on non-metallic fissile assemblies. Measurements of the cross-correlation for neutron and gamma-ray events were performed for plutonium oxide (PuO_2) powder samples of varying mass and burnup, stored in stainless steel containers [39], [40]. The time distributions of the cross-correlated events were determined by finding the difference between the detections in two detectors in a specified time window. These distributions were used to develop a model to determine the ^{240}Pu mass with less than 1.3% error [39]. The measurements that have been done to determine ^{240}Pu mass have not been expanded to determine ^{240}Pu content from ^{240}Pu mass, therefore this attribute still needs to be analyzed.

2.3 MCNP-PoliMi Validation

A number of validation tests have been conducted to demonstrate MCNP-PoliMi capability to accurately model time correlation measurements. MCNP-PoliMi simulations were compared with some of the measurements discussed in Section 2.2. For example, the time correlation measurements for different enrichments of heavily shielded uranium metal were modeled using geometry and materials information [37]. The simulation predicts the time correlations expected from fast plastic scintillation detectors, of dimension $27 \times 27 \times 10$ cm, for each modeled enrichment. The simulated time correlations were compared with the measured time correlations, and the best match was used to determine the actual enrichment. In [37], the simulated time distribution of the auto-correlated events showed more high energy neutrons than were observed in the measurement. For the depleted uranium (DU) casting the simulated fission neutron peak was 31% higher than the measured peak [37]. This difference was attributed to the modeling of each pixel's neutron emission beam from the D-

T generator as a circular cone when in actual measurements, the neutron beam is an elliptical cone [37]. This issue has been updated in the latest version of MCNP-PoliMi.

In another study, NMIS experimental data was compared to simulated time distributions of cross-correlated events, using MCNP-PoliMi, for three delta-phase Pu metal shells with 1.77% ^{240}Pu [41], [42]. Simulations of both active and passive time correlation measurements were conducted on the Pu shells. For the passive measurements, two Pu shells were simulated and the time cross-correlated distribution between two $10.2 \times 10.2 \times 10.2$ cm was compared with the measured distributions between two similar sized detectors. Both the simulated and measured distributions were normalized to the total area of the cross-correlation distribution. A comparison of the simulated and measured time distributions show the RMS error in the gamma-gamma peak is 4.77% and 1.64% in the neutron peak [41]. The analysis shows a good agreement between the measured and simulated cross-correlation, but the simulated gamma-gamma pair peak width is 1 ns smaller than the measured peak width. It was concluded that this difference could be due to the timing of the energy in the post processing code [41].

In another study, MCNP-PoliMi passive correlation measurements were used to evaluate the effects of placing Pu shells inside a container [43]. The AT-400R is a stainless steel container with a polyethylene moderator or neutron shield, designed for Pu storage. The simulations were validated with experimental results from measurements using a ^{252}Cf source as a surrogate for Pu. The Pu shell used for the simulation was ~2% ^{240}Pu. The simulations were conducted with and without the container in order to understand its attenuation properties, and the cross-correlated distributions showed an attenuation when the container is present [43]. The results show that the presence of the container reduces the

neutron-neutron correlations by a factor of 50, the gamma-gamma correlations by 30%, and the neutron-gamma correlations by a factor of 20 [43]. The simulations were repeated for bare Pu shells of varying masses, and the cross-correlated distributions were used to find a relationship between the ^{239}Pu content and the cross-correlated counts. The resulting quadratic equation can be used to estimate the ^{239}Pu content for spherical shells, if the correlated counts are known for a known isotopic content [43].

A number of studies have been completed to show that MCNP-PoliMi is able to distinguish between the observables from Pu oxide and Pu metal [20], [44]. MCNP-PoliMi passive measurement simulations were done on Pu spheres and cylinders with 6% ^{240}Pu content. PuO_2 objects with the same mass as the Pu metal objects were simulated using the same measurement configuration for all samples. The resulting distributions were normalized to the total number of spontaneous fissions (7×10^5 spontaneous fissions of ^{240}Pu). The cross-correlation distributions show a distinct difference between Pu metal and oxide. It was possible to distinguish between the metal and the oxide because the gamma ray attenuation is much higher in the metal than the oxide [20].

2.4 Original Work and Justification

It was postulated that the ^{240}Pu content of a Pu sample could be determined from time coincidence data obtained during an NMIS measurement; however, a method has not been developed to confirm this statement. Since 2001, work has been done to develop the attribute estimation capability for NMIS/FNMIS, and results have shown that it is possible to determine the mass and radial thickness of Pu metal spherical shells from NMIS measurements [19]. However, the estimation of ^{240}Pu content has not been addressed, and

providing this analysis would not only expand the attribute estimation capability of NMIS but also provide an alternative method to identify the presence of WGPu. The vast majority of studies with NMIS measurements have been conducted for uranium, and, therefore, any Pu quantification work is relatively new.

The goal of this research is to identify the presence of WGPu, by determining the ^{240}Pu content of the Pu sample. WGPu samples have a ^{240}Pu content of <7%. In order to develop the method, this research employs Monte Carlo simulations of NMIS passive time correlation measurements, in order to estimate the ^{240}Pu content in Pu metal assemblies. Currently, there are no known analyses that have been completed for Pu that provide a method to estimate ^{240}Pu content from only NMIS passive time coincidence data. The resulting method could be easily incorporated into NMIS, in order to expand its attribute estimation capabilities.

Although a few methods have been discussed that calculate the ^{240}Pu mass [19], [39], which can be used to determine the ^{240}Pu content if the total Pu mass is known (this typically requires a neutron coincidence or multiplicity measurement and gamma spectrometry), this research offers an alternative method to current analysis, by utilizing NMIS neutron detection capability in order to identify the presence of WGPu.

CHAPTER 3

METHODS AND MATERIALS

3.1 Materials and Simulation Configuration

The Pu samples simulated to develop the method are Pu spherical shells and spheres. Their dimensions and isotopic compositions are based on existing Pu assemblies. The Pu spherical shell is modeled on Russian plutonium assemblies at the Russian Federal Nuclear Center, All-Russia Scientific Research Institute of Experimental Physics (RFNC-VNIIEF). Each delta-phase plutonium metal sphere assembly, as shown in Figure 3-1, contains approximately 97.20% ^{239}Pu, 1.80% ^{240}Pu, and ~1% gallium by mass. The assembly has an inner radius of 5.35 cm, outer radius of 6.00 cm, mass of 4004.4 g and density of 15.21 g/cm^3 [45].

The Pu sphere modeled was the beryllium-reflected Pu metal sphere (BeRP Ball), fabricated by Los Alamos National Laboratory in 1980 [46]. It is an alpha-phase, WGPu spherical ball of radius 3.7938 cm, mass of 4483.9 g and a density of 19.60 g/cm^3. The BeRP ball is composed of 93.73% ^{239}Pu, 5.96% ^{240}Pu, and ~0.31% other isotopes (^{238}Pu, ^{241}Pu, ^{242}Pu, ^{241}Am) [47], [46], [48].

The measurement configuration used for the simulations is shown in Figure 3-2. Four plastic scintillation detectors, were positioned around the assembly, with the two small detectors (10.2 × 10.2 × 10.2 cm), and the two large detectors (15.2 × 15.2 × 10.2 cm), placed opposite each other, respectively. The detectors were located 12.8 cm from the center of the sample. The measurement time used in each simulation was 256 seconds.

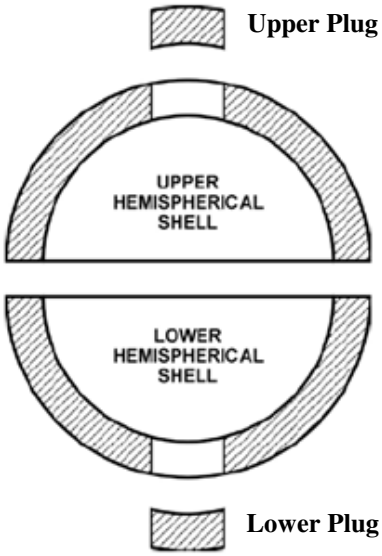

Figure 3-1. Illustration showing a cross-sectional side view of a delta-phase Pu shell component (parts shaded).

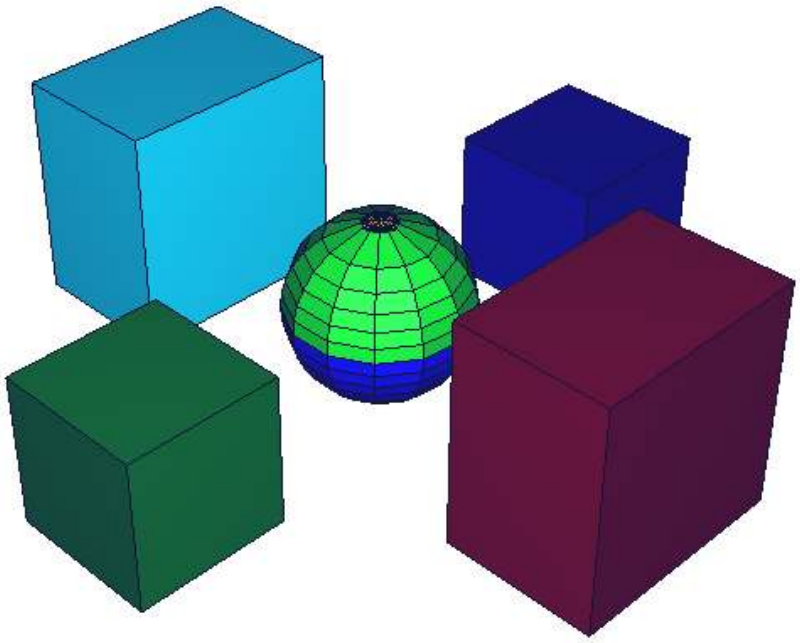

Figure 3-2. Configurations of detectors for simulation of passive measurements of the bare delta-phase Pu spherical shell assemblies.

In addition to analyzing bare Pu samples, simulations were also completed for passive measurements of Pu samples surrounded by reflectors and shielding. Neutron reflectors increase the multiplication of a fissile material. The reflectors used in the analysis were beryllium and graphite due to their distinction as both a good reflector and moderator. Moderators turn fast neutrons to thermal neutrons, and reflect them back into the sample, resulting in a sustained nuclear chain reaction [49].

Simulations were completed with various thicknesses of beryllium and graphite surrounding the Pu assembly. Figure 3-3 and Figure 3-4 shows the cross section of the measurement configuration used for simulations of the reflector and Pu spherical shell and Pu sphere respectively. In both figures the red represents the reflector, the blue represents the Pu assembly and the green represents the detectors.

In order to provide a comprehensive analysis on the effects of different shielding materials on the time correlated distributions, simulations were done with high density (depleted uranium, lead), and low Z (aluminum, polyethylene, steel) materials, to see their effects on the gammas and neutrons. Figure 3-5 shows the simulated measurement configuration, where the cylindrical object represents the shielding material.

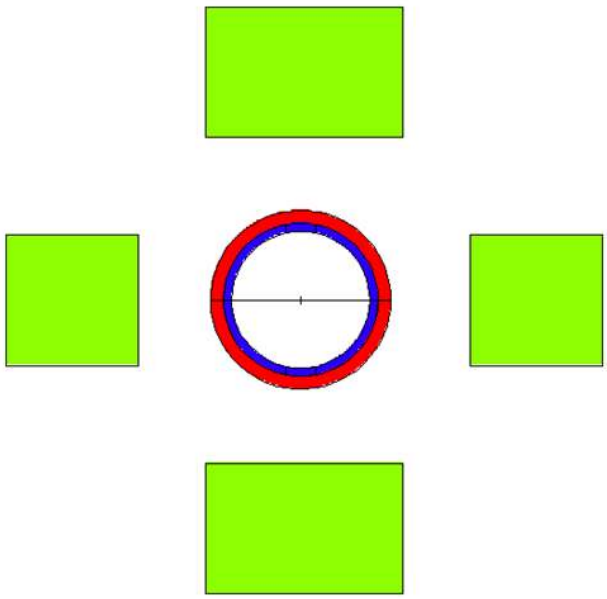

Figure 3-3. Diagram of the simulation configuration for the Pu spherical shell (blue) and a reflector (red).

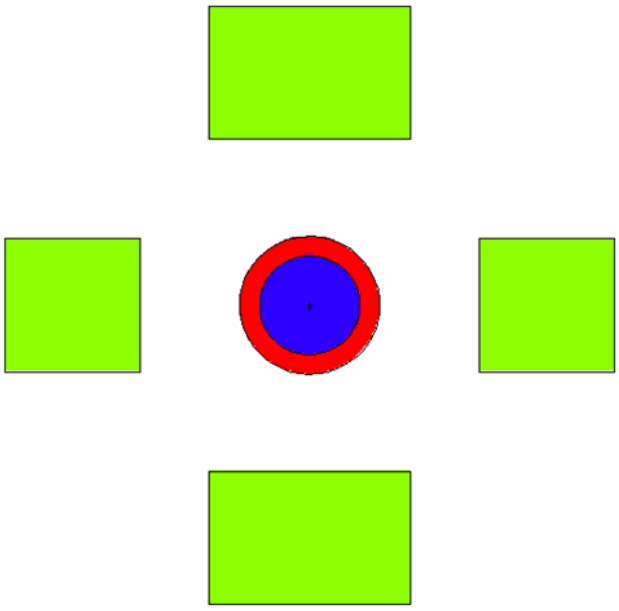

Figure 3-4. Diagram of the simulation configuration for the Pu sphere (blue) and a reflector (red).

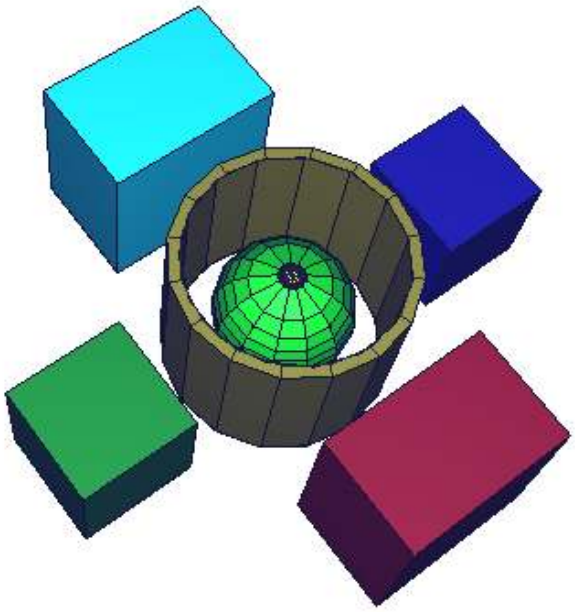

Figure 3-5. Diagram of the simulation configuration for the Pu sample surrounded by shielding.

Table 3-1. Summary of material information used in to develop the method to determine ^{240}Pu content.

Pu Shapes	Spherical Shell, Solid Sphere
Pu Allotropes	Delta, Alpha
Pu Mass (kg)	0.06-14.4
Pu Thickness (cm)	0.25-2.50
Pu Outer Radius (cm)	1.0-10.0
Reflector Materials	Beryllium, Graphite
Shielding Materials	Aluminum, Depleted Uranium, Lead, Polyethylene, Stainless Steel
Reflector/Shielding Thickness (cm)	0.5-2.5
Energy Threshold (MeV)	1.0-2.0
Measurement Time (seconds)	256

3.2 Procedure

The Pu samples used in the simulations are alpha- and delta phase Pu spherical shells and spheres with the dimensions outlined in Section 3.1. In order to develop the method, an exhaustive set of simulations is completed in order to account for a variety of measurement conditions. The simulations conducted and the analyses performed, are outlined in the steps below.

1. Simulate varying ^{240}Pu content for each of the bare Pu samples and plot the cross-correlated time distributions.
    a. Determine the counts/second for each corresponding ^{240}Pu content by calculating the area of the 5 ns peak width centered on 0 ns.
    b. Generate the equations to calculate ^{240}Pu content, for each bare Pu sample.
2. Simulate varying energy thresholds for the Pu samples and plot the cross-correlated time distributions.
    a. Use the ^{240}Pu content equation to calculate the ^{240}Pu content for various energy thresholds. Calculate the differences between the actual and calculated values of ^{240}Pu content and use this difference to develop an equation to correct for varying energy thresholds.
3. Simulate varying Pu spherical shell thicknesses for the alpha- and delta-phase Pu spherical shells and plot the cross-correlated time distributions.
    a. Use the ^{240}Pu content equation to calculate the ^{240}Pu content for various shell thicknesses. Calculate the differences between the actual and calculated

values of ^{240}Pu content and use this difference to develop an equation to correct for changing thicknesses of the Pu spherical shell.

4. Simulate varying the outer radii of the alpha- and delta-phase Pu spherical shells and spheres and plot the cross-correlated time distributions.
    a. Use the ^{240}Pu content equation to calculate the ^{240}Pu content for various Pu sample outer radii. Calculate the differences between the actual and calculated values of ^{240}Pu content and use this difference to develop an equation to correct for changing sizes of the Pu sample. The equations for each Pu sample are combined to provide ^{240}Pu content equations for bare Pu spherical shells and spheres.
5. Simulate the presence of varying thicknesses of reflectors, surrounding alpha- and delta-phase Pu spherical shells and spheres and plot the cross-correlated time distributions.
    a. Use the corrected ^{240}Pu content equation to calculate the ^{240}Pu content for Pu samples surrounded by reflectors. Calculate the differences between the actual and calculated values of ^{240}Pu content and use this difference to develop an equation to correct for the presence of each reflector surrounding the Pu sample.
6. Simulate the presence of varying thicknesses of shielding, surrounding alpha- and delta-phase Pu spherical shells and spheres and plot the cross-correlated time distributions.
    a. Use the corrected ^{240}Pu content equation to calculate the ^{240}Pu content for Pu samples surrounded by shielding. Calculate the differences between the

actual and calculated values of ^{240}Pu content and use this difference to develop an equation to correct for the presence of each reflector surrounding the Pu sample.

7. Create a script that includes these equations to calculate the ^{240}Pu content in a variety of shielded and unshielded configurations. The script requires the user to input the counts (as determined through analysis of the cross-correlated time distribution plot), inner and outer radius of the Pu sample, and thickness of the reflector or shielding, if present. When run, the script outputs the calculated ^{240}Pu content and the RMS error in percent (%).

Table 3-2 summarizes all the iterations of simulations that were completed to develop the ^{240}Pu content estimation method for bare Pu samples. Table 3-3 summarizes the simulations for Pu samples surrounded by shielding or reflectors. Configurations of shielding-shielding and shielding-reflector combinations were not analyzed.

Table 3-2. List of simulations to create the ^{240}Pu content estimation method for bare Pu assemblies.

Simulations	Shape	Pu Allotrope	^{240}Pu Content (%)	Energy Threshold (MeV)	Thickness (cm)	Outer Radius (cm)
1-10	Shell	Delta	1:1:10*	1.50	0.65	6.00
11-21	Shell	Delta	1.80	1:0.1:2	0.65	6.00
22-31	Shell	Delta	1.80	1.50	0.25:0.25:2.5	6.00
32-41	Shell	Delta	1.80	1.50	0.65	1:1:10
41-51	Shell	Alpha	1:1:10	1.50	0.65	6.00
52-62	Shell	Alpha	1.80	1:0.1:2	0.65	6.00
63-72	Shell	Alpha	1.80	1.50	0.25:0.25:2.5	6.00
73-82	Shell	Alpha	1.80	1.50	0.65	1:1:10
83-92	Sphere	Delta	1:1:10	1.50	0.00	3.79
93-103	Sphere	Delta	5.96	1:0.1:2	0.00	3.79
104-112	Sphere	Delta	5.96	1.50	0.00	1:0.5:5
113-122	Sphere	Alpha	1:1:10	1.50	0.00	3.79
123-133	Sphere	Alpha	5.96	1:0.1:2	0.00	3.79
134-141	Sphere	Alpha	5.96	1.50	0.00	1:0.5:4.5

* starting value:iteration value:ending value

Table 3-3. List of simulations to create the ^{240}Pu content estimation method for Pu assemblies surrounded by reflector or shielding.

Simulations	Shape	Pu Allotrope	Reflector/ Shielding	
			Material	Thickness (cm)
1-6	Shell	Delta	Beryllium	0:0.5:2.5
7-12	Shell	Delta	Graphite	0:0.5:2.5
13-18	Shell	Delta	Aluminum	0:0.5:2.5
19-24	Shell	Delta	Depleted Uranium	0:0.5:2.5
25-30	Shell	Delta	Lead	0:0.5:2.5
31-36	Shell	Delta	Polyethylene	0:0.5:2.5
37-42	Shell	Delta	Stainless Steel	0:0.5:2.5
43-48	Shell	Alpha	Beryllium	0:0.5:2.5
49-54	Shell	Alpha	Graphite	0:0.5:2.5
55-60	Shell	Alpha	Aluminum	0:0.5:2.5
61-66	Shell	Alpha	Depleted Uranium	0:0.5:2.5
67-72	Shell	Alpha	Lead	0:0.5:2.5
73-78	Shell	Alpha	Polyethylene	0:0.5:2.5
79-84	Shell	Alpha	Stainless Steel	0:0.5:2.5
85-90	Sphere	Delta	Beryllium	0:0.5:2.5
91-96	Sphere	Delta	Graphite	0:0.5:2.5
97-102	Sphere	Delta	Aluminum	0:0.5:2.5
103-108	Sphere	Delta	Depleted Uranium	0:0.5:2.5
109-114	Sphere	Delta	Lead	0:0.5:2.5
115-120	Sphere	Delta	Polyethylene	0:0.5:2.5
121-126	Sphere	Delta	Stainless Steel	0:0.5:2.5
127-132	Sphere	Alpha	Beryllium	0:0.5:2.5
133-138	Sphere	Alpha	Graphite	0:0.5:2.5
139-144	Sphere	Alpha	Aluminum	0:0.5:2.5
145-150	Sphere	Alpha	Depleted Uranium	0:0.5:2.5
151-156	Sphere	Alpha	Lead	0:0.5:2.5
157-162	Sphere	Alpha	Polyethylene	0:0.5:2.5
163-168	Sphere	Alpha	Stainless Steel	0:0.5:2.5

CHAPTER 4

DEVELOPMENT OF ^{240}PU CONTENT ESTIMATION METHOD

It is important, when developing the method that the end user is kept in mind. The ultimate goal is to incorporate this ^{240}Pu content determination method into NMIS which will be used by trained operators. As a result, the input values for the method should be relatively easy to determine.

The equations derived in this chapter are for the determination of ^{240}Pu content for Pu delta-phase spherical shells and alpha-phase spheres. These Pu assemblies have been discussed in Section 3.1. The analyses were repeated in the Appendix D and Appendix E, for Pu alpha-phase spherical shells and delta-phase spheres respectively. The method assumes that only one shielding or reflector material is present at a time, and considers only the two reflectors and five shielding materials previously discussed. Since the simulations were conducted using a 1.5 MeV energy threshold, additional analysis has been completed in Appendix J to study the effects of energy threshold on count rates, in order to accommodate a range of thresholds in the calculation. The definitions of the variables used in the equations are provided in Table A-1 in Appendix A.

4.1 Plutonium Spherical Shell

Simulations were completed for ^{240}Pu content ranging from 1% to 10.0%, as shown in Figure 4-1, for a delta-phase, Pu spherical shell. These simulations show an observable relationship between ^{240}Pu content and the NMIS passive time distributions. As the ^{240}Pu content increases the spontaneous fission of the Pu sample increases, resulting in increased

counts/second. The time distributions shown are for cross-correlated events between the two large detectors.

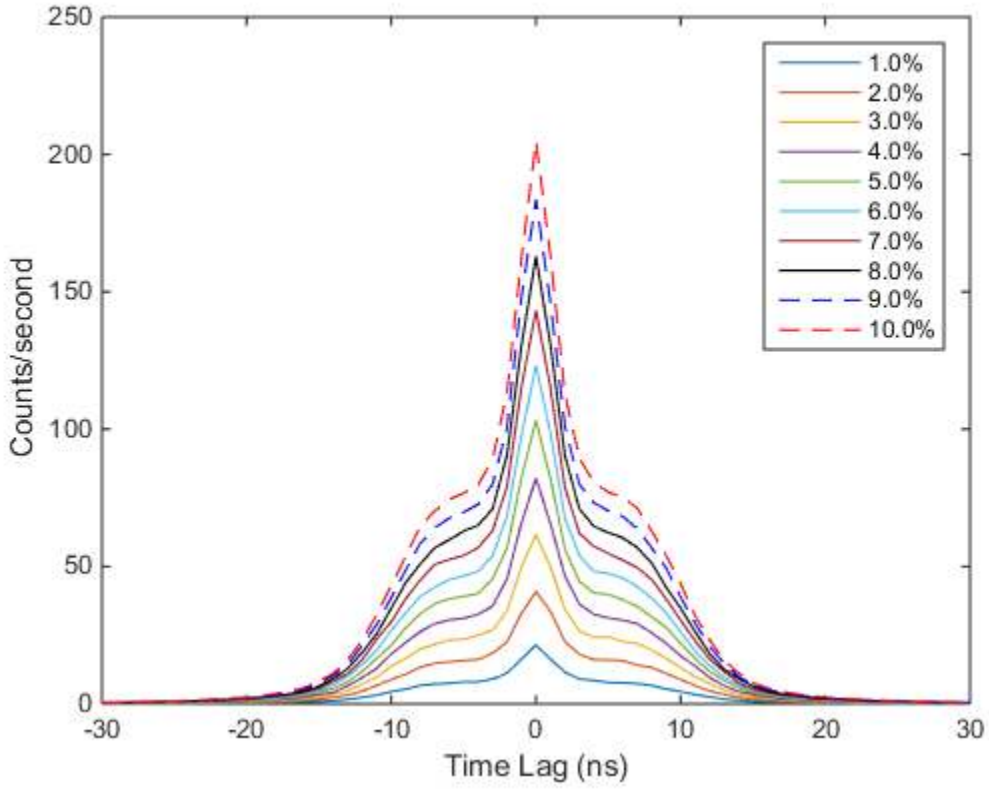

Figure 4-1. Simulation of time distributions for cross correlated events between two large detectors for various 240Pu content for a delta-phase Pu spherical shell.

4.1.1 ^{240}Pu Content Analysis

The area of the 5 ns peak width centered on 0 ns, shown in Figure 4-1, was calculated for each ^{240}Pu content. The resulting counts/second for the Pu spherical shell was then

plotted against the corresponding ^{240}Pu percentages, shown in Figure 4-2. The data is then fitted, and the equation of the line is

$$^{240}Pu\ Content\ (\%) = 0.0133C - 0.0384 \tag{4-1}$$

where C is the counts/second, determined by calculating the area of the 5 ns peak width of the time distribution for cross correlated events between the two large detectors.

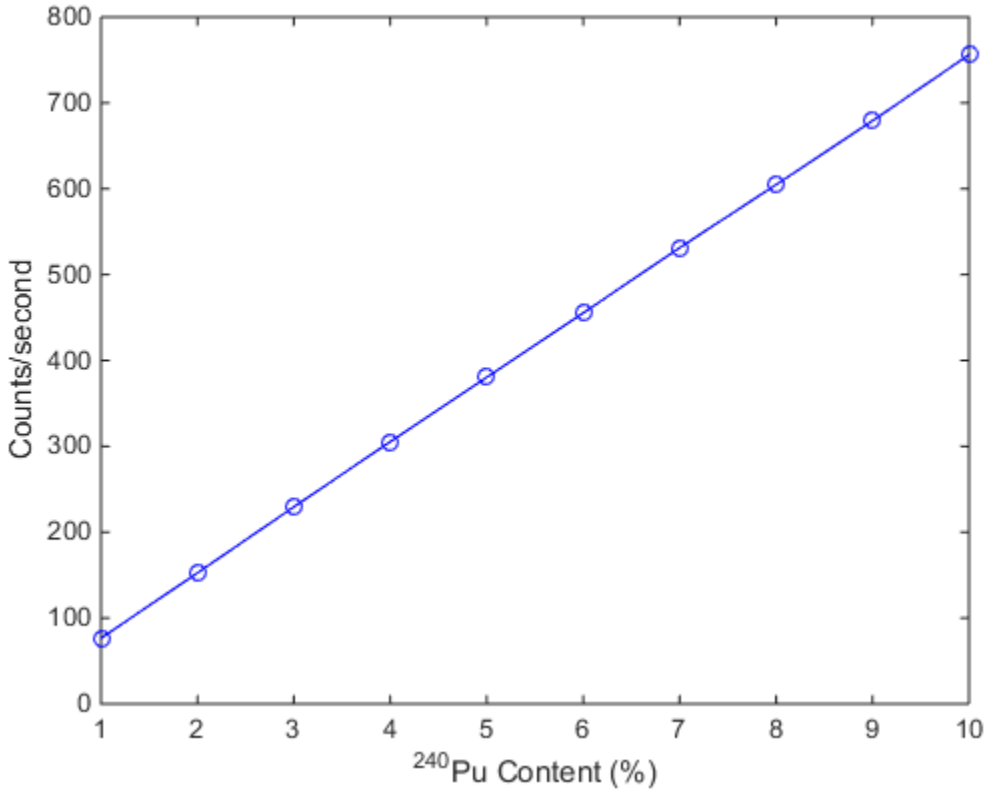

Figure 4-2. Relationship between various ^{240}Pu content and peak counts for a delta-phase Pu spherical shell.

4.1.2 Thickness Analysis

The data in Figure 4-3 shows the time distributions of cross-correlated events between the two large detectors, for shell thicknesses ranging from 0.25-2.50 cm. The ^{240}Pu content for varying shell thickness was calculated using Equation 4-1 in order to test the accuracy in estimating the ^{240}Pu content for spherical shells of varying thicknesses. The results in Table 4-1 show the differences between the calculated ^{240}Pu content and the actual value of 1.80%, for various shell thicknesses.

These differences were plotted against their corresponding thicknesses, in Figure 4-4, in order to generate an equation to correct for varying shell thicknesses. The data in Figure 4-4 is then fitted, and the equation of the curve is provided by Equation 4-2, which accounts for varying shell thicknesses in Equation 4-1.

Table 4-1. Differences between actual and calculated values of ^{240}Pu content for various thicknesses for a delta-phase Pu spherical shell.

Outer Radius (cm)	Inner Radius (cm)	Thickness (cm)	Mass (g)	Counts/second	Actual ^{240}Pu Content (%)	Calculated ^{240}Pu Content (%)	Difference (%)
6.00	5.75	0.25	1649.1	99	1.80	1.27	0.53
6.00	5.50	0.50	3160.8	128	1.80	1.66	0.14
6.00	5.25	0.75	4541.2	142	1.80	1.84	-0.04
6.00	5.00	1.00	5796.1	156	1.80	2.03	-0.23
6.00	4.75	1.25	6931.7	176	1.80	2.29	-0.49
6.00	4.50	1.50	7953.8	203	1.80	2.65	-0.85
6.00	4.25	1.75	8868.4	239	1.80	3.13	-1.33
6.00	4.00	2.00	9681.4	285	1.80	3.74	-1.94
6.00	3.75	2.25	10399.0	347	1.80	4.57	-2.77
6.00	3.50	2.50	11027.0	419	1.80	5.52	-3.72

$$Thickness\ \ Correction\ (\%) = 0.2617T^6 - 2.28T^5 + 7.949T^4 - 14.44T^3 + 13.85T^2 - 7.236T + 1.671 \quad (4\text{-}2)$$

where T represents non-zero values of shell thicknesses, in cm.

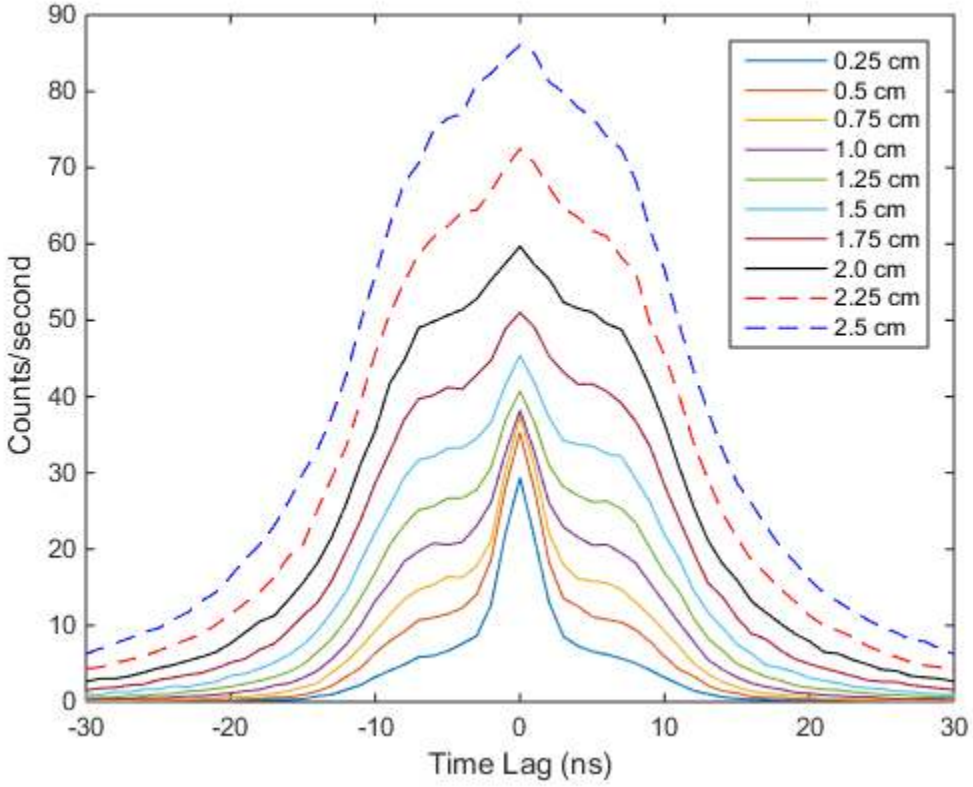

Figure 4-3. Simulation of time distributions for cross correlated events between two large detectors for various shell thicknesses for a delta-phase Pu spherical shell.

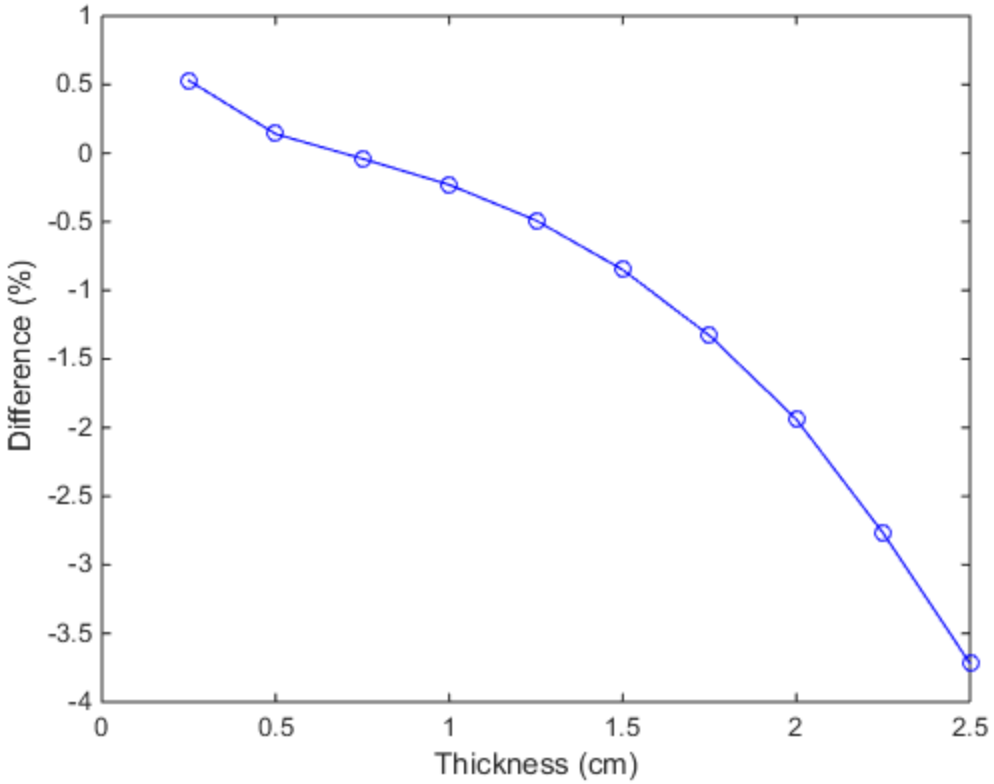

Figure 4-4. Differences between actual and calculated ^{240}Pu content plotted against various delta-phase Pu spherical shell thicknesses.

4.1.3 Size Analysis

The data in Figure 4-5 shows the time distributions of cross-correlated events between the two large detectors, for shell outer radii ranging from 1.0-10.0 cm. The ^{240}Pu content for varying outer radius values was calculated using a combination of Equation 4.1 and Equation 4.2, in order to test the accuracy in estimating the ^{240}Pu content for spherical shells of varying outer radius values. The results in Table 4-2 show the differences between the calculated ^{240}Pu content and the actual value of 1.80%, for various shell outer radii.

These differences were plotted against their corresponding outer radii in Figure 4-6, in order to generate an equation to correct for varying shell outer radii. The data in Figure 4-6 is then fitted, and the equation of the curve is provided by Equation 4-3, which adjusts the previous estimation for varying shell outer radii.

Table 4-2. Differences between actual and calculated values of ^{240}Pu content for various outer radii for a Pu spherical shell.

Outer Radius (cm)	Inner Radius (cm)	Thickness (cm)	Mass (g)	Counts/ second	Actual ^{240}Pu Content (%)	Calculated ^{240}Pu Content (%)	Difference (%)
1.00	0.35	0.65	61.0	3	1.80	0.03	1.77
2.00	1.35	0.65	352.8	15	1.80	0.19	1.61
3.00	2.35	0.65	893.1	36	1.80	0.47	1.33
4.00	3.35	0.65	1681.8	64	1.80	0.83	0.97
5.00	4.35	0.65	2718.9	98	1.80	1.29	0.51
6.00	5.35	0.65	4004.4	139	1.80	1.83	-0.03
7.00	6.35	0.65	5538.3	184	1.80	2.42	-0.62
8.00	7.35	0.65	7320.6	235	1.80	3.11	-1.31
9.00	8.35	0.65	9351.3	289	1.80	3.83	-2.03
10.00	9.35	0.65	11630.4	351	1.80	4.64	-2.84

$$Size\ Correction\ (\%) = 0.00107O^3 - 0.05649O^2 - 0.009526O + 1.839 \qquad (4\text{-}3)$$

where O represents non-zero values of outer radius, in cm.

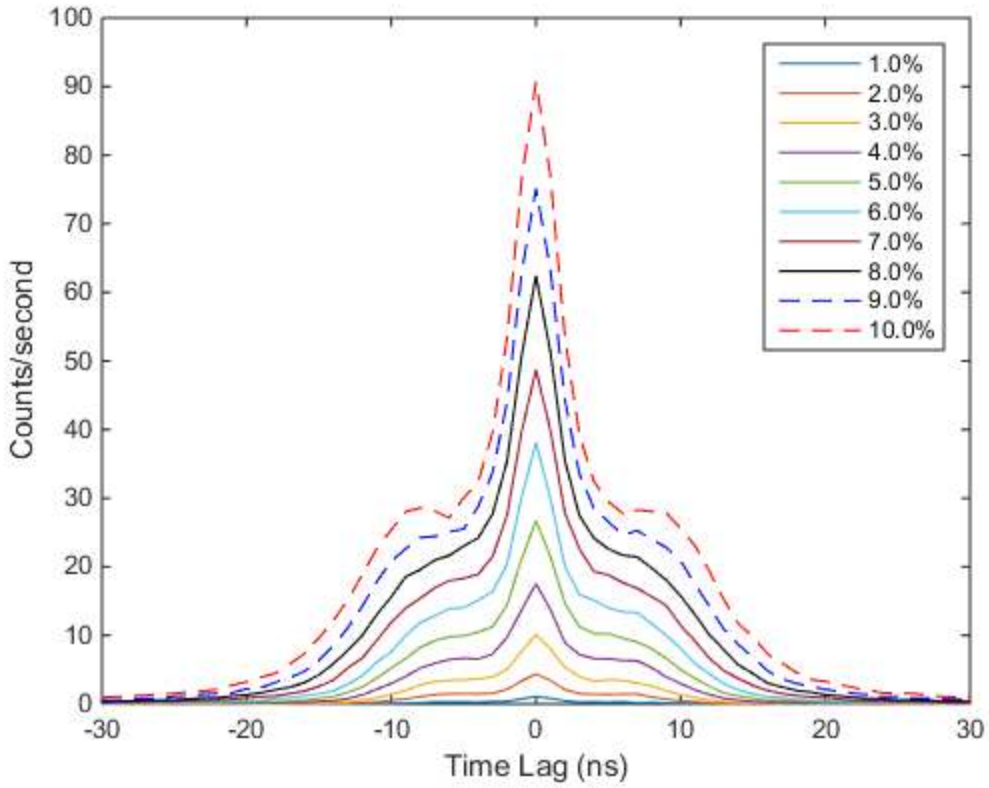

Figure 4-5. Simulation of time distributions for cross correlated events between two large detectors for various shell outer radii for a delta-phase Pu spherical shell.

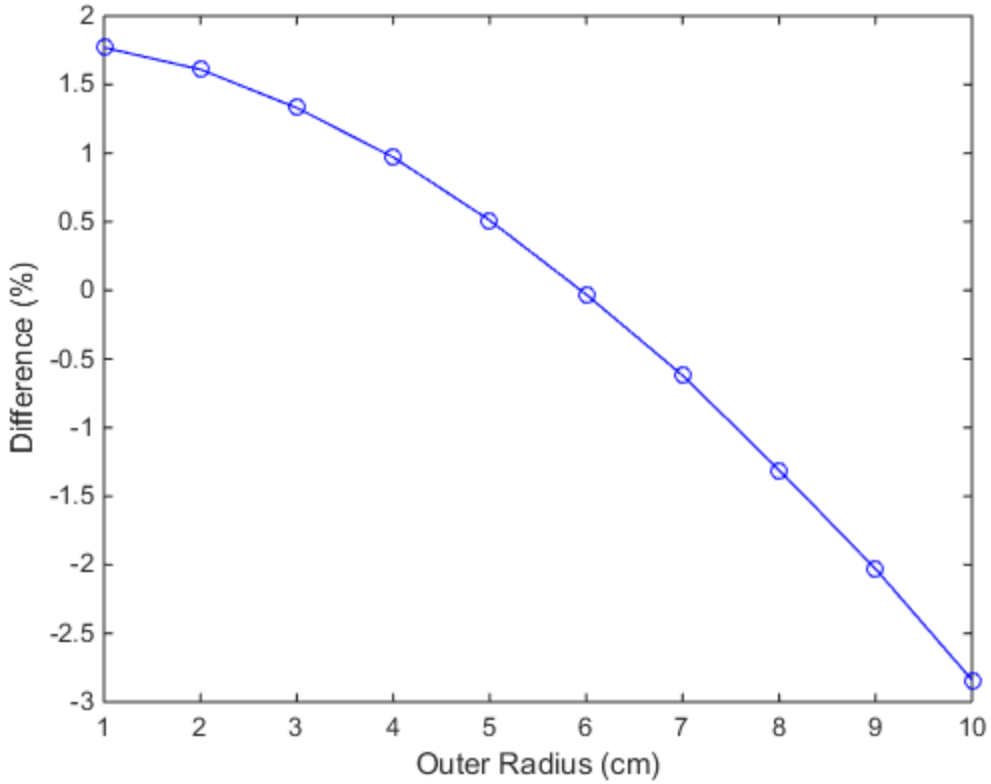

Figure 4-6. Differences between actual and calculated ^{240}Pu content plotted against various delta-phase Pu spherical shell outer radii.

4.1.4 Final Method

The equations derived in Section 4.1 are combined to provide a method to determine ^{240}Pu content for bare Pu spherical shells of various thickness, and outer radius values, shown in Equation 4.4. The results in Table 4-3 provide an updated comparison of the calculated ^{240}Pu content and the actual value of 1.80%, previously presented in Table 4-1 and Table 4-2, using:

$$^{240}Pu\ Content\ for\ Bare\ Pu\ Spherical\ Shells\ (\%) = 0.0133C + 0.2617T^6 - 2.28T^5 + 7.949T^4 - 14.44T^3 + 13.85T^2 - 7.236T + 0.00107O^3 - 0.05649O^2 - 0.009526O + 3.4716 \quad (4\text{-}4)$$

Table 4-3. Estimation of ^{240}Pu content for various thicknesses and outer radii of a delta-phase Pu spherical shell.

Outer Radius (cm)	Inner Radius (cm)	Thickness (cm)	Mass (g)	Counts/ second	Actual ^{240}Pu Content (%)	Calculated ^{240}Pu Content (%)
1.00	0.35	0.65	61.0	3	1.80	1.81
2.00	1.35	0.65	352.8	15	1.80	1.80
3.00	2.35	0.65	893.1	36	1.80	1.80
4.00	3.35	0.65	1681.8	64	1.80	1.80
5.00	4.35	0.65	2718.9	98	1.80	1.81
6.00	3.50	2.50	11027.0	419	1.80	1.76
6.00	3.75	2.25	10399.0	347	1.80	1.78
6.00	4.00	2.00	9681.4	285	1.80	1.77
6.00	4.25	1.75	8868.4	239	1.80	1.79
6.00	4.50	1.50	7953.8	203	1.80	1.78
6.00	4.75	1.25	6931.7	176	1.80	1.78
6.00	5.00	1.00	5796.1	156	1.80	1.78
6.00	5.25	0.75	4541.2	142	1.80	1.78
6.00	5.35	0.65	4004.4	139	1.80	1.81
6.00	5.50	0.50	3160.8	128	1.80	1.78
6.00	5.75	0.25	1649.1	99	1.80	1.78
7.00	6.35	0.65	5538.3	184	1.80	1.80
8.00	7.35	0.65	7320.6	235	1.80	1.81
9.00	8.35	0.65	9351.3	289	1.80	1.79
10.00	9.35	0.65	11630.4	351	1.80	1.81

The method is able to estimate the ^{240}Pu content for various thicknesses and outer radii, of bare Pu spherical shells, within ±0.04% of the actual ^{240}Pu content value.

4.2 Plutonium Sphere

Simulations were completed for ^{240}Pu content ranging from 1% to 10.0%, as shown in Figure 4-7, for an alpha-phase Pu sphere. The time distributions shown are for cross-correlated events between the large detectors.

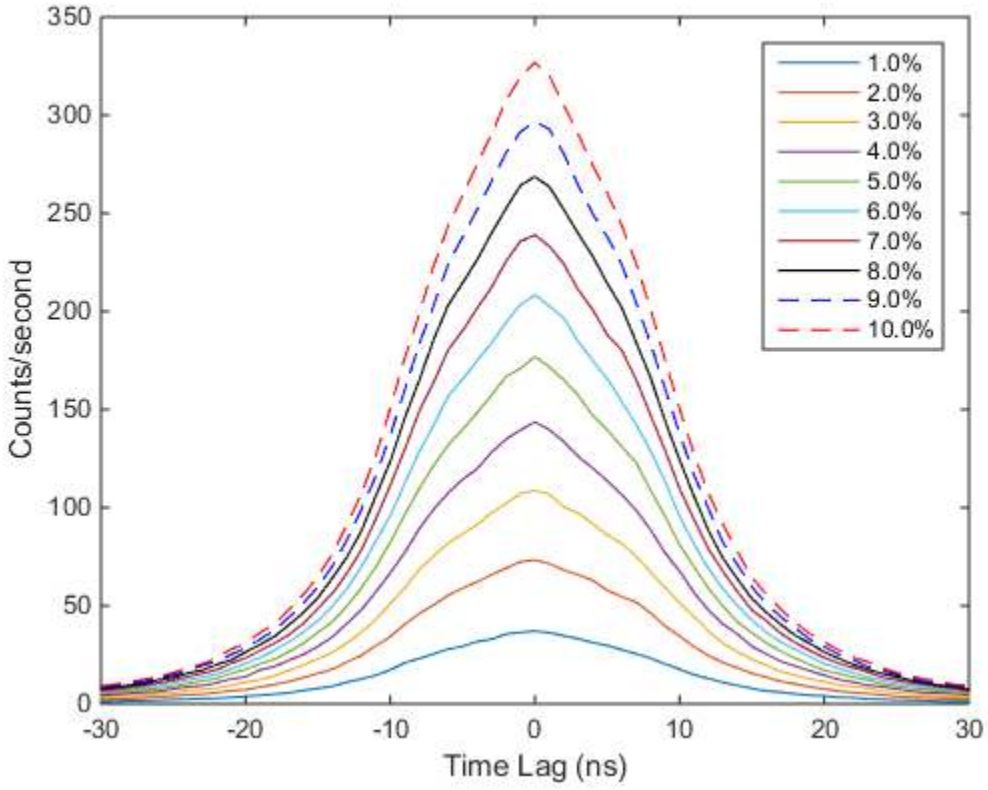

Figure 4-7. Simulation of time correlation distributions for various ^{240}Pu content for an alpha-phase solid Pu sphere.

4.2.1 ^{240}Pu Content Analysis

The area of the 5 ns peak widths, shown in Figure 4-7, was calculated for each ^{240}Pu content. The resulting counts/second for the Pu sphere was then plotted against the

corresponding ^{240}Pu percentages, shown in Figure 4-8. The data is then fitted and the equation of the curve is

$$^{240}Pu\ Content\ (\%) = \frac{\left(-182.6 + \sqrt{\left(182.6^2 + (9.924)(0.2083 - C)\right)}\right)}{-4.962} \tag{4-5}$$

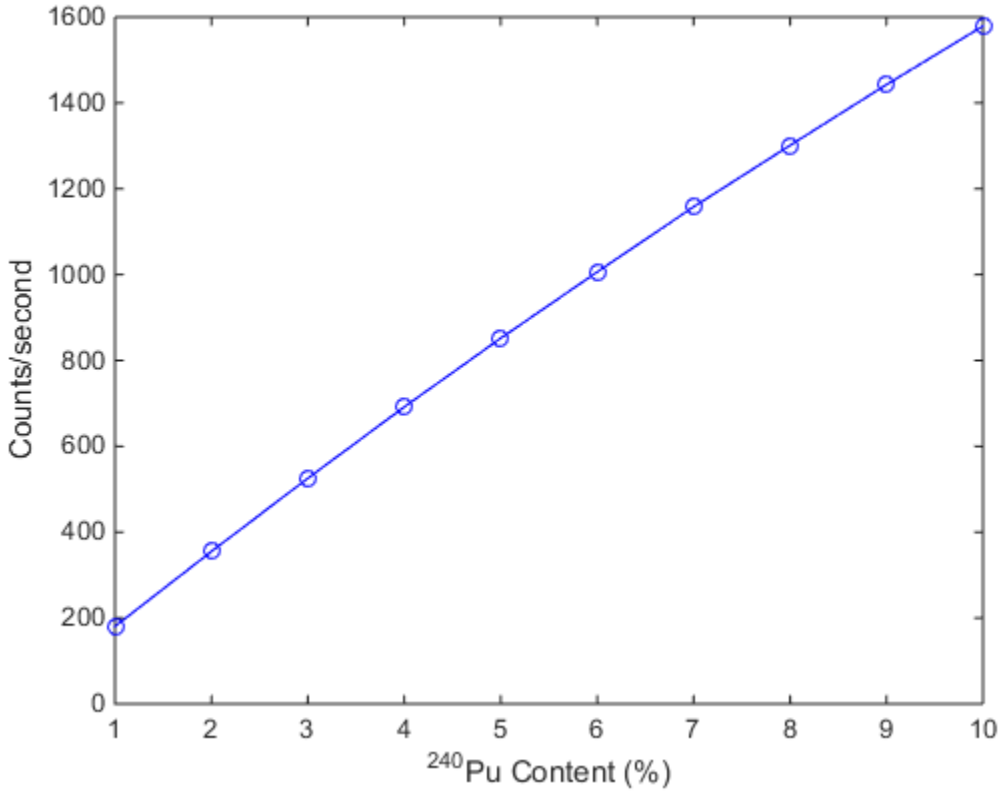

Figure 4-8. Relationship between various ^{240}Pu content and peak counts for an alpha-phase Pu sphere.

4.2.2 Size Analysis

The data in Figure 4-9 shows the time distributions of cross-correlated events between the two large detectors, for sphere outer radii ranging from 1.0-4.5 cm. The ^{240}Pu

content for varying outer radius values was calculated using Equation 4-5, in order to test the accuracy of the equation in estimating the ^{240}Pu content for Pu spheres of varying outer radius values. The results in Table 4-4 show the differences between the calculated ^{240}Pu content and the actual value of 5.96%.

Table 4-4. Differences between actual and calculated values of ^{240}Pu content for various outer radii for an alpha-phase solid Pu sphere.

Outer Radius (cm)	Mass (g)	Counts/ second	Actual ^{240}Pu Content (%)	Calculated ^{240}Pu Content (%)	Difference (%)
1.00	83.11	14	5.96	0.07	5.89
1.50	280.48	35	5.96	0.19	5.77
2.00	664.84	76	5.96	0.42	5.54
2.50	1298.52	153	5.96	0.84	5.12
3.00	2243.85	312	5.96	1.75	4.21
3.50	3563.15	645	5.96	3.72	2.24
4.00	5318.76	1365	5.96	8.44	-2.48
4.50	7573.00	3041	5.96	25.46	-19.50

These differences were plotted against their corresponding outer radii in Figure 4-10, in order to generate an equation to correct for varying shell outer radii. The data in Figure 4-10 is then fitted, and the equation of the curve is

$$\begin{aligned} \textit{Size Correction (\%)} = &-0.2973O^6 + 4.314O^5 - 25.4O^4 + 76.94O^3 \\ &- 125.9O^2 + 104.7O - 28.49 \end{aligned} \tag{4-6}$$

which adjusts the previous estimation for varying shell outer radii.

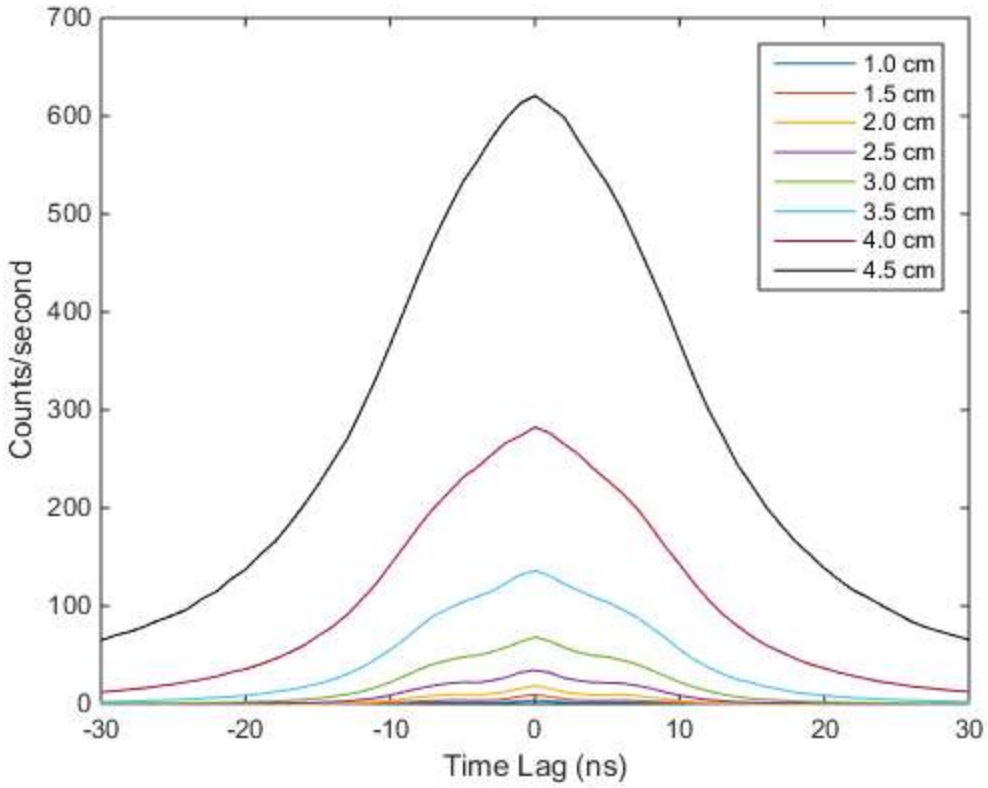

Figure 4-9. Simulation of time correlated distributions for various outer radii for an alpha-phase Pu sphere.

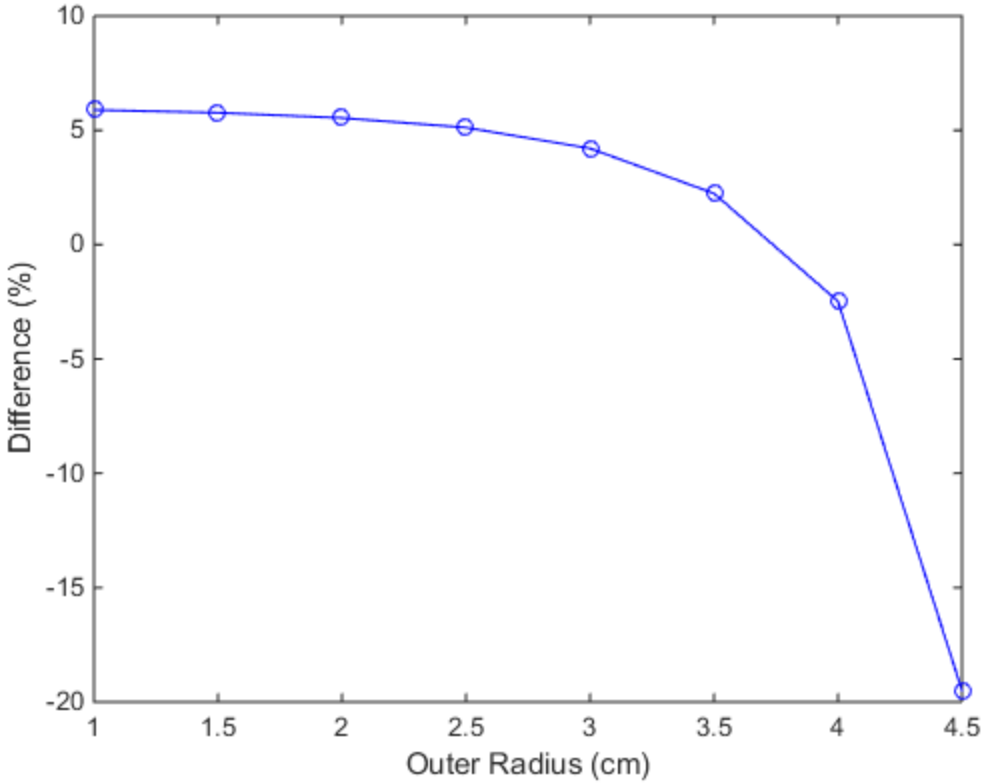

Figure 4-10. Differences between actual and calculated ^{240}Pu content plotted against varying Pu spherical shell outer radii.

4.2.3 Final Method

The equations derived in Section 4.2 are combined to provide a method to determine ^{240}Pu content for bare Pu spheres of various outer radius values, shown in Equation 4-7. The results in Table 4-5 provide an updated comparison of the calculated ^{240}Pu content and the actual value of 5.96%, previously presented in Table 4-4, using:

$$^{240}Pu\ Content\ for\ Bare\ Pu\ Spheres\ (\%) = \frac{\left(-182.6 + \sqrt{\left(182.6^2 + (9.924)(0.2083 - C)\right)}\right)}{-4.962}$$
$$-0.2973O^6 + 4.314O^5 - 25.4O^4 + 76.94O^3 - 125.9O^2 + 104.7O - 28.49 \quad (4\text{-}7)$$

Table 4-5. Estimation of ^{240}Pu content for various sizes of an alpha-phase solid Pu sphere.

Outer Radius (cm)	Mass (g)	Counts/ second	Actual ^{240}Pu Content (%)	Calculated ^{240}Pu Content (%)
1.00	83.11	14	5.96	5.94
1.50	280.48	35	5.96	5.94
2.00	664.84	76	5.96	5.87
2.50	1298.52	153	5.96	5.94
3.00	2243.85	312	5.96	5.81
3.50	3563.15	645	5.96	5.90
4.00	5318.76	1365	5.96	5.91
4.50	7573.00	3041	5.96	6.05

The method is able to estimate the ^{240}Pu content for various Pu sphere sizes, within ±0.15%, for all iterations tested, of the actual ^{240}Pu content value.

4.3 Different Reflectors

The following section provides analysis on the effects of beryllium and graphite thicknesses ranging from 0.5-2.5 cm, on the accuracy of the ^{240}Pu content estimation method for the Pu delta-phase spherical shell and alpha-phase sphere. The analysis results for alpha-phase spherical shells and delta-phase spheres are provided in Appendix F and Appendix G respectively. The details on the Pu samples used can be found in Chapter 3.

4.3.1 Beryllium

4.3.1.1 Delta-Phase Plutonium Spherical Shell

The data in Figure 4-11 shows the time correlated distributions of cross-correlated events between the two large detectors, for thicknesses of beryllium metal ranging from 0.5-2.5 cm. The ^{240}Pu content for varying thicknesses of beryllium metal, surrounding a delta-phase Pu spherical shell, was calculated using Equation 4-4. The results in Table 4-6 show the differences between the calculated ^{240}Pu content and the actual value of 1.80%.

Table 4-6. Differences between actual and calculated values of ^{240}Pu content for various thicknesses of beryllium metal surrounding a delta-phase Pu spherical shell.

Reflector thickness (cm)	Counts/ second	Actual ^{240}Pu content (%)	Calculated ^{240}Pu content (%)	Differences (%)
0.0	138	1.80	1.80	0.00
0.5	137	1.80	1.78	0.02
1.0	135	1.80	1.76	0.04
1.5	129	1.80	1.68	0.12
2.0	126	1.80	1.64	0.16
2.5	123	1.80	1.60	0.20

These differences were plotted against the corresponding beryllium metal thicknesses in Figure 4-12, in order to generate an equation to adjust for the presence of beryllium metal. The data in Figure 4-12 is then fitted, and the equation of the curve is

$$\begin{aligned} \textit{Beryllium Correction (\%)} = &-0.00667B^4 + 0.0111B^3 - 0.045B^2 \\ &+ 0.00127B - 0.00119 \end{aligned} \tag{4-8}$$

where B represents non-zero values of thickness of the beryllium metal reflector, in cm.

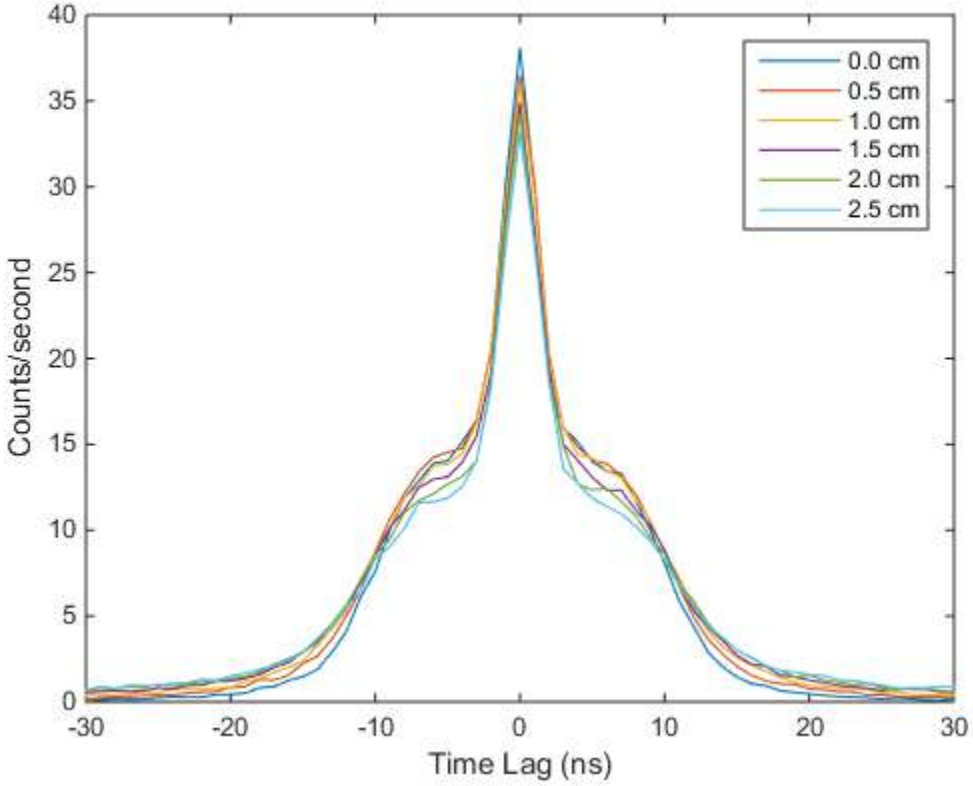

Figure 4-11. Simulation of time correlated distributions for various beryllium metal thicknesses surrounding a delta-phase Pu spherical shell.

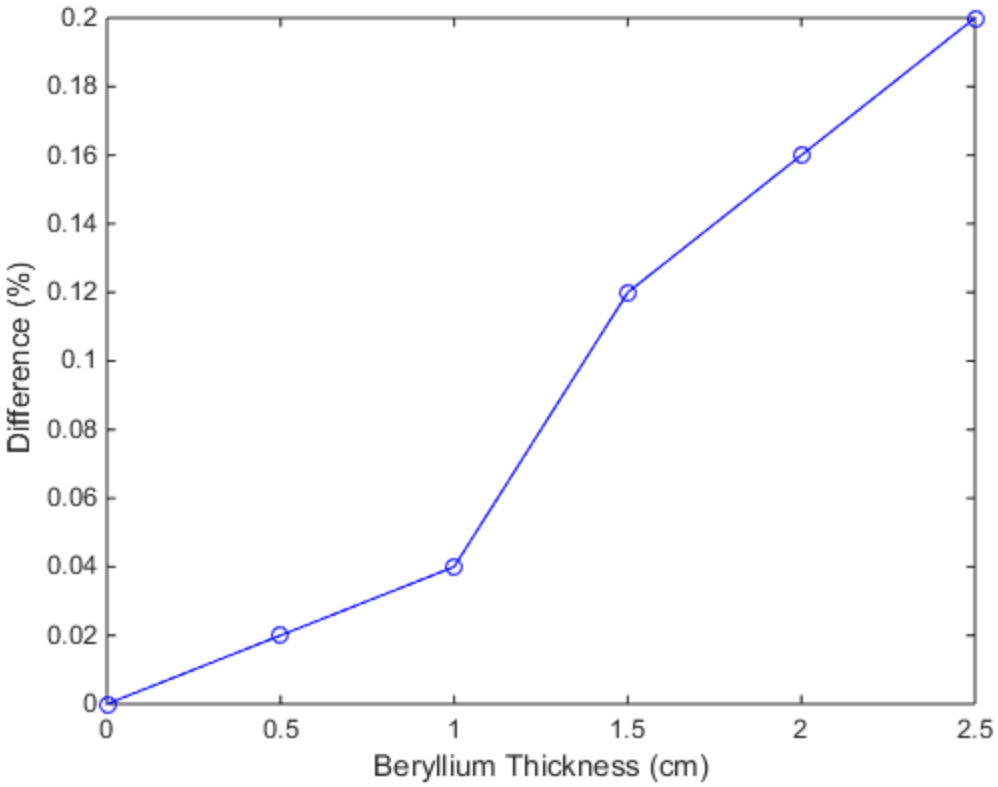

Figure 4-12. Differences between actual and calculated ^{240}Pu content plotted against various thicknesses of beryllium metal surrounding a delta-phase Pu spherical shell.

4.3.1.2 Alpha-Phase Plutonium Sphere

The data in Figure 4-13 shows the time correlated distributions of cross-correlated events between the two large detectors, for thicknesses of beryllium metal ranging from 0.5-2.5 cm. The ^{240}Pu content for varying thicknesses of beryllium metal, surrounding an alpha-phase Pu sphere, was calculated using Equation 4-7. The results in Table 4-7 show the differences between the calculated ^{240}Pu content and the actual value of 5.96%.

Table 4-7. Differences between actual and calculated values of ^{240}Pu content for various thicknesses of beryllium metal surrounding an alpha-phase Pu sphere.

Reflector thickness (cm)	Peak Count (s^{-1})	Actual ^{240}Pu content (%)	Calculated ^{240}Pu content (%)	Difference (%)
0.0	998	5.96	6.08	-0.12
0.5	1162	5.96	7.17	-1.21
1.0	1288	5.96	8.03	-2.07
1.5	1399	5.96	8.82	-2.86
2.0	1495	5.96	9.52	-3.56
2.5	1603	5.96	10.32	-4.36

These differences were plotted against their corresponding beryllium metal thicknesses in Figure 4-14, in order to generate an equation to adjust for the presence of beryllium metal. The data in Figure 4-14 is then fitted, and the equation of the curve is

$$Beryllium\,Correction\,(\%) = -0.1178B^3 + 0.591B^2 - 2.436B - 0.121 \qquad (4\text{-}9)$$

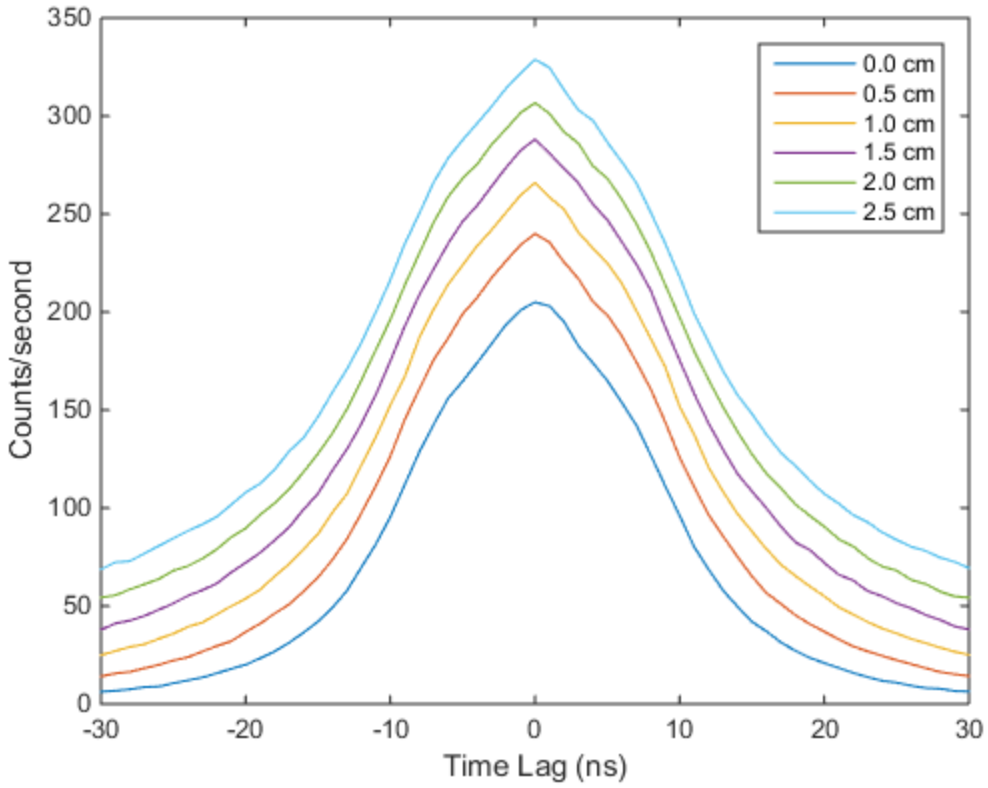

Figure 4-13. Simulation of time correlated distributions for various thicknesses of beryllium metal surrounding an alpha-phase Pu sphere.

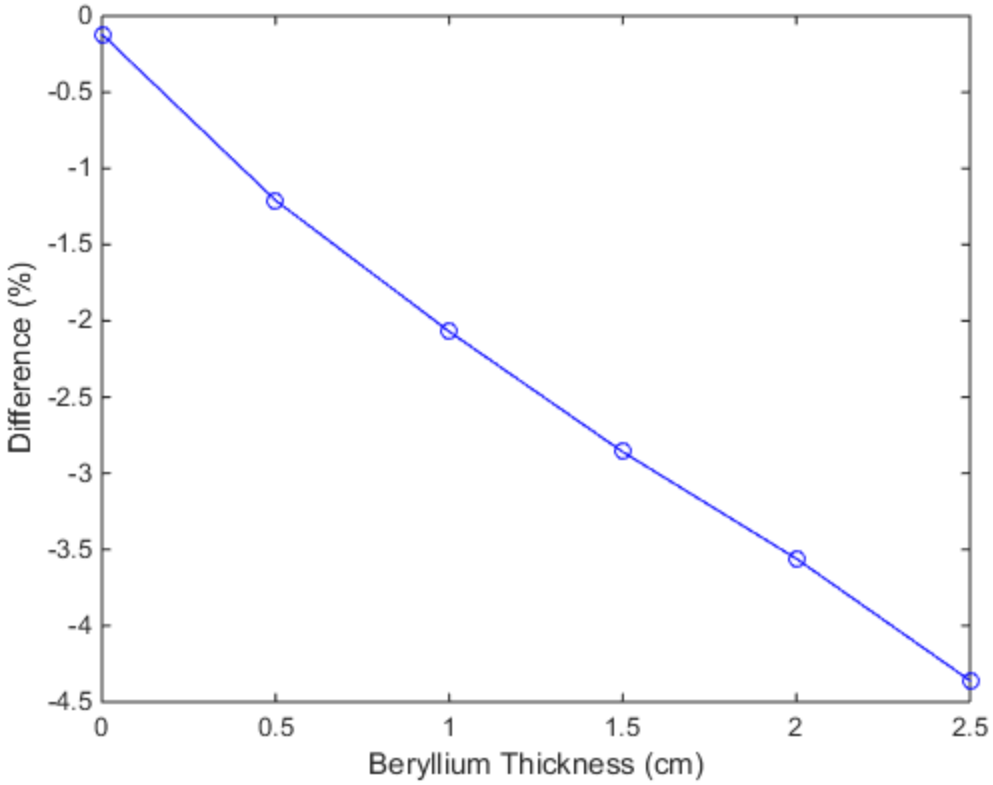

Figure 4-14. Differences between actual and calculated ^{240}Pu content plotted against various thicknesses of beryllium metal surrounding an alpha-phase Pu sphere.

4.3.2 Graphite

4.3.2.1 Delta-Phase Plutonium Spherical Shell

The data in Figure 4-15 shows the time correlated distributions of cross-correlated events between the two large detectors, for thicknesses of graphite ranging from 0.5-2.5 cm. The ^{240}Pu content for varying thicknesses of graphite, surrounding a delta-phase Pu spherical shell, was calculated using Equation 4-4. The results in Table 4-8 show the differences between the calculated ^{240}Pu content and the actual value of 1.80%.

Table 4-8. Differences between actual and calculated values of ^{240}Pu content for various thicknesses of graphite surrounding a delta-phase Pu spherical shell.

Reflector thickness (cm)	Counts/ second	Actual ^{240}Pu content (%)	Calculated ^{240}Pu content (%)	Differences (%)
0.0	138	1.80	1.80	0.00
0.5	135	1.80	1.75	0.05
1.0	131	1.80	1.71	0.09
1.5	127	1.80	1.65	0.15
2.0	123	1.80	1.60	0.20
2.5	118	1.80	1.53	0.27

These differences were plotted against their corresponding graphite thicknesses in Figure 4-16, in order to generate an equation to adjust for the presence of graphite. The data in Figure 4-16 is then fitted, and the equation of the curve is

$$\begin{aligned} \textit{Graphite Correction (\%)} = {} & 1.73\times10^{-17}G^4 + 0.0044G^3 - 0.0667G^2 \\ & + 0.09651G + 0.000476 \end{aligned} \tag{4-10}$$

where G is the non-zero thickness of the graphite reflector, in cm.

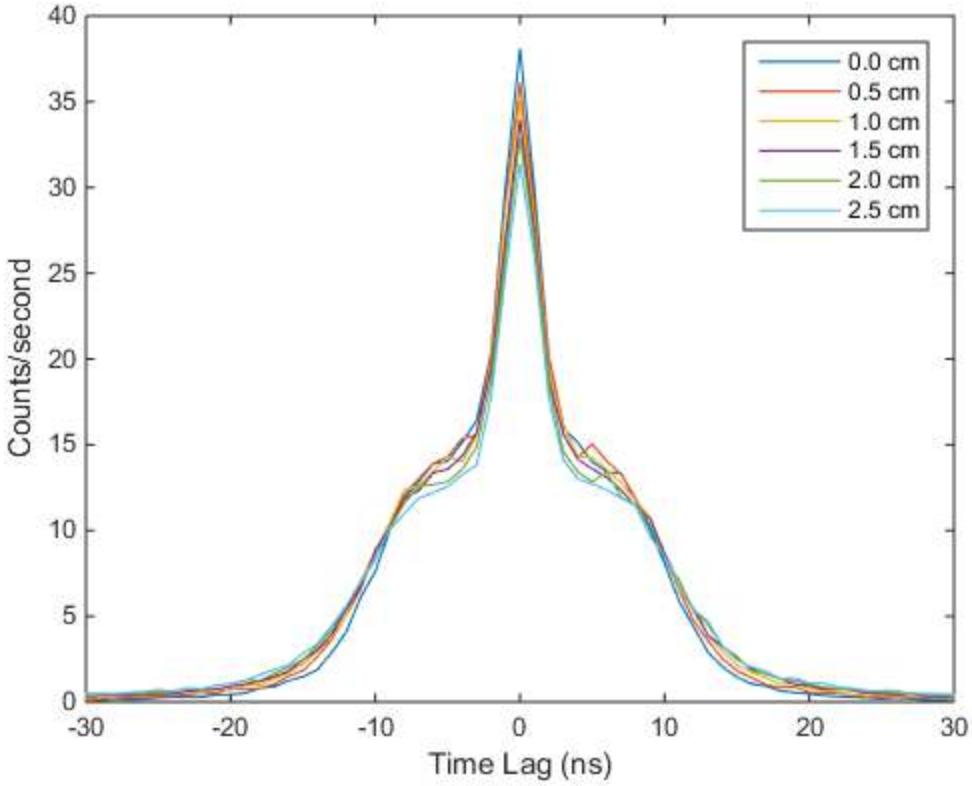

Figure 4-15. Simulation of time correlated distributions for various graphite thicknesses surrounding a delta-phase Pu spherical shell.

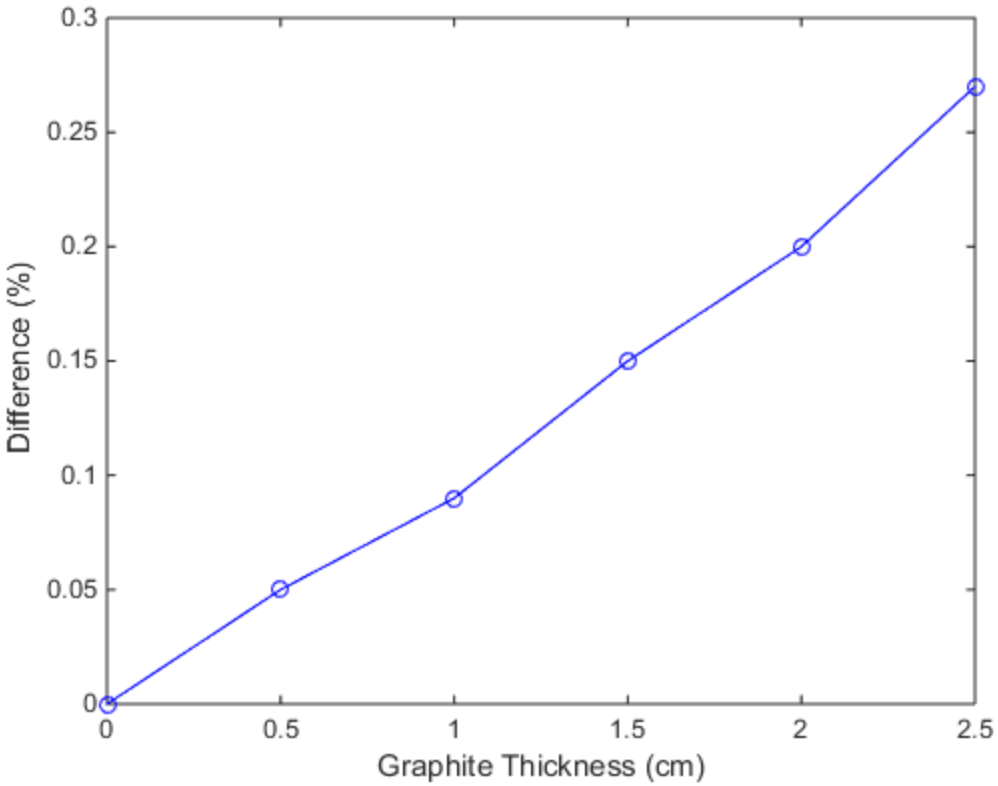

Figure 4-16. Differences between actual and calculated ^{240}Pu content plotted against various thicknesses of graphite surrounding a delta-phase Pu spherical shell.

4.3.2.2 Alpha-Phase Plutonium Sphere

The data in Figure 4-17 shows the time correlated distributions of cross-correlated events between the two large detectors, for thicknesses of graphite ranging from 0.5-2.5 cm. The ^{240}Pu content for varying thicknesses of graphite, surrounding an alpha-phase Pu sphere, was calculated using Equation 4-7. The results in Table 4-9 show the differences between the calculated ^{240}Pu content and the actual value of 5.96%.

Table 4-9. Differences between actual and calculated values of ^{240}Pu content for various thicknesses of graphite surrounding a delta-phase Pu sphere.

Reflector thickness (cm)	Peak Count (s^{-1})	Actual ^{240}Pu content (%)	Calculated ^{240}Pu content (%)	Differences (%)
0.0	92.77	5.96	5.97	-0.01
0.5	103.63	5.96	6.74	-0.78
1.0	109.97	5.96	7.20	-1.24
1.5	114.40	5.96	7.52	-1.56
2.0	117.80	5.96	7.78	-1.82
2.5	119.28	5.96	7.89	-1.93

These differences were plotted against their corresponding graphite thicknesses in Figure 4-18, in order to generate an equation to adjust for the presence of graphite. The data in Figure 4-18 is then fitted, and the equation of the curve is

$$Graphite\ Correction\ (\%) = 0.07G^4 - 0.4204G^3 + 1.086G^2 - 1.946G - 0.012 \quad (4\text{-}11)$$

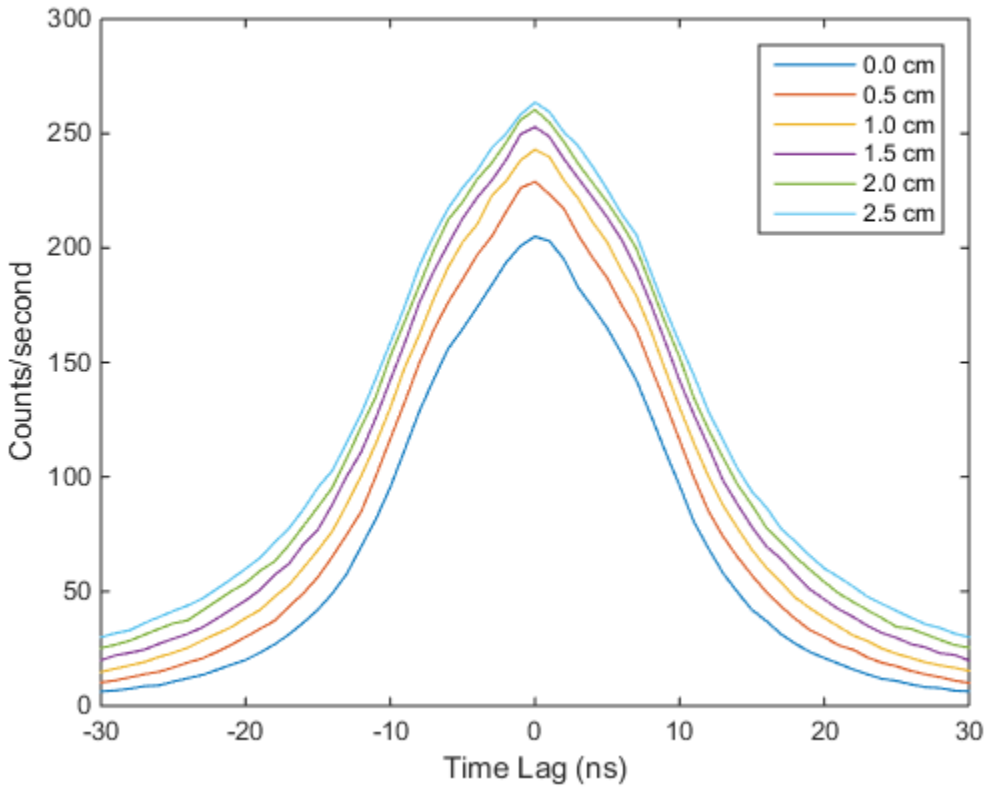

Figure 4-17. Simulation of time correlated distributions for various thicknesses of graphite surrounding an alpha-phase Pu sphere.

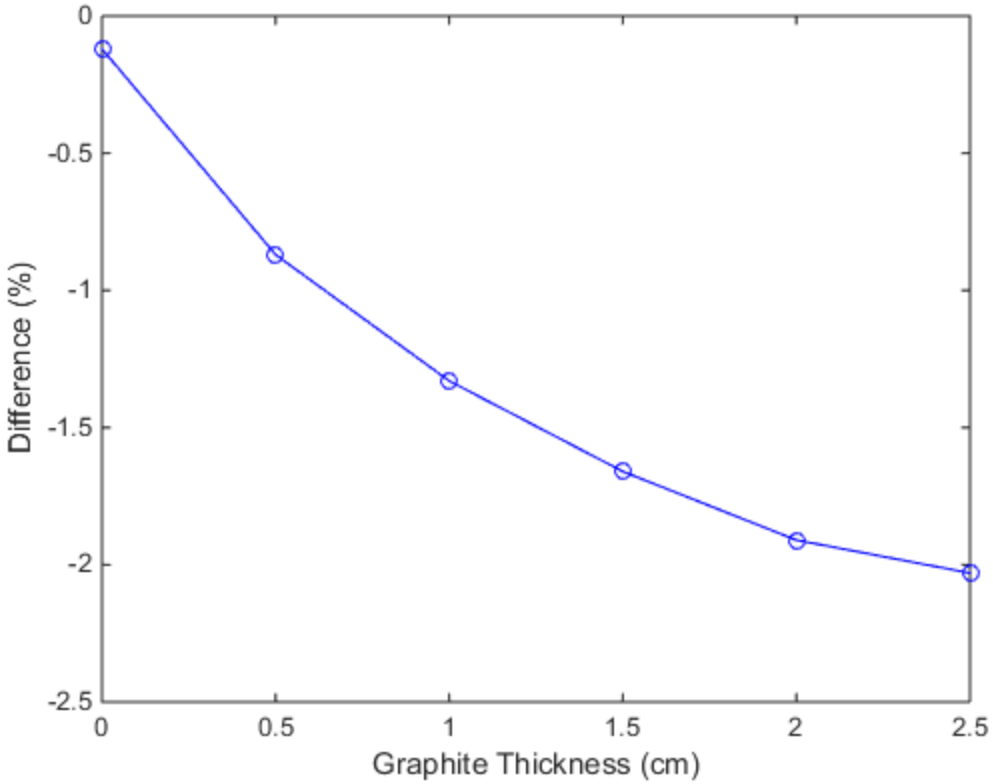

Figure 4-18. Differences between actual and calculated ^{240}Pu content plotted against various thicknesses of graphite surrounding an alpha-phase Pu sphere.

4.4 Different Shielding Materials

The following section provides analysis on the effects of different shielding materials on the accuracy of the ^{240}Pu content estimation method for the Pu delta-phase spherical shell and alpha-phase sphere. The analysis results for alpha-phase spherical shells and delta-phase spheres are provided in Appendix H and Appendix I respectively. The details on the Pu samples used can be found in Chapter 3.

4.4.1 Aluminum

4.4.1.1 Delta Phase Plutonium Spherical Shell

The data in Figure 4-19 shows the time correlated distributions of cross-correlated events between the two large detectors, for thicknesses of aluminum ranging from 0.5-2.5 cm. The ^{240}Pu content for varying thicknesses of aluminum, surrounding a delta-phase Pu spherical shell, was calculated using Equation 4-4. The results in Table 4-10 show the differences between the calculated ^{240}Pu content and the actual value of 1.80%.

Table 4-10. Differences between actual and calculated values of ^{240}Pu content for various thicknesses of aluminum surrounding a delta-phase Pu spherical shell.

Shielding Thickness (cm)	Counts/ second	Actual ^{240}Pu content (%)	Calculated ^{240}Pu content (%)	Difference (%)
0.0	138	1.80	1.80	0.00
0.5	129	1.80	1.69	0.11
1.0	123	1.80	1.60	0.20
1.5	116	1.80	1.51	0.29
2.0	108	1.80	1.41	0.39
2.5	102	1.80	1.33	0.47

These differences were plotted against their corresponding aluminum thicknesses in Figure 4-20, in order to generate an equation to adjust for the presence of aluminum. The data in Figure 4-20 is then fitted, and the equation of the curve is

$$\begin{aligned} Aluminum\ Correction\ (\%) = &-0.0167A^4 + 0.0856A^3 - 0.1442A^2 \\ &+ 0.2742A - 0.000119 \end{aligned} \tag{4-12}$$

where A is the thickness, in cm, of the aluminum shielding.

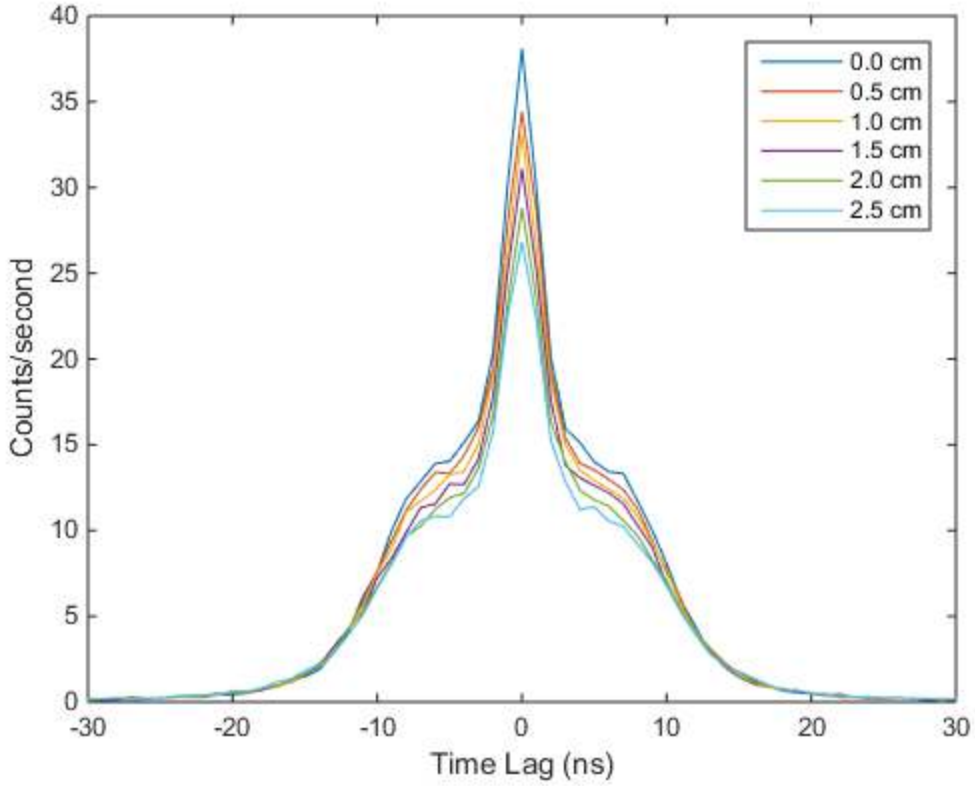

Figure 4-19. Simulation of time correlated distributions for various aluminum thicknesses surrounding a delta-phase Pu spherical shell.

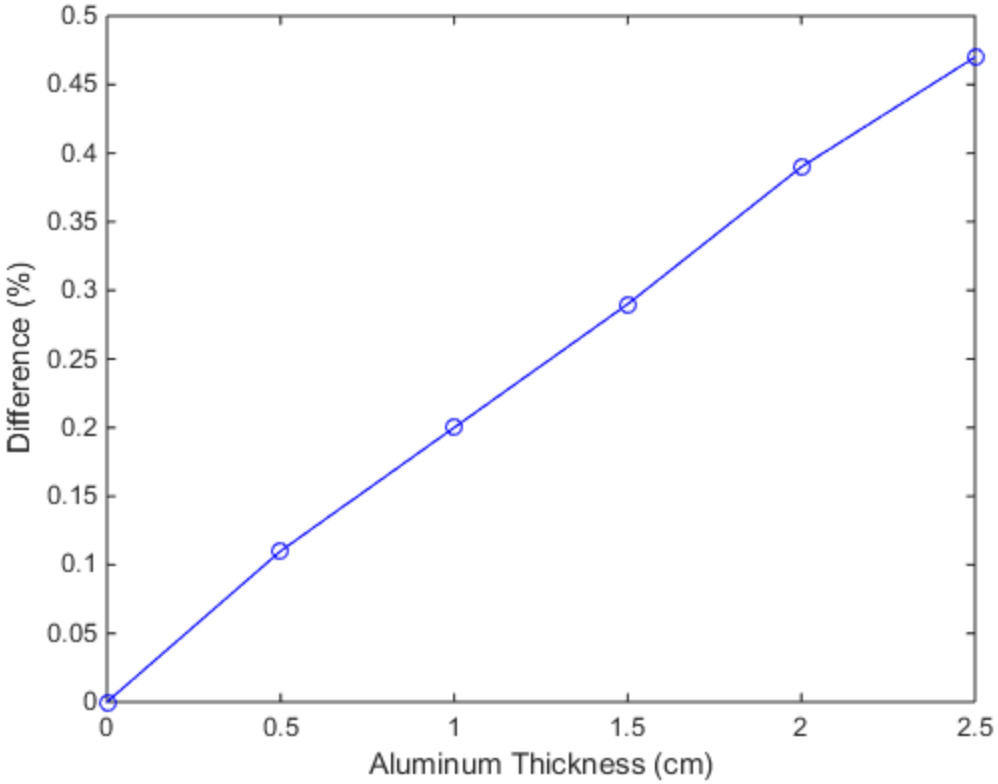

Figure 4-20. Differences between actual and calculated ^{240}Pu content plotted against various aluminum thicknesses surrounding a delta-phase Pu spherical shell.

4.4.1.2 Alpha-Phase Plutonium Sphere

The data in Figure 4-21 shows the time correlated distributions of cross-correlated events between the two large detectors, for thicknesses of aluminum ranging from 0.5-2.5 cm. The ^{240}Pu content for varying thicknesses of aluminum, surrounding an alpha-phase Pu sphere, was calculated using Equation 4-7. The results in Table 4-11 show the differences between the calculated ^{240}Pu content and the actual value of 5.96%.

Table 4-11. Differences between actual and calculated values of ^{240}Pu content for various thicknesses of aluminum surrounding an alpha-phase Pu sphere.

Shielding Thickness (cm)	Counts/ second	Actual ^{240}Pu content (%)	Calculated ^{240}Pu content (%)	Difference (%)
0.0	998	5.96	6.08	-0.12
0.5	1035	5.96	6.32	-0.36
1.0	1010	5.96	6.15	-0.19
1.5	984	5.96	5.99	-0.03
2.0	961	5.96	5.84	0.12
2.5	937	5.96	5.68	0.28

These differences were plotted against their corresponding aluminum thicknesses in Figure 4-22, in order to generate an equation to adjust for the presence of aluminum. The data in Figure 4-22 is then fitted, and the equation of the curve is

$$Aluminum\ Correction\,(\%) = 0.1467A^4 - 0.8815A^3 + 1.819A^2 - 1.168A - 0.1216 \quad (4\text{-}13)$$

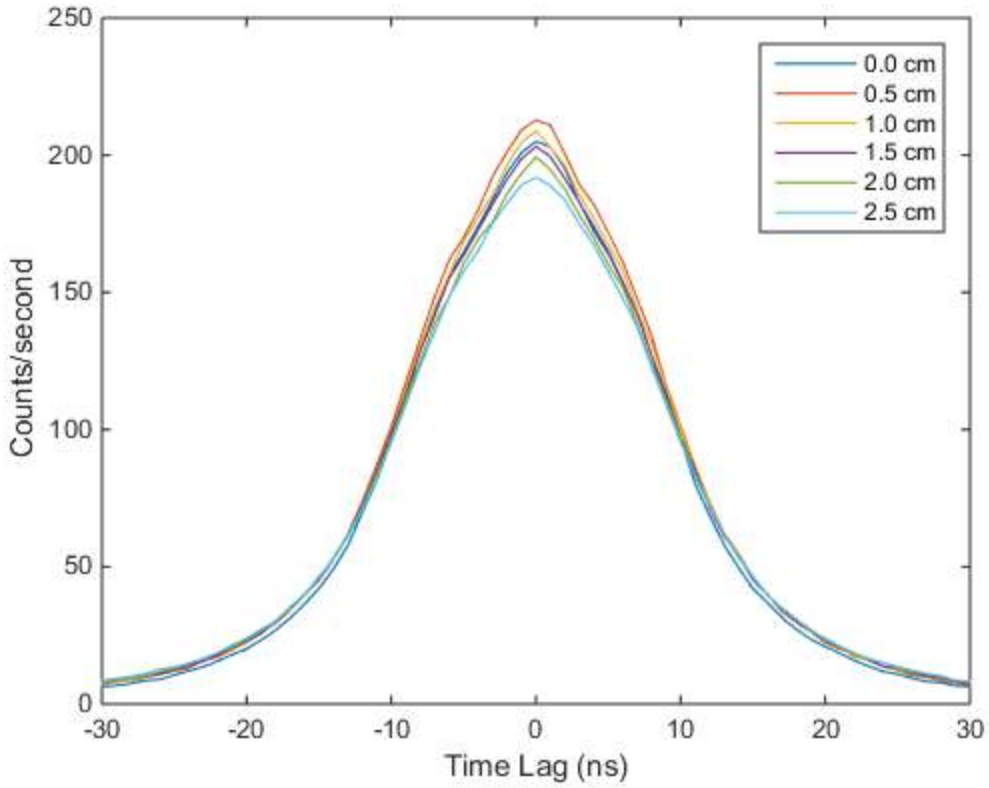

Figure 4-21. Simulation of time correlated distributions for various aluminum thicknesses surrounding an alpha-phase Pu sphere.

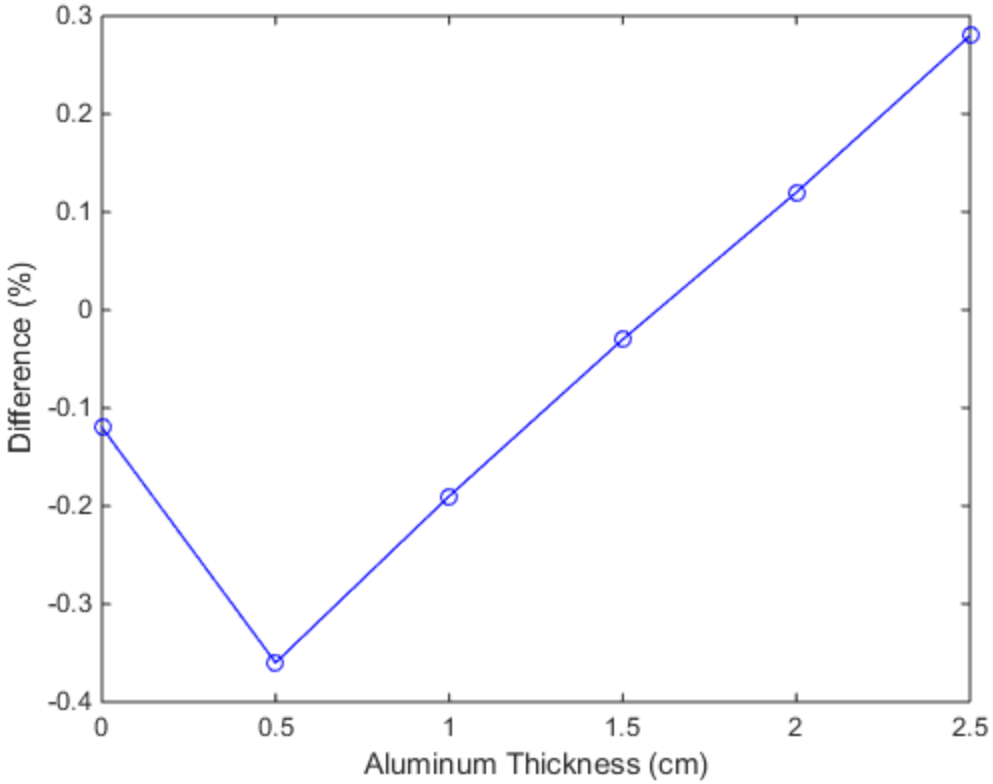

Figure 4-22. Differences between actual and calculated ^{240}Pu content plotted against various aluminum thicknesses surrounding an alpha-phase Pu sphere.

4.4.2 Depleted Uranium

4.4.2.1 Delta-Phase Plutonium Spherical Shell

The data in Figure 4-23 shows the time correlated distributions of cross-correlated events between the two large detectors, for thicknesses of depleted uranium ranging from 0.5-2.5 cm. The ^{240}Pu content for varying thicknesses of depleted uranium, surrounding a delta-phase Pu spherical shell, was calculated using Equation 4-4. The results in Table 4-12 show the differences between the calculated ^{240}Pu content and the actual value of 1.80%.

Table 4-12. Differences between actual and calculated values of ^{240}Pu content for various thicknesses of depleted uranium surrounding a delta-phase Pu spherical shell.

Shielding Thickness (cm)	Peak Count (s^{-1})	Actual ^{240}Pu content (%)	Calculated ^{240}Pu content (%)	Differences (%)
0.0	138	1.80	1.80	0.00
0.5	69	1.80	0.89	0.91
1.0	42	1.80	0.52	1.28
1.5	29	1.80	0.35	1.45
2.0	22	1.80	0.26	1.54
2.5	18	1.80	0.20	1.60

These differences were plotted against their corresponding depleted uranium thicknesses in Figure 4-24, in order to generate an equation to adjust for the presence of depleted uranium. The data in Figure 4-24 is then fitted, and the equation of the curve is

$$\begin{aligned} \textit{Depleted Uranium Correction (\%)} = &-0.09667D^4 + 0.6989D^3 - 1.934D^2 \\ &+ 2.617D + 0.00595 \end{aligned} \tag{4-14}$$

where D is the thickness, in cm, of the depleted uranium shielding.

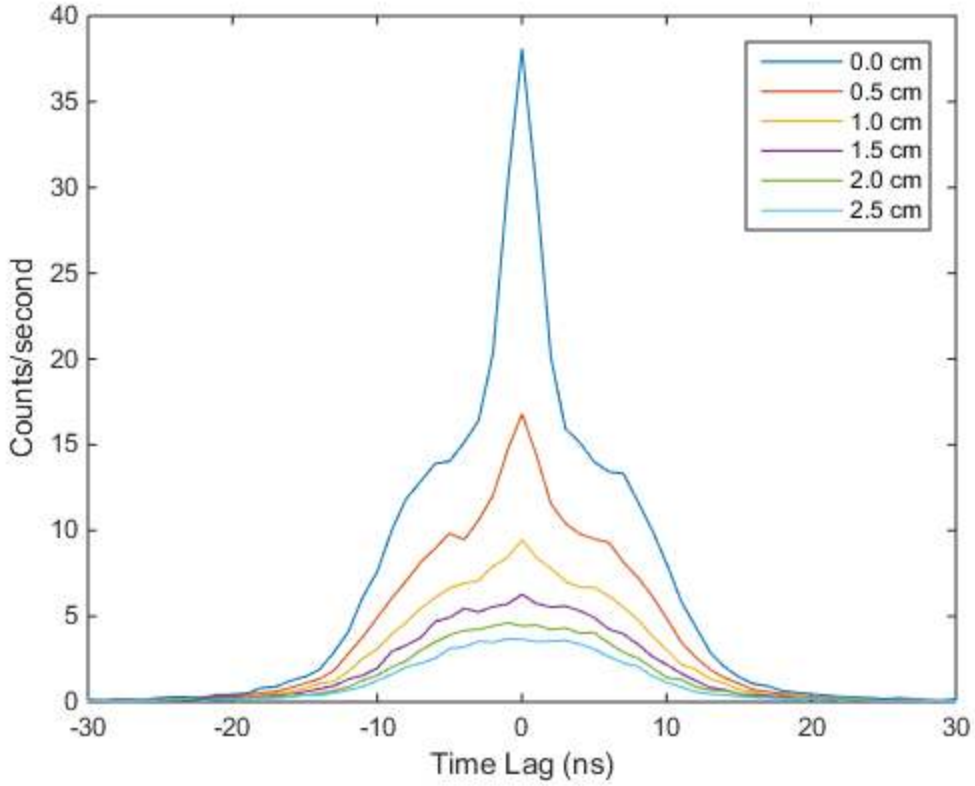

Figure 4-23. Simulation of time correlated distributions for various depleted uranium thicknesses surrounding a delta-phase Pu spherical shell.

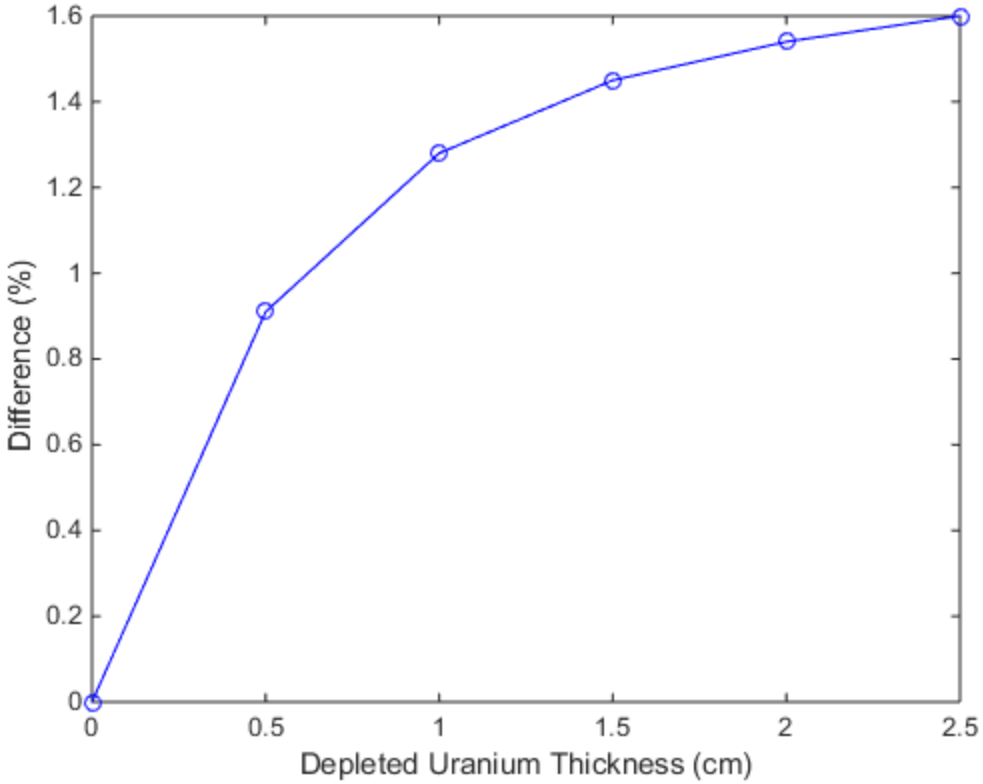

Figure 4-24. Differences between actual and calculated ^{240}Pu content plotted against various depleted uranium thicknesses surrounding a delta-phase Pu spherical shell.

4.4.2.2 Alpha-Phase Plutonium Sphere

The data in Figure 4-25 shows the time correlated distributions of cross-correlated events between the two large detectors, for thicknesses of depleted uranium ranging from 0.5-2.5 cm. The ^{240}Pu content for varying thicknesses of depleted uranium, surrounding an alpha-phase Pu sphere, was calculated using Equation 4-7. The results in Table 4-13 show the differences between the calculated ^{240}Pu content and the actual value of 5.96%.

Table 4-13. Differences between actual and calculated values of ^{240}Pu content for various thicknesses of depleted uranium surrounding an alpha-phase Pu sphere.

Shielding Thickness (cm)	Counts/ second	Actual ^{240}Pu content (%)	Calculated ^{240}Pu content (%)	Difference (%)
0.0	998	5.96	6.08	-0.12
0.5	912	5.96	5.52	0.44
1.0	788	5.96	4.73	1.23
1.5	683	5.96	4.09	1.87
2.0	594	5.96	3.54	2.42
2.5	534	5.96	3.18	2.78

These differences were plotted against their corresponding depleted uranium thicknesses in Figure 4-26, in order to generate an equation to adjust for the presence of depleted uranium. The data in Figure 4-26 is then fitted, and the equation of the curve is

$$\begin{aligned} \textit{Depleted Uranium Correction}(\%) = {} & 0.0933D^4 - 0.6089D^3 + 1.11D^2 \\ & + 0.7341D - 0.1224 \end{aligned} \tag{4-15}$$

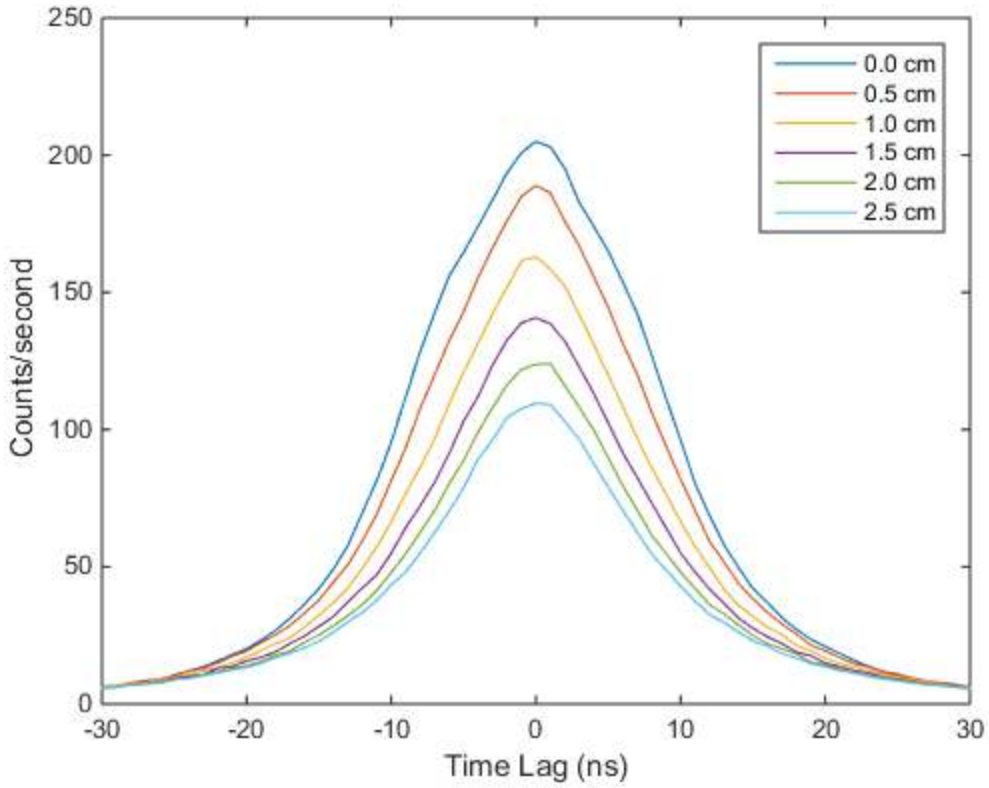

Figure 4-25. Simulation of time correlated distributions for various depleted uranium thicknesses surrounding an alpha-phase Pu sphere.

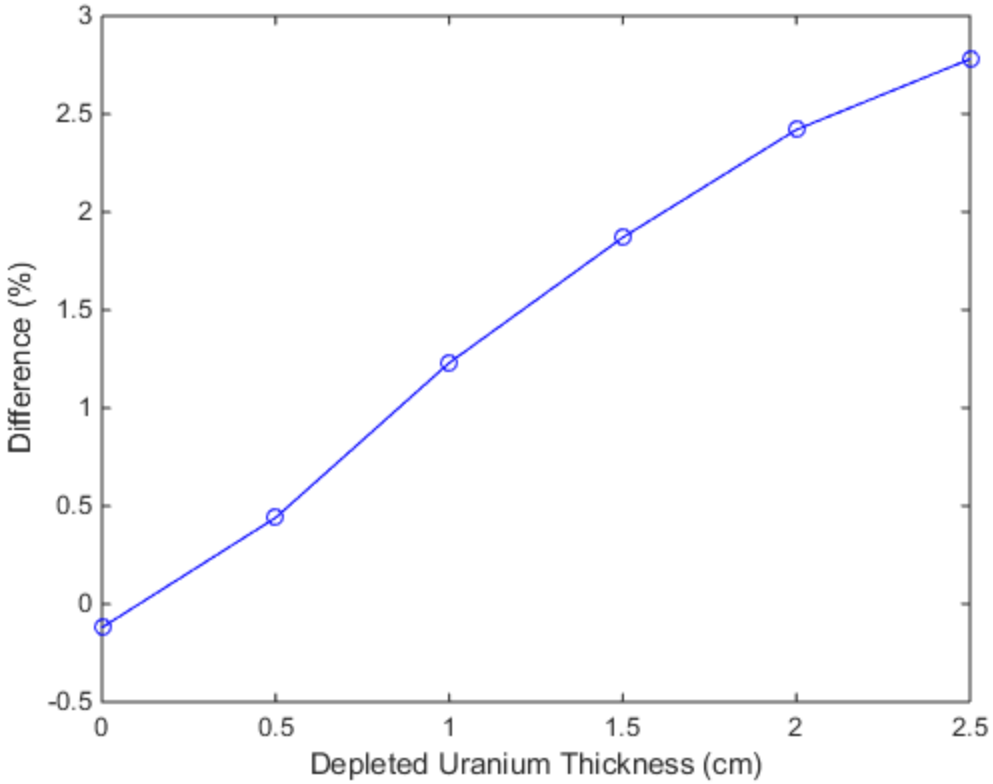

Figure 4-26. Differences between actual and calculated ^{240}Pu content plotted against various depleted uranium thicknesses surrounding an alpha-phase Pu sphere.

4.4.3 Lead

4.4.3.1 Delta-Phase Plutonium Spherical Shell

The data in Figure 4-27 shows the time correlated distributions of cross-correlated events between the two large detectors, for thicknesses of lead ranging from 0.5-2.5 cm. The ^{240}Pu content for varying thicknesses of lead, surrounding a delta-phase Pu spherical shell, was calculated using Equation 4-4. The results in Table 4-14 show the differences between the calculated ^{240}Pu content and the actual value of 1.80%.

Table 4-14. Differences between actual and calculated values of ^{240}Pu content for various thicknesses of lead surrounding a delta-phase Pu spherical shell.

Shielding Thickness (cm)	Counts/ second	Actual ^{240}Pu content (%)	Calculated ^{240}Pu content (%)	Differences (%)
0.0	138	1.80	1.80	0.00
0.5	93	1.80	1.21	0.59
1.0	65	1.80	0.83	0.97
1.5	48	1.80	0.60	1.20
2.0	36	1.80	0.44	1.36
2.5	29	1.80	0.36	1.44

These differences were plotted against their corresponding lead thicknesses in Figure 4-28, in order to generate an equation to adjust for the presence of lead. The data in Figure 4-28 is then fitted, and the equation of the curve is

$$Lead\ Correction\ (\%) = -0.02333L^4 + 0.1826L^3 - 0.6714L^2 + 1.478L - 0.0004 \qquad (4\text{-}16)$$

where L is the thickness, in cm, of the lead shielding.

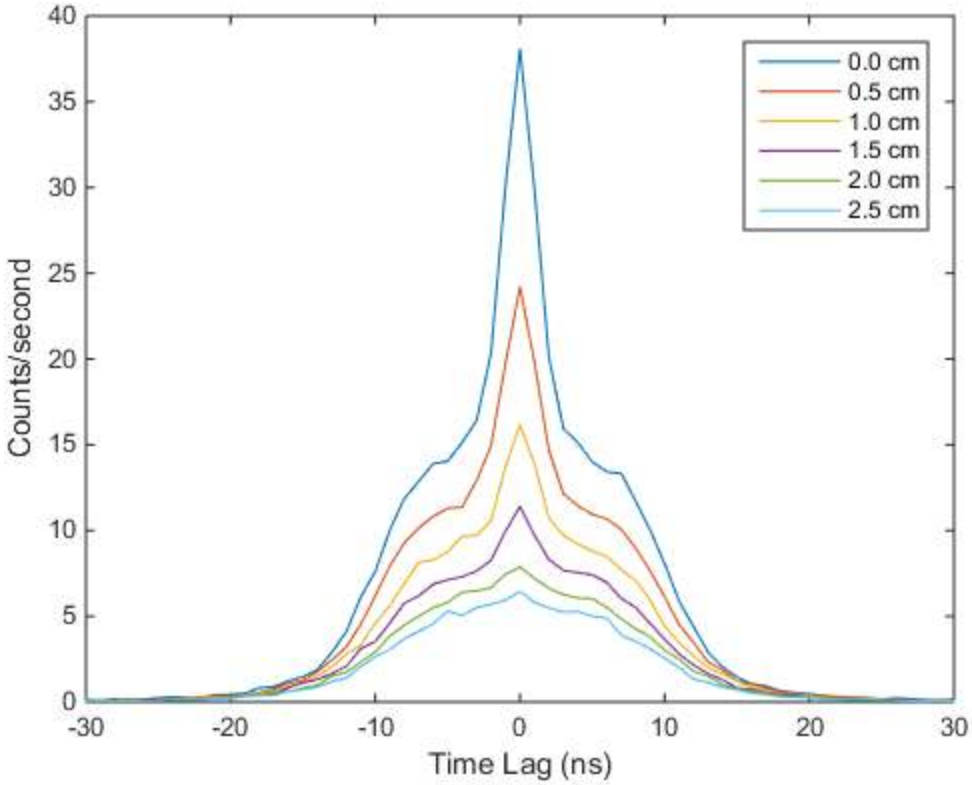

Figure 4-27. Simulation of time correlated distributions for various lead thicknesses surrounding a delta-phase Pu spherical shell.

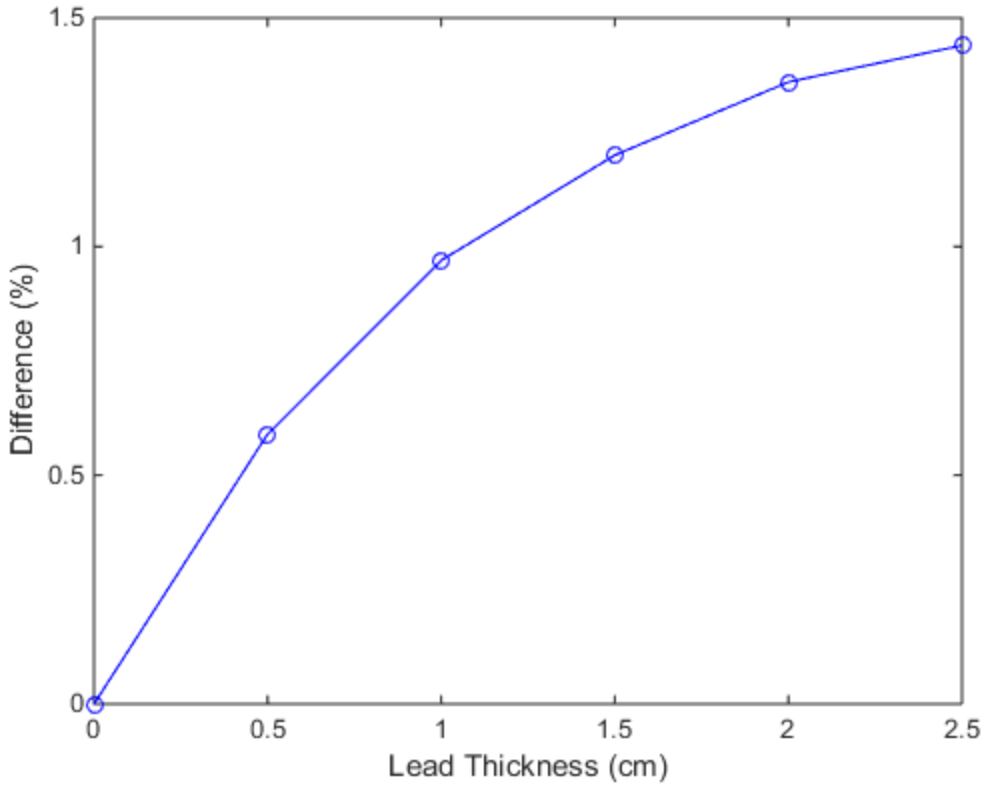

Figure 4-28. Differences between actual and calculated 240Pu content plotted against various lead thicknesses surrounding a delta-phase Pu spherical shell.

4.4.3.2 Alpha-Phase Pu Sphere

The data in Figure 4-29 shows the time correlated distributions of cross-correlated events between the two large detectors, for thicknesses of lead ranging from 0.5-2.5 cm. The ^{240}Pu content for varying thicknesses of lead, surrounding an alpha-phase Pu sphere, was calculated using Equation 4-7. The results in Table 4-15 show the differences between the calculated ^{240}Pu content and the actual value of 5.96%.

Table 4-15. Differences between actual and calculated values of ^{240}Pu content for various thicknesses of lead surrounding an alpha-phase Pu sphere.

Shielding Thickness (cm)	Counts/ second	Actual ^{240}Pu content (%)	Calculated ^{240}Pu content (%)	Differences (%)
0.0	998	5.96	6.08	-0.12
0.5	957	5.96	5.81	0.15
1.0	866	5.96	5.23	0.73
1.5	788	5.96	4.73	1.23
2.0	725	5.96	4.34	1.62
2.5	671	5.96	4.01	1.95

These differences were plotted against their corresponding lead thicknesses in Figure 4-30, in order to generate an equation to adjust for the presence of lead. The data in Figure 4-30 is then fitted, and the equation of the curve is

$$Lead\ Correction\ (\%) = 0.1467L^4 - 0.877L^3 + 1.632L^2 - 0.0619Pb - 0.1211 \qquad (4\text{-}17)$$

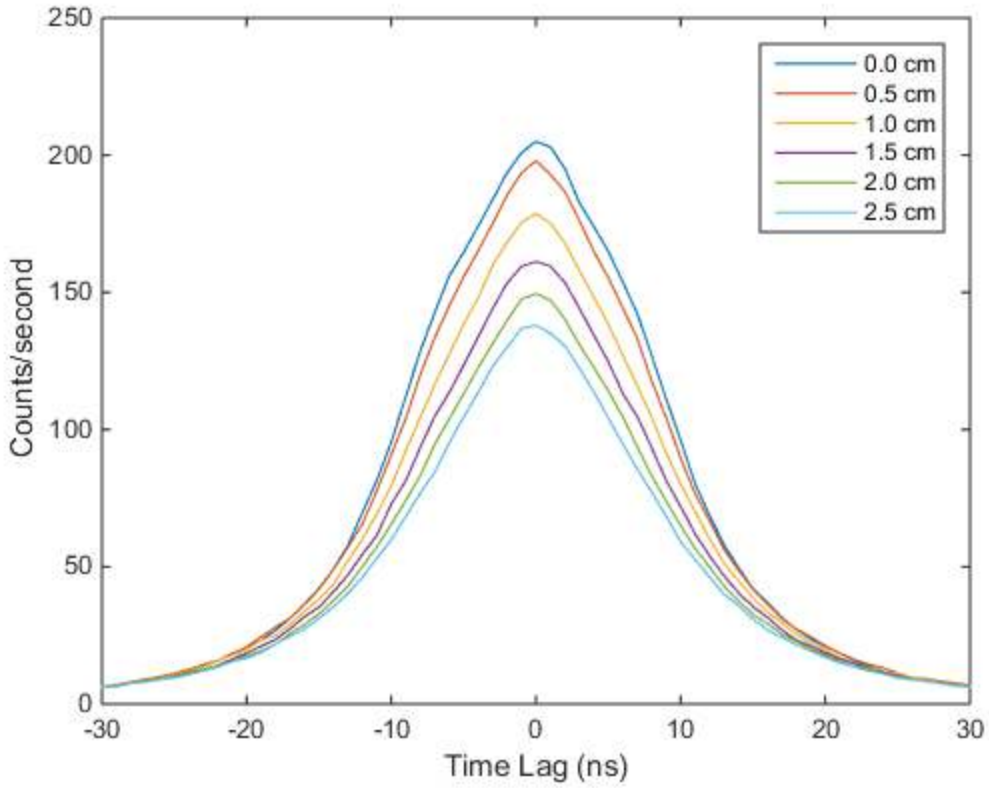

Figure 4-29. Simulation of time correlated distributions for various lead thicknesses surrounding an alpha-phase Pu sphere.

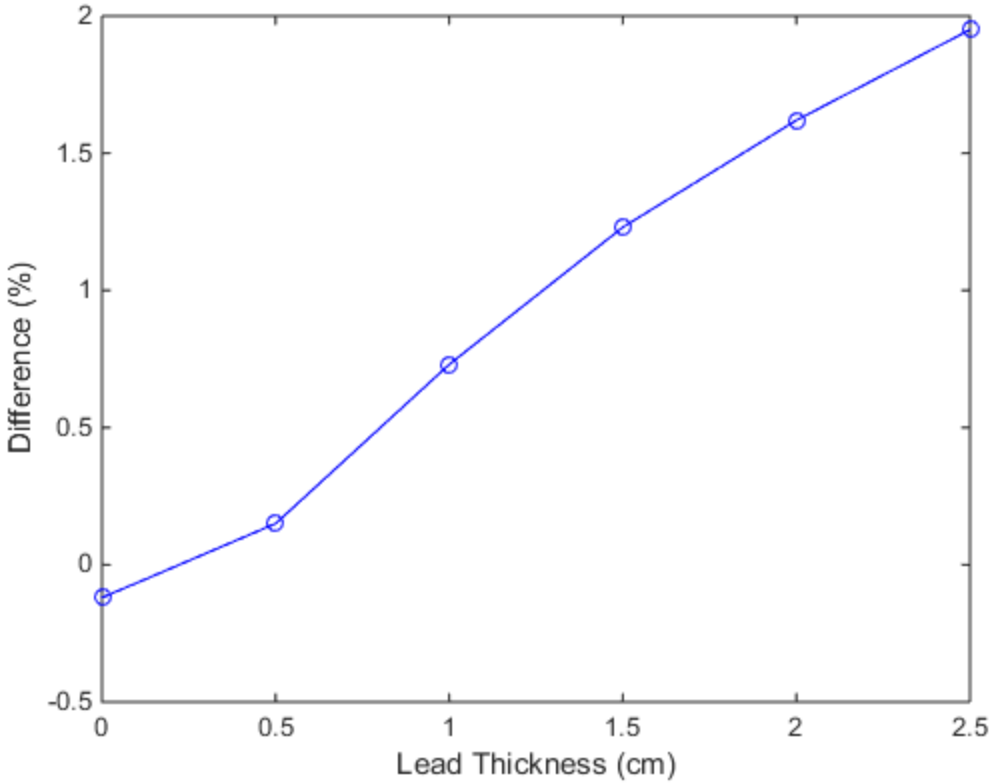

Figure 4-30. Differences between actual and calculated ^{240}Pu content plotted against various lead thicknesses surrounding an alpha-phase Pu sphere.

4.4.4 Polyethylene (non-borated)

4.4.4.1 Delta-Phase Plutonium Spherical Shell

The data in Figure 4-31 shows the time correlated distributions of cross-correlated events between the two large detectors, for thicknesses of polyethylene ranging from 0.5-2.5 cm. The ^{240}Pu content for varying thicknesses of polyethylene, surrounding a delta-phase Pu spherical shell, was calculated using Equation 4-4. The results in Table 4-16 show the differences between the calculated ^{240}Pu content and the actual value of 1.80%.

Table 4-16. Differences between actual and calculated values of ^{240}Pu content for various thicknesses of polyethylene surrounding a delta-phase Pu spherical shell.

Shielding Thickness (cm)	Counts/ second	Actual ^{240}Pu content (%)	Calculated ^{240}Pu content (%)	Difference (%)
0.0	138	1.80	1.80	0.00
0.5	130	1.80	1.70	0.10
1.0	122	1.80	1.59	0.21
1.5	116	1.80	1.51	0.29
2.0	111	1.80	1.44	0.36
2.5	105	1.80	1.37	0.43

These differences were plotted against their corresponding polyethylene thicknesses in Figure 4-32, in order to generate an equation to adjust for the presence of polyethylene. The data in Figure 4-32 is then fitted, and the equation of the curve is

$$\begin{aligned} \textit{Polyethylene Correction (\%)} = {} & 0.01667P^4 - 0.08259P^3 + 0.1031P^2 \\ & + 0.1704P - 0.000278 \end{aligned} \tag{4-18}$$

where P is the thickness, in cm, of the polyethylene shielding.

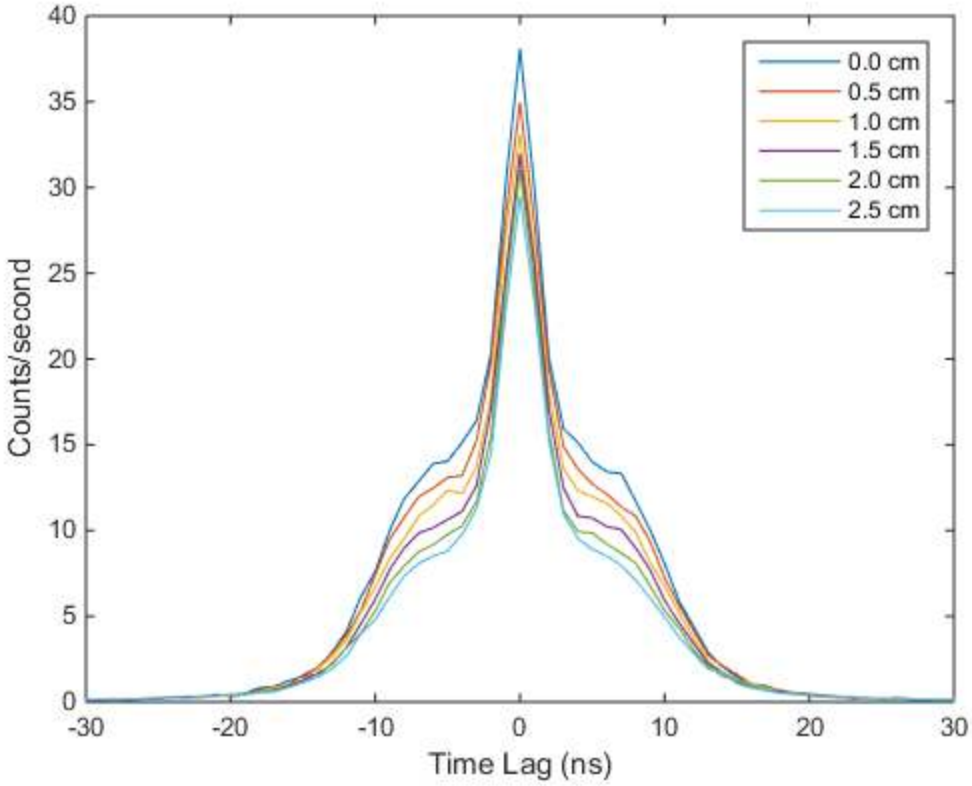

Figure 4-31. Simulation of time correlated distributions for various polyethylene thicknesses surrounding a delta-phase Pu spherical shell.

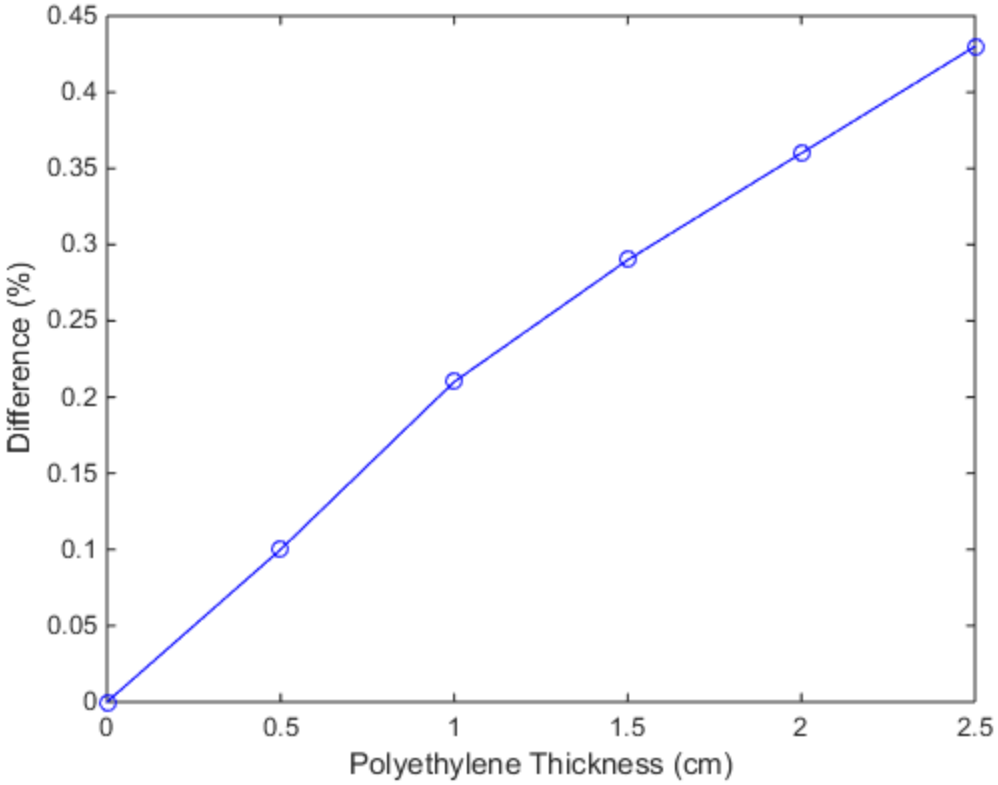

Figure 4-32. Differences between actual and calculated ^{240}Pu content plotted against various polyethylene thicknesses surrounding a delta-phase Pu spherical shell.

4.4.4.2 Alpha-Phase Plutonium Sphere

The data in Figure 4-33 shows the time correlated distributions of cross-correlated events between the two large detectors, for thicknesses of polyethylene ranging from 0.5-2.5 cm. The ^{240}Pu content for varying thicknesses of polyethylene, surrounding an alpha-phase Pu sphere, was calculated using Equation 4-7. The results in Table 4-17 show the differences between the calculated ^{240}Pu content and the actual value of 5.96%.

Table 4-17. Differences between actual and calculated values of ^{240}Pu content for various thicknesses of polyethylene surrounding an alpha-phase Pu sphere.

Shielding Thickness (cm)	Counts/ second	Actual ^{240}Pu content (%)	Calculated ^{240}Pu content (%)	Difference (%)
0.0	998	5.96	6.08	-0.12
0.5	966	5.96	5.86	0.10
1.0	886	5.96	5.35	0.61
1.5	811	5.96	4.88	1.08
2.0	744	5.96	4.46	1.50
2.5	682	5.96	4.08	1.88

These differences were plotted against their corresponding polyethylene thicknesses in Figure 4-34, in order to generate an equation to adjust for the presence of polyethylene. The data in Figure 4-34 is then fitted, and the equation of the curve is

$$\begin{aligned} \textit{Polyethylene Correction (\%)} = {} & 0.1133P^4 - 0.6911P^3 + 1.368P^2 \\ & - 0.0713P - 0.1212 \end{aligned} \tag{4-19}$$

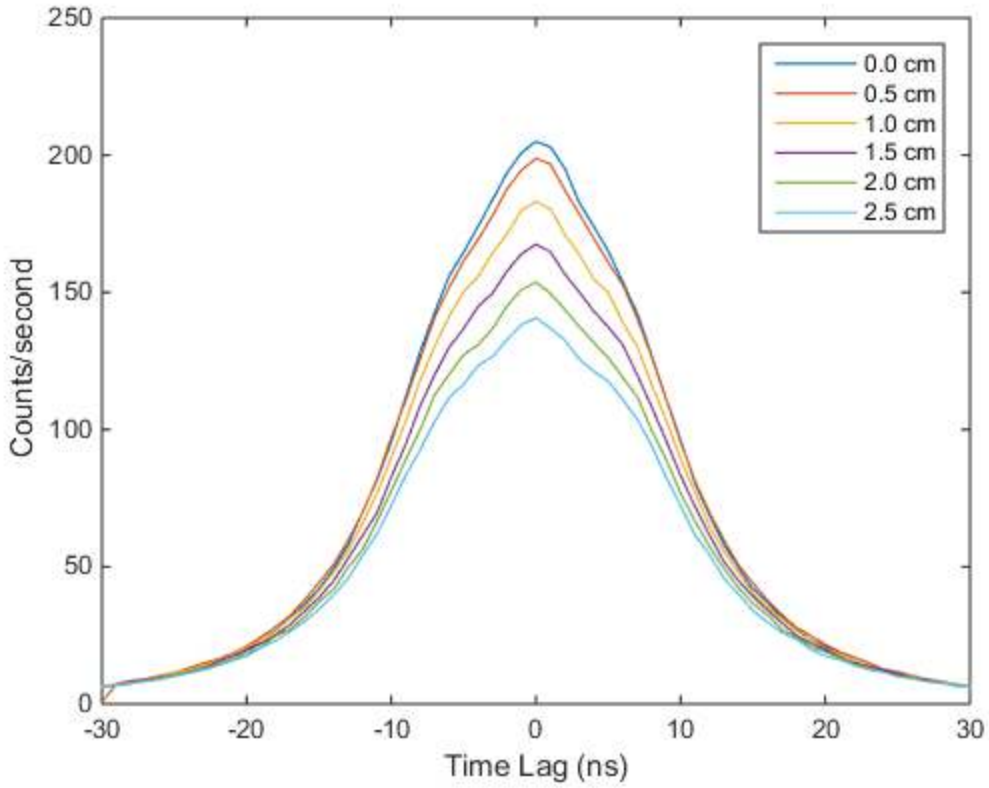

Figure 4-33. Simulation of time correlated distributions for various polyethylene thicknesses surrounding an alpha-phase Pu sphere.

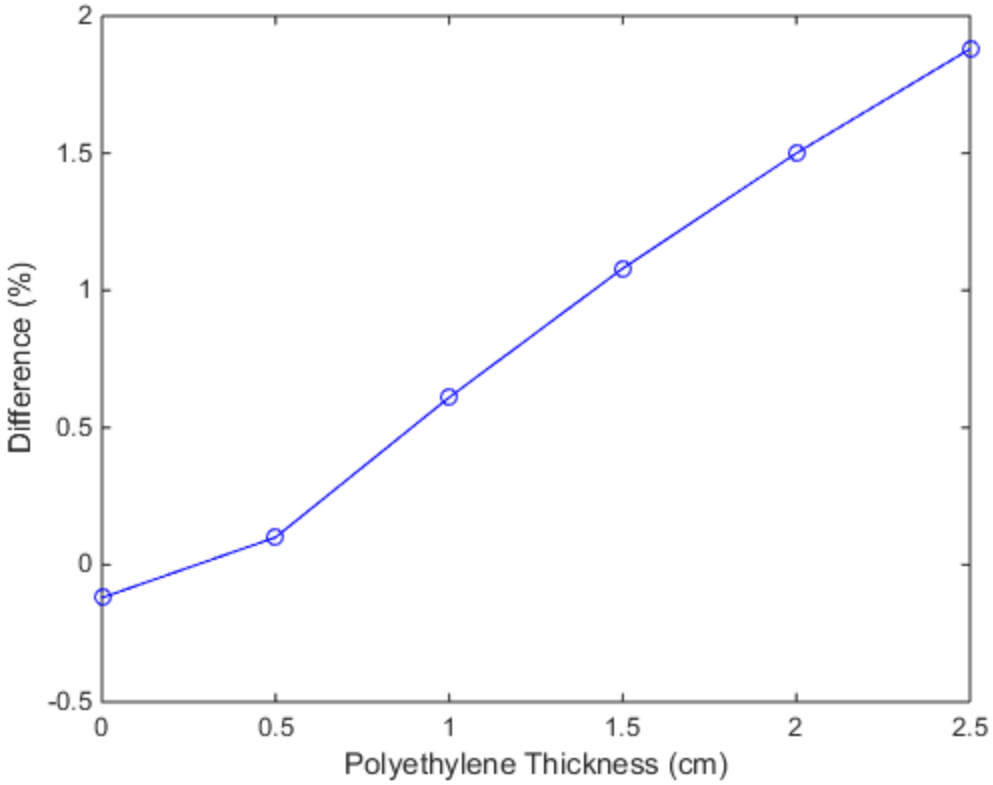

Figure 4-34. Differences between actual and calculated ^{240}Pu content plotted against various polyethylene thicknesses surrounding an alpha-phase Pu sphere.

4.4.5 Stainless Steel

4.4.5.1 Delta-Phase Plutonium Spherical Shell

The data in Figure 4-35 shows the time correlated distributions of cross-correlated events between the two large detectors, for thicknesses of stainless steel ranging from 0.5-2.5 cm. The ^{240}Pu content for varying thicknesses of stainless steel, surrounding a delta-phase Pu spherical shell, was calculated using Equation 4-4. The results in Table 4-18 show the differences between the calculated ^{240}Pu content and the actual value of 1.80%.

Table 4-18. Differences between actual and calculated values of ^{240}Pu content for various thicknesses of stainless steel surrounding a delta-phase Pu spherical shell.

Shielding Thickness (cm)	Counts/ second	Actual ^{240}Pu content (%)	Calculated ^{240}Pu content (%)	Difference (%)
0.0	138	1.80	1.80	0.00
0.5	118	1.80	1.53	0.27
1.0	99	1.80	1.29	0.51
1.5	82	1.80	1.06	0.74
2.0	69	1.80	0.88	0.92
2.5	56	1.80	0.71	1.09

These differences were plotted against their corresponding stainless steel thicknesses in Figure 4-36, in order to generate an equation to adjust for the presence of stainless steel. The data in Figure 4-36 is then fitted, and the equation of the curve is

$$\begin{aligned} \textit{Stainless Steel Correction (\%)} = {} & 0.00667S^4 - 0.03481S^3 + 0.00389S^2 \\ & + 0.5393S - 0.000556 \end{aligned} \tag{4-20}$$

where S is the thickness, in cm, of the stainless steel shielding.

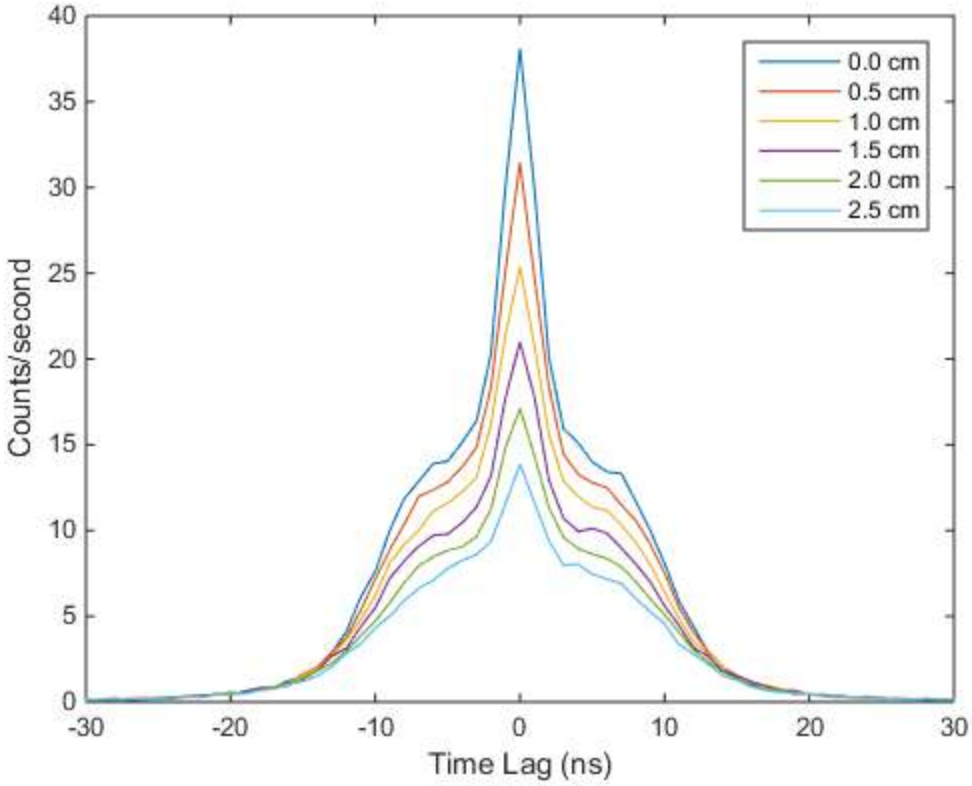

Figure 4-35. Simulation of time correlated distributions for various stainless steel thicknesses surrounding a delta-phase Pu spherical shell.

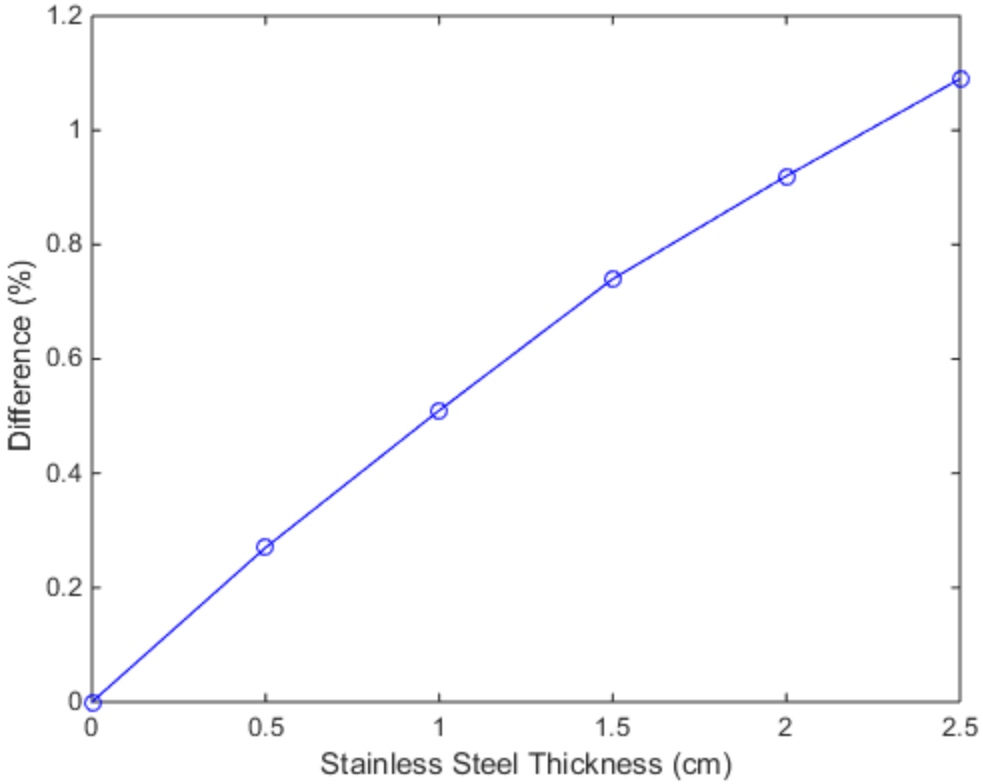

Figure 4-36. Differences between actual and calculated ^{240}Pu content plotted against various stainless steel thicknesses surrounding a delta-phase Pu spherical shell.

4.4.5.2 Alpha-Phase Plutonium Sphere

The data in Figure 4-37 shows the time correlated distributions of cross-correlated events between the two large detectors, for thicknesses of stainless steel ranging from 0.5-2.5 cm. The ^{240}Pu content for varying thicknesses of stainless steel, surrounding an alpha-phase Pu sphere, was calculated using Equation 4-7. The results in Table 4-19 show the differences between the calculated ^{240}Pu content and the actual value of 5.96%.

Table 4-19. Differences between actual and calculated values of ^{240}Pu content for various thicknesses of stainless steel surrounding an alpha-phase Pu sphere.

Shielding Thickness (cm)	Counts/ second	Actual ^{240}Pu content (%)	Calculated ^{240}Pu content (%)	Differences (%)
0.0	998	5.96	6.08	-0.12
0.5	1020	5.96	6.22	-0.26
1.0	970	5.96	5.90	0.06
1.5	915	5.96	5.54	0.42
2.0	856	5.96	5.16	0.80
2.5	799	5.96	4.80	1.16

These differences were plotted against their corresponding stainless steel thicknesses in Figure 4-38, in order to generate an equation to adjust for the presence of stainless steel. The data in Figure 4-38 is then fitted, and the equation of the curve is

$$\begin{aligned} \textit{Stainless Steel Correction (\%)} = {} & 0.1267S^4 - 0.8156S^3 + 1.852S^2 \\ & - 0.9978S - 0.1217 \end{aligned} \qquad (4\text{-}21)$$

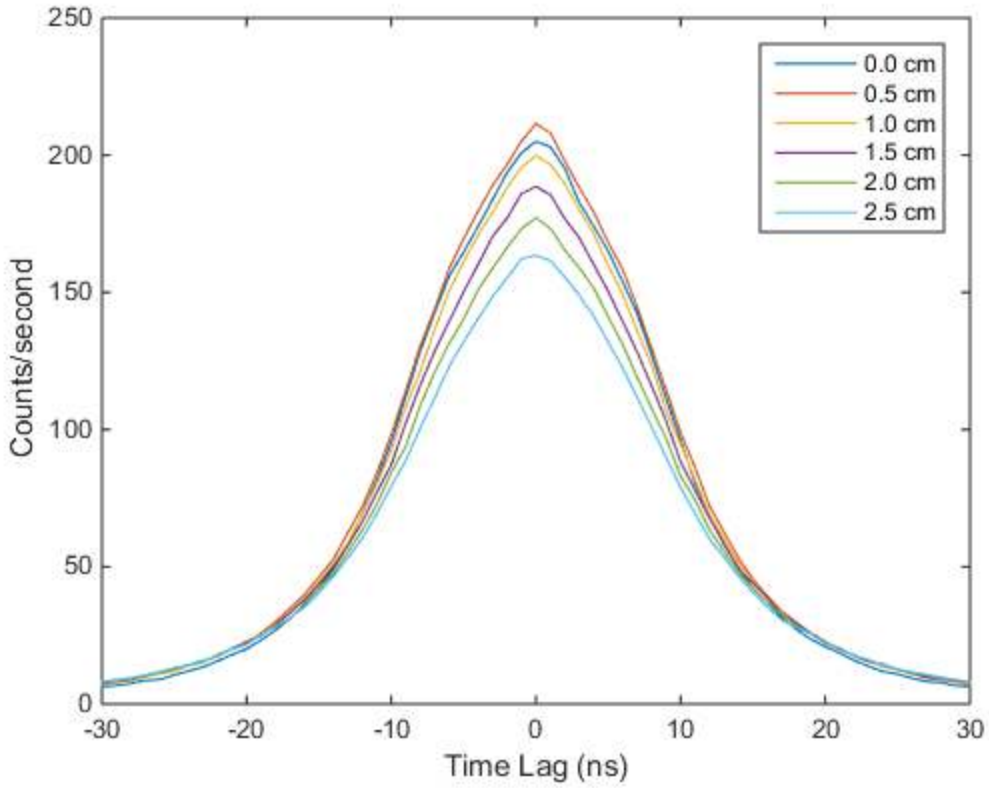

Figure 4-37. Simulation of time correlated distributions for various stainless steel thicknesses surrounding an alpha-phase Pu sphere.

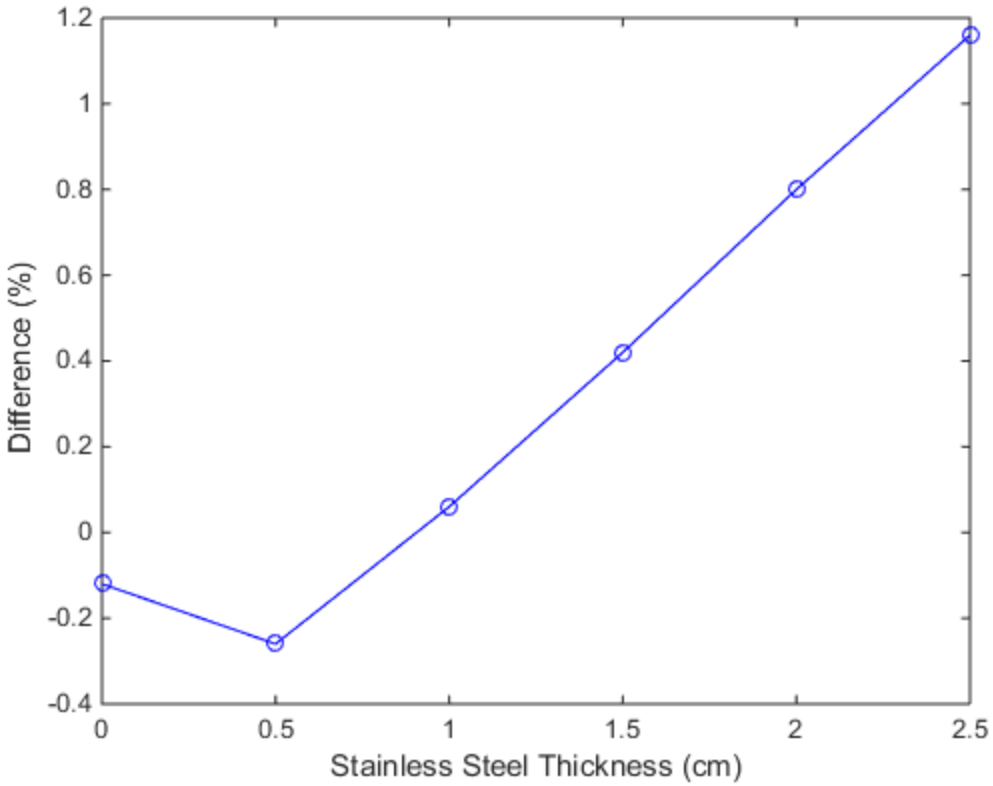

Figure 4-38. Differences between actual and calculated ^{240}Pu content plotted against various stainless steel thicknesses surrounding an alpha-phase Pu sphere.

CHAPTER 5

METHOD VERIFICATION

The method developed in this dissertation was tested using a blind simulation test and measured data. The goal of these verification tests was two-fold: to determine how accurately the method can 1) determine the ^{240}Pu content, and 2) identify the presence of WGPu.

In order to complete the verification study, the equations were implemented in a Matlab® program for quick calculation of the ^{240}Pu content. The program requires the user to input the sample inner and outer radius, reflector or shielding thickness, measurement time and energy threshold. The program outputs the ^{240}Pu content along with the uncertainty of the results, and a statement identifying whether or not the sample is WGPu. The uncertainty analysis used in the calculations is explained in Appendix C. For this verification study, the system defined any sample with a ^{240}Pu content below 7% as WGPu. A screenshot of the user interface is shown in Figure 5-1.

```
% 240Pu estimation method to determine the plutonium 240 content in a Pu metal assembly
% Detects the presence of WGPu

% User Defined Options
data = 1;       % measurement: data = 0; simulation: data = 1
Pu = 0;         % delta phase: Pu = 1; alpha phase: Pu = 0
time = 249;     % measurement time in seconds
E = 1.36;       % CFD threshold in MeV
W = 71082;      % total counts calculated by finding the area of the 5ns gamma-gamma peak width
I = 9.862/2;    % inner radius of the plutonium sample in cm. Solid sphere I=0
O = 11.252/2;   % outer radius of the plutonium sample in cm

% Shielding Materials
S = 0.0;        % thickness of stainless steel shield in cm. S=0 if no stainless steel shield is present
A = 0.0;        % thickness of aluminum shield in cm. A=0 if no aluminum shield is present
L = 3.2;        % thickness of lead shield in cm. L=0 if no lead shield is present
P = 0.0;        % thickness of polyethylene (non borated) shield in cm. P=0 if no polyethylene shield is present
D = 0.0;        % thickness of depleted uranium shield in cm. D=0 if no depleted uranium shield is present

% Reflector Materials
B = 0.0;        % thickness of beryllium reflector in cm. B=0 if no beryllium reflector is present
G = 0.0;        % thickness of graphite reflector in cm. G=0 if no graphite reflector is present
```

Command Window

```
    Academic License

>> PuCalc
Plutonium-240 Content = 5.16+/-0.76%
This assembly contains weapons-grade plutonium.
>>
```

Figure 5-1. Image of ^{240}Pu content calculator.

5.1 Simulations

Simulated passive Pu measurement data, with sample and shielding material information, was provided to test the determination of the presence of WGPu. These simulated blind tests were done to compensate for the lack of a wide array of Pu measurement data. The tests were designed by a third party to recreate a number of different Pu samples and measurement scenarios. The simulations were "blind" because the ^{240}Pu content was not known, in order to simulate an actual measurement scenario. The inner and outer diameter and allotrope of the Pu sample, thickness of any reflector or shielding present, energy threshold and measurement time was provided. Table 5-1 provides a summary of the parameters used in the simulated blind tests. Once the analysis was complete, the actual ^{240}Pu content was provided and compared to the calculated value, and the results are shown in Table 5-2. Test cases 2, 3, 4 and 6 were beyond-design basis, meaning that these cases exceeded the parameters used to build the model.

The method was able to accurately detect the presence of WGPu in nine out of ten cases and never misidentified WGPu as non-WGPu. In test case 6, the calculated ^{240}Pu content was 6.01%, which resulted in a misidentification of the sample as WGPu, but the estimation was less than 2% different from the actual ^{240}Pu content of 7.08%. In eight out of ten cases, the calculated values were within 2% of the actual ^{240}Pu content value. In test case 1, the calculated value was 2.11% less than the actual calculated ^{240}Pu content, and in test case 10, the calculated value was 3.16% greater than the actual calculated ^{240}Pu content. In both cases the program was still able to detect the presence of WGPu.

Table 5-1. Summary of material and measurement information provided for the simulated blind test.

Pu Shapes	Spherical Shells, Solid Spheres
Pu Allotropes	Delta, Alpha
Pu Mass (kg)	2.7-24.4
Pu Thickness (cm)	0.45-2.52
Pu Outer Radius (cm)	3.3-10.6
Reflector Materials	Beryllium, Graphite
Shielding Materials	Aluminum, Lead, Polyethylene, Stainless Steel
Reflector/Shielding Thickness (cm)	0.5-4.3
Energy Threshold (MeV)	1.04-1.88
Measurement Time (seconds)	40-1842

The simulated measurement set-up used to build the verification test differed from the configuration used to build the method. An example simulated measurement setup for the blind test was provided after the analysis and is shown in Figure 5-2. The image shows test case 9 which is a delta sphere (shown in blue), surrounded by a spherical shell of polyethylene (shown in yellow). The detectors (shown in red) are 15.2×15.2×11.2 cm plastic scintillators. The detectors were located ~20 cm from the center of the sample.

The measurement setup discussed in Chapter 3 shows that in the blind test the detectors were further away from the Pu sample, the detectors were slightly larger than the ones used to develop the model, and the shielding material used was a different density and shape than the one used to develop the method. These factors could account for the differences between the actual and calculated ^{240}Pu content. Since the method does not

directly account for variables such as detector to source distance, and shielding or reflector configuration, any changes to the measurement setup will affect the accuracy of the estimation. In spite of this fact, the method is able to detect the presence of WGPu in nine out of ten scenarios tested.

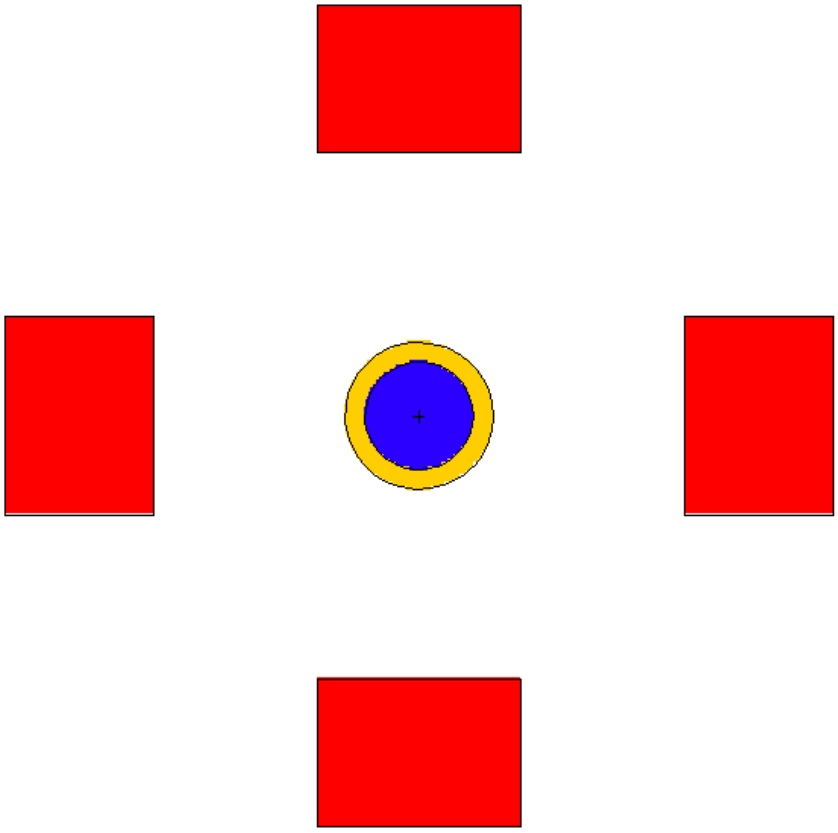

Figure 5-2. Diagram of the blind test simulation configuration for a Pu sphere (blue) surrounded by a polyethylene shield (yellow). The red boxes represent the detector positions. See text for details.

Table 5-2. Estimation of ^{240}Pu content and determination of WGPu presence for various samples.

Test Cases	Shape	Phase	Inner Diameter (cm)	Outer Diameter (cm)	Reflector /Shield*	Reflector /Shield Thickness (cm)	Energy Threshold (MeV)	Measurement Time (seconds)	Estimated ^{240}Pu Content (%)	Actual ^{240}Pu Content (%)	Correctly Predicted Presence of WGPu**
1	Shell	Alpha	5.439	9.341	S	2.3	1.26	357	1.55±0.07	3.73	Y
2	Shell	Alpha	13.056	17.276	N/A	0	1.32	226	1.95±0.07	1.58	Y
3	Shell	Alpha	9.682	11.252	L	3.2	1.36	249	5.01±0.07	5.86	Y
4	Shell	Alpha	20.298	21.189	N/A	0	1.84	40	15.89±0.07	16.41	Y
5	Shell	Delta	7.118	8.819	A	0.5	1.25	1842	3.03±0.02	2.18	Y
6	Shell	Delta	9.03	14.069	G	4.3	1.72	72	6.01±0.02	7.08	N
7	Sphere	Alpha	0	6.491	B	1.5	1.72	1342	1.21±0.09	2.86	Y
8	Sphere	Delta	0	7.448	G	0.6	1.04	182	9.51±0.05	8.51	Y
9	Sphere	Delta	0	8.175	P	1.5	1.17	477	4.58±0.05	5.01	Y
10	Sphere	Delta	0	8.838	N/A	0	1.88	457	5.94±0.05	2.73	Y

*A-Aluminum, B-Beryllium, G-Graphite, L-Lead, P-Polyethylene, S-Stainless Steel

**Y-Yes, N-No

5.2 Measurements

Data from previous passive NMIS measurements on delta-phase plutonium spherical shells was used to test the ^{240}Pu content estimation method. Four assemblies were analyzed of various sizes and masses, ranging from 2-4.5 kg. The measurement setup was similar to the one shown in Figure 3-2. The sample dimensions were obtained from the Criticality Handbook [45]. The counts were calculated by finding the area of the 5 ns peak width centered on 0 ns for the cross-correlated distribution. Table 5-3 provides a summary of the parameters used in the measurements.

Table 5-3. Summary of material and measurement information for Pu spherical shell measurements.

Pu Shapes	Spherical Shells
Pu Allotropes	Delta
Pu Mass (kg)	2.2-4.5
Pu Thickness (cm)	0.64-1.51
Pu Outer Radius (cm)	4.0-5.4
Reflector Materials	N/A
Shielding Materials	N/A
Reflector/Shielding Thickness (cm)	N/A
Energy Threshold (MeV)	1.5
Measurement Time (seconds)	2048

The results in Table 5-4 show the differences between the actual and calculated values of ^{240}Pu content, using the ^{240}Pu content estimation method developed in this

dissertation. The method is able to estimate the ^{240}Pu content for the plutonium assemblies within 0.25% of the actual ^{240}Pu content value and detect the presence of WGPu in all cases.

Table 5-4. Estimation of ^{240}Pu content for various delta-phase Pu spherical shell assemblies.

Measurement	Inner Radius (cm)	Outer Radius (cm)	Mass (g)	Counts	Actual ^{240}Pu Content (%)	Calculated ^{240}Pu Content (%)	Correctly Predicted Presence of WGPu
1	3.15	4.66	4468.3	92600	1.80	2.01±0.02	Y
2	4.02	4.66	2315.1	45660	1.80	1.77±0.02	Y
3	4.66	5.35	3316.1	66920	1.80	1.91±0.02	Y
4	3.15	4.02	2153.2	40270	1.80	1.77±0.02	Y

CHAPTER 6

CONCLUSION AND FUTURE WORK

A proof-of-concept method has been developed to identify the presence of WGPu by determining the ^{240}Pu content using NMIS passive measurement results. This method was used to develop an algorithm which can be incorporated into NMIS to extend the capabilities of the system.

The method was built using Monte Carlo simulations of NMIS passive measurements that have been validated by others, considering Pu spherical shells and spheres as the fission source. Through analysis of the time distribution of the cross-correlated events between the large detectors, and the effects of changes in thickness and size of the Pu sample on the time distributions, equations were developed to determine the ^{240}Pu content in bare alpha- and delta-phase Pu spherical shells and spheres. The method was extended to calculate the ^{240}Pu content when the Pu sample is surrounded by one layer of different types of reflectors or shielding materials with thicknesses up to 2.5 cm.

The verification tests used to measure the accuracy of the method show that, by calculating the ^{240}Pu content, the method is able to identify the presence of WGPu in nine out of ten blind simulated tests cases, and also in all four measurement-based test cases. In cases where the measurement configuration matches the one used for the development of the method, as shown in the verification tests for the measured data, the estimates were within 0.25% of the actual ^{240}Pu content. When the measurement setup does not match the one used to develop the method, which might be the case in an actual measurement scenario, the

results were within 2% of the actual ^{240}Pu content in eight out of ten cases. Due to the limited availability of measured data, more testing with measurement results from others is needed.

When compared with other isotopic composition analysis results of shielded Pu assemblies, for example the PC/FRAM analysis with Pu objects shielded by up to 25 mm of lead [26], the method developed here works for greater thicknesses of lead and yields an accurate answer much more quickly. The blind test results show that the method developed in this research was able to determine the ^{240}Pu content and identify the presence of WGPu in a Pu sample surrounded by 32 mm of lead, which is ~25% greater than the thickness used in the PC/FRAM study.

If the shape of the Pu sample and the details of the shielding or reflector material and measurement set up are precisely known ahead of time, then it is advised to use the method described in this work to develop a modified algorithm in order to provide the most accurate results. But in cases where only a rough estimate is needed to determine the ^{240}Pu content or identify the presence of WGPu, the work presented here suggests that the algorithm developed as a part of this work may be used. In the future, the method and associated algorithm can be expanded to account for a wider variety of configurations, but this will require even more extensive simulations.

LIST OF REFERENCES

[1] J. Shultis and R. Faw, *Fundamentals of Nuclear Science and Engineering*, 2nd ed. Boca Raton: CRC Press, 2007, p. 141.

[2] Department of Energy, "Nonproliferation and Arms Control Assessment of Weapons-Usable Fissile Material Storage and Excess Plutonium Disposition Alternatives," 1997.

[3] National Nuclear Security Administration, "Amendment to Federal Register Document 03-10151: Surplus Plutonium Disposition Program," 2003.

[4] European Safeguards Research & Development Association (ESARDA), "Passive Neutron Coincidence Counting Techniques for Pu Mass Determination," *ESARDA Bulletin*, no. 37, pp. 55–57, Dec-2007.

[5] National Nuclear Security Administration Office of Nonproliferation Research and Engineering, "Technology R&D for Arms Control," 2001.

[6] S. S. Hecker, "Plutonium and Its Alloys: From atoms to microstructure," *Los Alamos Science*, no. 26, pp. 290–335, 2000.

[7] J. Mullens, J. Breeding, R. Perez, J. Mihalczo, T. Valentine, and J. McEvers, "A Multipurpose Processor for Arms Control and Nonproliferation and NMC&A," in *40th Annual Meeting of the Institute of Nuclear Materials Management*, 1999.

[8] J. Mihalczo, J. Mattingly, and J. Mullens, "Oak ridge multiple attribute system (ORMAS) for Pu, HEU, HE, chemical agents, and drugs," *ORNL/TM-2001/175*, 2001.

[9] J. Mullens, J. Neal, S. Pozzi, and J. Mihalczo, "Tomographic Image and Detector Coincidence Measurements for HEU Object Inspection," in *Institute of Nuclear Materials Management Central Chapter Meeting*, 2004.

[10] P. Hausladen, M. A. Blackston, J. A. Mullens, S. M. McConchie, J. T. Mihalczo, P. R. Bingham, M. N. Ericson, and L. Fabris, "Induced-fission imaging of nuclear material," in *51st Annual Meeting of the Institute of Nuclear Materials Management*, 2010.

[11] J. A. Mullens, S. M. McConchie, P. Hausladen, J. T. Mihalczo, B. R. Grogan, and E. D. Sword, "Neutron radiography and fission mapping measurements of nuclear materials with varying composition and shielding," in *52nd Annual Meeting of the Institute of Nuclear Materials Management*, 2011.

[12] J. M. Crye, "Enrichment Determination of Uranium Metal in Shielded Configurations Without Calibration Standards," University of Tennessee, Knoxville, 2013.

[13] J. T. Mihalczo, P. R. Bingham, M. A. Blackston, J. M. Crye, B. R. Grogan, P. A. Hausladen, S. M. McConchie, and J. A. Mullens, "Fast-Neutron Imaging with API DT Neutron Generators," in *Portable Neutron Generators and Generator-Based Technologies International Conference*, 2012, pp. 1–17.

[14] T. A. Wellington, B. A. Palles, J. A. Mullens, J. T. Mihalczo, D. E. Archer, T. Thompson, C. L. Britton, N. D. Bull Ezell, M. N. Ericson, E. Farquhar, R. Lind, and J. Carter, "Recent Fast Neutron Imaging Measurements with the Fieldable Nuclear Materials Identification System. Accepted.," in *23rd Conference on Application of Accelerators in Research and Industry, CAARI 2014*, 2014.

[15] R. Walton and H. Menlove, "Nondestructive Assay for Nuclear Safeguards," *Los Alamos Science*, Los Alamos, pp. 88–115, 1980.

[16] P. Baeten, "Quantification of Transuranic Elements by Neutron Multiplicity Counting: A new approach by Time Interval Analysis," 1999.

[17] M. Bruggeman, P. Baeten, W. De Boeck, and R. Carchon, "Neutron coincidence counting based on time interval analysis with one- and two-dimensional Rossi-alpha distributions: an application for passive neutron waste assay," *Nucl. Instruments Methods Phys. Res. Sect. A Accel. Spectrometers, Detect. Assoc. Equip.*, vol. 382, no. 3, pp. 511–518, Nov. 1996.

[18] J. K. Mattingly, J. T. Mihalczo, L. G. Chiang, and J. S. Neal, "Preliminary Analysis of Joint RFNC-VNIIEF/ORNL Measurements Performed In Year 2000," 2001.

[19] J. K. Mattingly, "Plutonium Attribute Estimation from Passive NMIS Measurements at VNIIEF," *ORNL/TM-2002/20*, no. January, pp. 1–10, 2002.

[20] M. Flaska and S. A. Pozzi, "Identification of Radioactive Materials by Analysis of Simulations and Measurements of Cross-Correlation Functions," in *48th Annual Meeting of the Institute of Nuclear Material Management*, 2007.

[21] B. R. Grogan, "The Development of a Parameterized Scatter Removal Algorithm for Nuclear Materials Identification System Imaging," University of Tennessee, Knoxville, 2010.

[22] T. Sampson, "Plutonium Isotopic Composition by Gamma-Ray Spectroscopy," in *Passive Nondestructive Assay of Nuclear Materials (PANDA)*, 1991, pp. 221–272.

[23] J. Parker and T. Reilly, "Plutonium Isotopic Determination by Gamma-Ray Spectroscopy," *Nucl. Anal. Res. Dev. Progr. Status Rep.*, no. LA-5675-PR, 1974.

[24] T. E. Sampson, “Plutonium Isotopic Analysis using PC/FRAM,” in *Passive Nondestructive Assay of Nuclear Materials (PANDA) Addendum*, 2007, pp. 1–56.

[25] J. Parker, “General Topics in Passive Gamma-Ray Assay,” in *Passive Nondestructive Assay of Nuclear Materials (PANDA)*, 1991.

[26] P. A. Hypes, “Plutonium source isotopic analysis with up to 25 mm Pb shielding using the FRAM Isotopic Analysis Code,” in *41st Annual Meeting of the Institute of Nuclear Materials Management*, 2000.

[27] S. J. Luke, G. K. White, D. E. Archer, and T. B. Gosnell, “Neutron Symmetry and Gamma-Ray Measurements for the Fissile Material Transparency Technology Demonstration,” 2001.

[28] S. J. Luke, G. K. White, D. E. Archer, J. K. Wolford Jr, and T. B. Gosnell, “Verification of the presence of weapons-quality plutonium in sealed storage containers for the Trilateral Initiative demonstration,” *IAEA-SM-367/17/08*, pp. 1–7, 2001.

[29] S. J. Luke and D. E. Archer, “Gamma Attribute Measurements - Pu-300, Pu600, Pu900,” in *41st Annual Meeting of the Institute of Nuclear Materials Management*, 2000.

[30] E. Brandon, “Welding the AT-400A Containment Vessel,” 1998.

[31] L. F. Hansen, “A Comparison of the Shielding Performances of the AT-400A, Model FL and Model AL-R8 Containers,” 1995.

[32] R. Neibert, J. Zabriskie, C. Knight, and J. Jones, “Passive and Active Radiation Measurements Capability at the INL Zero Power Physics Reactor (ZPPR) Facility,” 2010.

[33] S. J. Luke, D. E. Archer, T. B. Gosnell, R. T. Lochner, G. K. White, and R. Weitz, “Results of Gamma-Ray Measurements from a Recent Demonstration for Russian Technical Experts,” in *42nd Annual Meeting of the Institute of Nuclear Materials Management*, 2001.

[34] M. Monterial, M. G. Paff, S. D. Clarke, E. Miller, S. A. Pozzi, P. Marleau, S. Kiff, A. Nowack, and J. Mattingly, “Time-Correlated-Pulse-Height Technique Measurements of Fissile Samples at the Device Assembly Facility,” in *54th Annual Meeting of the Institute of Nuclear Materials Management*, 2013, pp. 1–10.

[35] S. Mcconchie, P. Hausladen, and J. Mihalczo, “Time Correlation Measurements of Cf-252 Source-Driven Fission Chains in Bare HEU Metal Assemblies,” in *51st Annual Meeting of the Institute of Nuclear Materials Management*, 2010.

[36] C. Deyglun, C. Carasco, B. Pérot, C. Eléon, G. Sannié, K. Boudergui, G. Corre, V. Konzdrasovs, S. Normand, and P. Pras, "Passive and Active Correlation Techniques for the Detection of Nuclear Materials," in *3rd International Conference on Advancements in Nuclear Instrumentation Measurement Methods and their Applications (ANIMMA)*, 2013, pp. 1–7.

[37] J. Crye, S. McConchie, J. Mihalczo, K. Pena, and H. Hall, "Time Correlation Measurements of Heavily Shielded Uranium Metal," in *53rd Annual Meeting of the Institute of Nuclear Materials Management*, 2012.

[38] J. K. Mattingly, J. S. Neal, and J. T. Mihalczo, "NMIS Passive Time-Dependent Coincidence Measurements for Plutonium Mass and Multiplication," in *43rd Annual Meeting of the Institute of Nuclear Materials Management*, 2002.

[39] S. A. Pozzi, J. T. Mihalczo, P. Peerani, J. Loeschner, L. Cartegni, J. Mullens, and P. Hausladen, "Passive (NMIS) Measurements on Plutonium Oxide Samples," in *Proceedings of the INMM 46th Annual Meeting*, 2005, no. 1.

[40] S. D. Clarke, S. A. Pozzi, M. Flaska, and P. Peerani, "Simulations and Measurements of Plutonium-Oxide Powder Standards," in *50th Annual Meeting of the Institute of Nuclear Materials Management*, 2009.

[41] S. A. Pozzi, J. K. Mattingly, J. T. Mihalczo, and E. Padovani, "Validation of the MCNP-PoliMi Code for the Simulation of Nuclear Safeguards Experiments on Uranium and Plutonium Metal," in *American Nuclear Society Topical Meeting in Mathematics & Computations*, 2003.

[42] S. A. Pozzi, J. K. Mattingly, J. T. Mihalczo, and E. Padovani, "MCNP-PoliMi of Active and Passive Measurements on Uranium and Plutonium Objects," in *44th Annual Meeting of the Institute of Nuclear Materials Management*, 2003.

[43] S. A. Pozzi and J. T. Mihalczo, "Monte Carlo Evaluation of Passive Correlation Measurements on Containerized Plutonium Shells," in *44th Annual Meeting of the Institute of Nuclear Materials Management*, 2003.

[44] S. Pozzi, E. Padovani, J. Mattingly, and J. Mihalczo, "MCNP-PoliMi Evaluation of Time Dependent Coincidence between Detectors for Fissile Metal vs. Oxide Determination," in *43rd Annual Meeting of the Institute of Nuclear Materials Management*, 2002, pp. 1–8.

[45] M. Gorbatenko, V. Gorelov, V. Yegorov, V. Zagrafov, A. Zacharov, V. Ilyin, M. Kuvshinov, A. Malinkin, and V. Yuferev, "Bare Spherical Assembly of 239Pu(δ,98%), Identification No. PU-MET-FAST-022," in *International Handbook of Evaluated Criticality Safety Benchmark Experiments*, 1st ed., Nuclear Energy Agency, Nuclear Science Committee, 1999.

[46] J. Mattingly, “Polyethylene-Reflected Plutonium Metal Sphere: Subcritical Neutron and Gamma Measurements,” *SAND2009-5804*, pp. 11–14, 2009.

[47] J. Hutchinson, W. Myers, R. Sanchez, and D. Hayes, “Analysis of the BERP Ball : An Alpha-Phase Plutonium Sphere.” American Nuclear Society, Nuclear Criticality Safety Division, Atlanta, 2009.

[48] B. Richard and J. Hutchinson, “Nickel-Reflected Plutonium-Metal-Sphere Subcritical Measurements, Identification No. FUND-NCERC-PU-HE3-MULT-001,” in *International Handbook of Evaluated Criticality Safety Benchmark Experiments*, IX., vol. IX, Nuclear Energy Agency, Nuclear Science Committee, 2014.

[49] U.S. Department of Energy, *DOE Fundamentals Handbook: Nuclear Physics and Reactor Theory*, vol. 2, no. January. Washington, DC: U.S. Department of Energy, 1993, pp. 1–36.

APPENDICES

APPENDIX A. EQUATION VARIABLE DEFINITIONS

Table A-1. Definitions of variables used to determine ^{240}Pu content.

Variables	Definition
A	Thickness of aluminum shield in cm. A=0 if no aluminum shield is present
B	Thickness of beryllium reflector in cm. B=0 if no beryllium reflector is present
C	Total counts/second calculated by finding the area of the 5ns peak width centered on 0 ns
D	Thickness of depleted uranium shield in cm. D=0 if no depleted uranium shield is present
E	Energy threshold in MeV
G	Thickness of graphite reflector in cm. G=0 if no graphite reflector is present
I	Inner radius of the plutonium sample in cm. Solid sphere I=0
O	Outer radius of the plutonium sample in cm
L	Thickness of lead shield in cm. L=0 if no lead shield is present
P	Thickness of polyethylene (non-borated) shield in cm. P=0 if no polyethylene shield is present
S	Thickness of stainless steel shield in cm. S=0 if no stainless steel shield is present
T	Thickness of the plutonium assembly in cm

APPENDIX B. MEASUREMENT VERSUS SIMULATION

There is a known issue with the raw neutron counts reported from MCNP-PoliMi results that has yet to be solved [12]. In order to account for this difference, NMIS measurement data for the Pu spherical shell discussed in Section 3.1 was compared to MCNP-PoliMi simulation of the same Pu sample. The data in Figure B-1 shows the time distributions of cross-correlated distributions between two large detectors for NMIS measured and simulated data.

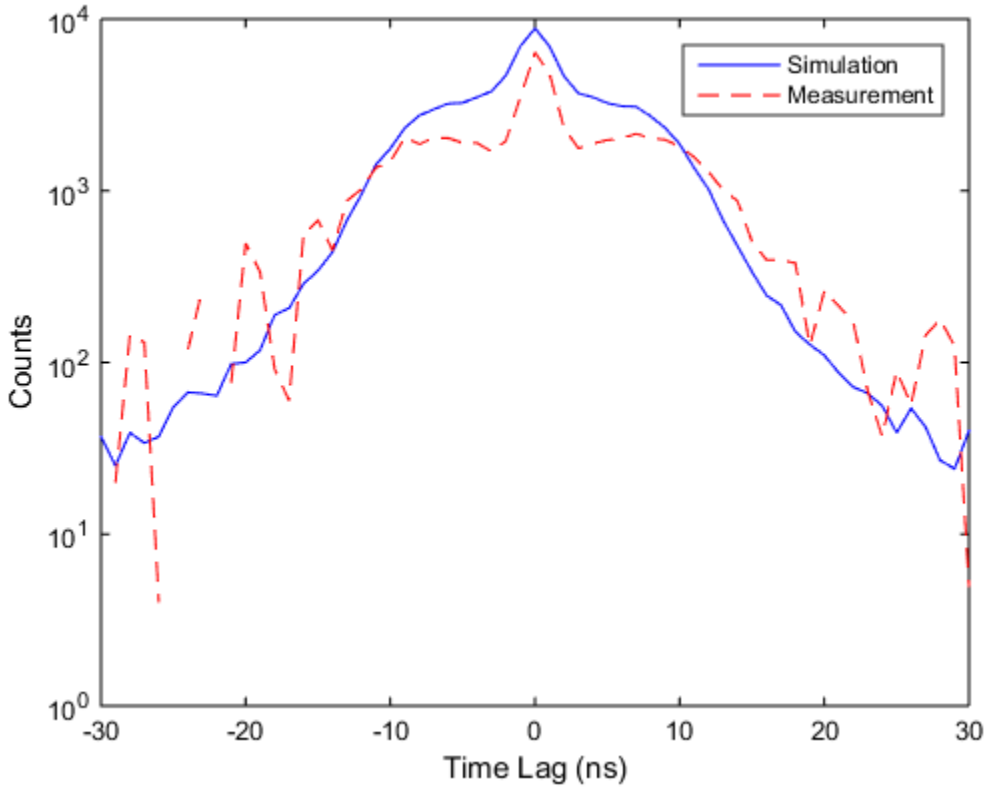

Figure B-1. Comparison of measurement results and simulated data.

Although the simulations and measurement have similar distributions, the peak at 0 ns is lower for than the simulation peak, which results in a lower counts/second when calculating the ^{240}Pu content. Since the method was built using simulation data, an analysis was conducted to compare how accurately MCNP-PoliMi calculates the neutron counts for NMIS measurement. The analysis shows that although time distributions for the simulated and measured data have the same shape, the peak counts are different, so there is not an absolute agreement. The difference may be due to how the detector is modeled in the MCNP calculations [12].In order to account for this difference, to allow the method to be used for both simulations and actual measurements, the method adjusts the reported neutron counts from NMIS measurements by increasing the area of the 5 ns peak width. The method will take into account this difference between the measured and simulated data in order to provide a more accurate estimation.

APPENDIX C. UNCERTAINTY ANALYSIS

A number of steps are taken to provide an accurate uncertainty value for the estimate. To determine the uncertainty in the initial calculation of the ^{240}Pu content, for example, in Equation 4-5, the uncertainty of the equation is calculated as

$$u_1 = \frac{\partial Pu}{\partial C}\Delta C = \frac{1}{\sqrt{33344.8 - 9.924C}} \times \Delta C \qquad \text{(C-1)}$$

where u_1 is the uncertainty in the initial calculation of the ^{240}Pu content, $\frac{\partial Pu}{\partial C}$ is the derivative of the initial ^{240}Pu equation with respect to the counts and ΔC is the uncertainty in the fit used to calculate the counts.

The uncertainty in Equation 4-6 (u_2) is combined with u_1, as shown in Equation C-2, to determine the total uncertainty in the determination of the ^{240}Pu content in alpha phase Pu spheres.

$$u_{total} = \sqrt{u_1^2 + u_2^2} \qquad \text{(C-2)}$$

where u_{total} is the combined uncertainty of the calculation.

APPENDIX D. METHOD DEVELOPMENT FOR ALPHA-PHASE PLUTONIUM SPHERICAL SHELLS

The analysis conducted in Section 4.1 was repeated for an alpha-phase Pu spherical shell. The equation from the analysis is given in Equation D-1. The results in Table D-1 provide a comparison of the calculated ^{240}Pu content and the actual value of 1.80%, using:

$$^{240}Pu\ Content\ (\%) = \frac{-88.96 + \sqrt{88.96^2 + 0.9376(0.7408 - C)}}{-0.4688} - 0.9731T^4 + 2.655T^3 - 3.393T^2 + 0.577T + 0.00105O^3 - 0.0549O^2 - 0.0115O + 2.338 \quad \text{(D-1)}$$

Table D-1. Estimation of ^{240}Pu content for various thicknesses and outer radii of an alpha-phase Pu spherical shell.

Outer Radius (cm)	Inner Radius (cm)	Thickness (cm)	Mass (g)	Counts/ second	Actual ^{240}Pu Content (%)	Calculated ^{240}Pu Content (%)
1.00	0.35	0.65	2151.66	4	1.80	1.81
2.00	1.35	0.65	4124.12	18	1.80	1.79
3.00	2.35	0.65	5925.17	42	1.80	1.80
4.00	3.35	0.65	7562.61	73	1.80	1.79
5.00	4.35	0.65	9044.23	114	1.80	1.82
6.00	3.50	2.50	14387.66	1493	1.80	1.82
6.00	3.75	2.25	13568.29	1014	1.80	1.70
6.00	4.00	2.00	12632.05	699	1.80	1.79
6.00	4.25	1.75	11571.16	493	1.80	1.86
6.00	4.50	1.50	10377.81	353	1.80	1.79
6.00	4.75	1.25	9044.23	265	1.80	1.74
6.00	5.00	1.00	7562.61	208	1.80	1.73
6.00	5.25	0.75	5925.17	170	1.80	1.77
6.00	5.35	0.65	10377.81	159	1.80	1.81
6.00	5.50	0.50	4124.12	144	1.80	1.85

Table 25. Continued

Outer Radius (cm)	Inner Radius (cm)	Thickness (cm)	Mass (g)	Counts/ second	Actual ^{240}Pu Content (%)	Calculated ^{240}Pu Content (%)
6.00	5.75	0.25	2151.66	113	1.80	1.75
7.00	6.35	0.65	11571.16	211	1.80	1.80
8.00	7.35	0.65	12632.05	269	1.80	1.81
9.00	8.35	0.65	13568.29	329	1.80	1.78
10.00	9.35	0.65	14387.66	398	1.80	1.80

The method is able to estimate the ^{240}Pu content for various thicknesses and outer radii within 0.10% of the actual ^{240}Pu content value.

APPENDIX E. METHOD DEVELOPMENT FOR DELTA-PHASE PLUTONIUM SPHERES

The analysis conducted in Section 4.2 was repeated for a delta-phase Pu sphere. The resulting equation from the analysis is given in Equation E-1. The results in Table E-1 provide a comparison of the calculated ^{240}Pu content and the actual value of 5.96%, using:

$$^{240}Pu\ Content\ (\%) = \frac{-79.97 + \sqrt{\left(79.97^2 + (2.6076)(1.812 - CC)\right)}}{-0.0988} - 0.07218O^6 + 1.103O^5 - 6.895O^4 + 22.11O^3 - 38.34O^2 + 33.36O - 5.441 \quad \text{(E-1)}$$

Table E-1. Estimation of ^{240}Pu content for various thicknesses and outer radii for a delta-phase Pu sphere.

Outer Radius (cm)	Mass (g)	Counts/ second	Actual ^{240}Pu Content (%)	Calculated ^{240}Pu Content (%)
1.00	66.18	12	5.96	5.96
1.50	223.37	31	5.96	5.97
2.00	529.46	62	5.96	5.91
2.50	1034.11	112	5.96	5.95
3.00	1786.94	193	5.96	5.90
3.50	2837.59	332	5.96	5.85
4.00	4235.70	573	5.96	5.91
4.50	6030.92	1007	5.96	5.88
5.00	8272.86	1799	5.96	5.94

The method is able to estimate the ^{240}Pu content for various sizes for a Pu sphere within 0.15% of the actual ^{240}Pu content value.

APPENDIX F. METHOD DEVELOPMENT FOR ALPHA-PHASE PLUTONIUM SPHERICAL SHELLS WITH DIFFERENT REFLECTORS

Beryllium

The analysis outlined in Section 4.3 was repeated for an alpha-phase Pu spherical shell surrounded by beryllium metal. The ^{240}Pu content for varying thicknesses of beryllium metal, surrounding an alpha-phase Pu spherical shell, was calculated using Equation D-1. The results in Table F-1 show the differences between the calculated ^{240}Pu content and the actual value of 1.80%, and the equation to adjust for the presence of beryllium metal is given in Equation F-1.

Table F-1. Estimation of ^{240}Pu content for various beryllium metal thicknesses surrounding an alpha-phase Pu spherical shell.

Reflector thickness (cm)	Counts/ second	Actual ^{240}Pu content (%)	Calculated ^{240}Pu content (%)	Difference (%)
0.0	159	1.80	1.81	-0.01
0.5	163	1.80	1.85	-0.05
1.0	164	1.80	1.86	-0.06
1.5	161	1.80	1.83	-0.03
2.0	158	1.80	1.80	0.00
2.5	155	1.80	1.76	0.04

$$\textit{Beryllium Correction (\%)} = -9.529\times10^{-17}B^4 - 0.0163B^3 - 0.101B^2 - 0.1312B - 0.0096 \quad \text{(F-1)}$$

Graphite

The analysis outlined in Section 4.3 was repeated for an alpha-phase Pu spherical shell surrounded by graphite. The ^{240}Pu content for varying thicknesses of graphite, surrounding an alpha-phase Pu spherical shell, was calculated using Equation D-1. The results in Table F-2 show the differences between the calculated ^{240}Pu content and the actual value of 1.80%, and the equation to adjust for the presence of graphite is given in Equation F-2.

Table F-2. Estimation of ^{240}Pu content for various graphite thicknesses surrounding an alpha-phase Pu spherical shell.

Reflector thickness (cm)	Counts/ second	Actual ^{240}Pu content (%)	Calculated ^{240}Pu content (%)	Difference (%)
0.0	159	1.80	1.81	-0.01
0.5	160	1.80	1.81	-0.01
1.0	156	1.80	1.77	0.03
1.5	154	1.80	1.75	0.05
2.0	151	1.80	1.71	0.09
2.5	146	1.80	1.65	0.15

$$\textit{Graphite Correction (\%)} = 0.02G^4 - 0.0985G^3 + 0.1694G^2 - 0.056G - 0.0106 \qquad \text{(F-2)}$$

APPENDIX G. METHOD DEVELOPMENT FOR DELTA-PHASE PLUTONIUM SPHERES WITH DIFFERENT REFLECTORS

Beryllium

The analysis outlined in Section 4.3 was repeated for a delta-phase Pu sphere surrounded by beryllium metal. The ^{240}Pu content for varying thicknesses of beryllium metal, surrounding a delta-phase Pu sphere, was calculated using Equation E-1. The results in Table G-1 show the differences between the calculated ^{240}Pu content and the actual value of 5.96%, and the equation to adjust for the presence of beryllium metal is given in Equation G-1.

Table G-1. Estimation of ^{240}Pu content for various beryllium thicknesses surrounding a delta-phase Pu sphere.

Reflector thickness (cm)	Counts/ second	Actual ^{240}Pu content (%)	Calculated ^{240}Pu content (%)	Difference (%)
0.0	455	5.96	5.85	0.11
0.5	491	5.96	6.35	-0.39
1.0	513	5.96	6.66	-0.70
1.5	522	5.96	6.79	-0.83
2.0	525	5.96	6.83	-0.87
2.5	523	5.96	6.80	-0.84

$$Beryllium\ Correction\ (\%) = -0.0644B^3 + 0.5081B^2 - 1.248B + 0.111 \qquad \text{(G-1)}$$

Graphite

The analysis outlined in Section 4.3 was repeated for a delta-phase Pu sphere surrounded by graphite. The ^{240}Pu content for varying thicknesses of graphite, surrounding a delta-phase Pu sphere, was calculated using Equation E-1. The results in Table G-2 show the differences between the calculated ^{240}Pu content and the actual value of 5.96%, and the equation to adjust for the presence of graphite is given in Equation G-2.

Table G-2. Estimation of ^{240}Pu content for various graphite thicknesses surrounding a delta-phase Pu sphere.

Reflector thickness (cm)	Counts/ second	Actual ^{240}Pu content (%)	Calculated ^{240}Pu content (%)	Differences (%)
0.0	455	5.96	5.85	0.11
0.5	482	5.96	6.22	-0.26
1.0	491	5.96	6.35	-0.39
1.5	498	5.96	6.45	-0.49
2.0	498	5.96	6.45	-0.49
2.5	491	5.96	6.35	-0.39

$$\textit{Graphite Correction (\%)} = 0.07G^4 - 0.3863G^3 + 0.8786G^2 - 1.075G + 1.1086 \qquad \text{(G-2)}$$

APPENDIX H. METHOD DEVELOPMENT FOR ALPHA-PHASE PLUTONIUM SPHERICAL SHELLS WITH DIFFERENT SHIELDING MATERIALS

Aluminum

The analysis outlined in Section 4.4 was repeated for an alpha-phase Pu spherical shell surrounded by aluminum. The ^{240}Pu content for varying thicknesses of aluminum, surrounding an alpha-phase Pu spherical shell, was calculated using Equation D-1. The results in Table H-1 show the differences between the calculated ^{240}Pu content and the actual value of 1.80%, and the equation to adjust for the presence of aluminum is given in Equation H-1.

Table H-1. Estimation of ^{240}Pu content for various aluminum thicknesses surrounding an alpha-phase Pu spherical shell.

Shielding Thickness (cm)	Counts/ second	Actual ^{240}Pu content (%)	Calculated ^{240}Pu content (%)	Difference (%)
0.0	159	1.80	1.81	-0.01
0.5	151	1.80	1.71	0.09
1.0	143	1.80	1.62	0.18
1.5	136	1.80	1.55	0.25
2.0	129	1.80	1.46	0.34
2.5	122	1.80	1.38	0.42

$$Aluminum\ Correction\ (\%) = 0.00889A^3 - 0.0405A^2 + 0.218A - 0.009762 \qquad \text{(H-1)}$$

Depleted Uranium

The analysis outlined in Section 4.4 was repeated for an alpha-phase Pu spherical shell surrounded by depleted uranium. The ^{240}Pu content for varying thicknesses of depleted uranium, surrounding an alpha-phase Pu spherical shell, was calculated using Equation D-1. The results in Table H-2 show the differences between the calculated ^{240}Pu content and the actual value of 1.80%, and the equation to adjust for the presence of depleted uranium is given in Equation H-2.

Table H-2. Estimation of ^{240}Pu content for various depleted uranium thicknesses surrounding an alpha-phase Pu spherical shell.

Shielding Thickness (cm)	Peak Counts (s^{-1})	Actual ^{240}Pu content (%)	Calculated ^{240}Pu content (%)	Difference (%)
0.0	159	1.80	1.81	-0.01
0.5	88	1.80	1.01	0.79
1.0	58	1.80	0.66	1.14
1.5	42	1.80	0.49	1.31
2.0	34	1.80	0.39	1.41
2.5	28	1.80	0.32	1.48

$$\textit{Depleted Uranium Correction}\,(\%) = -0.0767D^4 + 0.5633D^3 - 1.596D^2 + 2.262D - 0.0096 \qquad \text{(H-2)}$$

Lead

The analysis outlined in Section 4.4 was repeated for an alpha-phase Pu spherical shell surrounded by lead. The ^{240}Pu content for varying thicknesses of lead, surrounding an alpha-phase Pu spherical shell, was calculated using Equation D-1. The results in Table H-3 show the differences between the calculated ^{240}Pu content and the actual value of 1.80%, and the equation to adjust for the presence of lead is given in Equation H-3.

Table H-3. Estimation of ^{240}Pu content for various lead thicknesses surrounding an alpha-phase Pu spherical shell.

Shielding Thickness (cm)	Counts/ second	Actual ^{240}Pu content (%)	Calculated ^{240}Pu content (%)	Differences (%)
0.00	159	1.80	1.81	-0.01
0.50	114	1.80	1.29	0.51
1.00	83	1.80	0.94	0.86
1.50	65	1.80	0.74	1.06
2.00	52	1.80	0.60	1.20
2.50	42	1.80	0.49	1.31

$$\textit{Lead Correction (\%)} = 0.07185L^3 - 0.4759L^2 + 1.269L - 0.01087 \qquad \text{(H-3)}$$

Polyethylene (non-borated)

The analysis outlined in Section 4.4 was repeated for an alpha-phase Pu spherical shell surrounded by polyethylene. The ^{240}Pu content for varying thicknesses of polyethylene, surrounding an alpha-phase Pu spherical shell, was calculated using Equation D-1. The results in Table H-4 show the differences between the calculated ^{240}Pu content and the actual value of 1.80%, and the equation to adjust for the presence of polyethylene is given in Equation H-4.

Table H-4. Estimation of ^{240}Pu content for various polyethylene thicknesses surrounding an alpha-phase Pu spherical shell.

Shielding Thickness (cm)	Counts/ second	Actual ^{240}Pu content (%)	Calculated ^{240}Pu content (%)	Differences (%)
0.00	159	1.80	1.81	-0.01
0.50	149	1.80	1.69	0.11
1.00	140	1.80	1.59	0.21
1.50	132	1.80	1.50	0.30
2.00	125	1.80	1.42	0.38
2.50	118	1.80	1.34	0.46

$$Polyethylene\ Correction\,(\%) = 0.007407P^3 - 0.0478P^2 + 0.2611P - 0.00992 \qquad \text{(H-4)}$$

Stainless Steel

The analysis outlined in Section 4.4 was repeated for an alpha-phase Pu spherical shell surrounded by stainless steel. The ^{240}Pu content for varying thicknesses of stainless steel, surrounding an alpha-phase Pu spherical shell, was calculated using Equation D-1. The results in Table H-5 show the differences between the calculated ^{240}Pu content and the actual value of 1.80%, and the equation to adjust for the presence of stainless steel is given in Equation H-5.

Table H-5. Estimation of ^{240}Pu content for various stainless steel thicknesses surrounding an alpha-phase Pu spherical shell.

Shielding Thickness (cm)	Counts/ second	Actual ^{240}Pu content (%)	Calculated ^{240}Pu content (%)	Difference (%)
0.00	159	1.80	1.81	-0.01
0.50	140	1.80	1.58	0.22
1.00	119	1.80	1.35	0.45
1.50	101	1.80	1.15	0.65
2.00	86	1.80	0.98	0.82
2.50	73	1.80	0.83	0.97

$$\textit{Stainless Steel Correction (\%)} = 0.0133S^4 - 0.0741S^3 + 0.0844S^2 + 0.4356S - 0.0101 \quad \text{(H-5)}$$

APPENDIX I. METHOD DEVELOPMENT FOR DELTA-PHASE PLUTONIUM SPHERES WITH DIFFERENT SHIELDING MATERIALS

Aluminum

The analysis outlined in Section 4.4 was repeated for a delta-phase Pu sphere surrounded by aluminum. The ^{240}Pu content for varying thicknesses of aluminum, surrounding a delta-phase Pu sphere, was calculated using Equation E-1. The results in Table I-1 show the differences between the calculated ^{240}Pu content and the actual value of 5.96%, and the equation to adjust for the presence of aluminum is given in Equation I-1.

Table I-1. Estimation of ^{240}Pu content for various aluminum thicknesses surrounding a delta-phase Pu sphere.

Shielding Thickness (cm)	Counts/ second	Actual ^{240}Pu content (%)	Calculated ^{240}Pu content (%)	Difference (%)
0.0	455	5.96	5.85	0.11
0.5	442	5.96	5.66	0.30
1.0	425	5.96	5.43	0.53
1.5	410	5.96	5.24	0.72
2.0	396	5.96	5.04	0.92
2.5	385	5.96	4.88	1.08

$$Aluminum\ Correction\ (\%) = -0.01852A^3 + 0.05016A^2 + 0.3791A - 0.108 \qquad \text{(I-1)}$$

Depleted Uranium

The analysis outlined in Section 4.4 was repeated for a delta-phase Pu sphere surrounded by depleted uranium. The ^{240}Pu content for varying thicknesses of depleted uranium, surrounding a delta-phase Pu sphere, was calculated using Equation E-1. The results in Table I-2 show the differences between the calculated ^{240}Pu content and the actual value of 5.96%, and the equation to adjust for the presence of depleted uranium is given in Equation I-2.

Table I-2. Estimation of ^{240}Pu content for various depleted uranium thicknesses surrounding a delta-phase Pu sphere.

Shielding Thickness (cm)	Counts/ second	Actual ^{240}Pu content (%)	Calculated ^{240}Pu content (%)	Difference (%)
0.0	455	5.96	5.85	0.11
0.5	370	5.96	4.68	1.28
1.0	303	5.96	3.78	2.18
1.5	253	5.96	3.12	2.84
2.0	217	5.96	2.64	3.32
2.5	187	5.96	2.25	3.71

$$\textit{Depleted Uranium Correction (\%)} = 0.08D^3 - 0.699D^2 + 2.686D + 0.108 \qquad \text{(I-2)}$$

Lead

The analysis outlined in Section 4.4 was repeated for a delta-phase Pu sphere surrounded by lead. The ^{240}Pu content for varying thicknesses of lead, surrounding a delta-phase Pu sphere, was calculated using Equation E-1. The results in Table I-3 show the differences between the calculated ^{240}Pu content and the actual value of 5.96%, and the equation to adjust for the presence of lead is given in Equation I-3.

Table I-3. Estimation of ^{240}Pu content for various lead thicknesses surrounding a delta-phase Pu sphere.

Shielding Thickness (cm)	Peak Counts (s^{-1})	Actual ^{240}Pu content (%)	Calculated ^{240}Pu content (%)	Difference (%)
0.0	455	5.96	5.85	0.11
0.5	393	5.96	5.00	0.96
1.0	342	5.96	4.31	1.65
1.5	303	5.96	3.78	2.18
2.0	272	5.96	3.36	2.60
2.5	244	5.96	3.00	2.96

$$Lead\ Correction\ (\%) = 0.04815L^3 - 0.4327L^2 + 1.921L - 0.108 \qquad \text{(I-3)}$$

Polyethylene

The analysis outlined in Section 4.4 was repeated for a delta-phase Pu sphere surrounded by polyethylene. The ^{240}Pu content for varying thicknesses of polyethylene, surrounding a delta-phase Pu sphere, was calculated using Equation E-1. The results in Table I-4 show the differences between the calculated ^{240}Pu content and the actual value of 5.96%, and the equation to adjust for the presence of polyethylene is given in Equation I-4.

Table I-4. Estimation of ^{240}Pu content for various polyethylene thicknesses surrounding a delta-phase Pu sphere.

Shielding Thickness (cm)	Counts/ second	Actual ^{240}Pu content (%)	Calculated ^{240}Pu content (%)	Difference (%)
0.0	455	5.96	5.85	0.11
0.5	415	5.96	5.29	0.67
1.0	376	5.96	4.76	1.20
1.5	340	5.96	4.27	1.69
2.0	310	5.96	3.87	2.09
2.5	284	5.96	3.53	2.43

$$Polyethylene\ Correction\ (\%) = -0.0222P^3 - 0.0324P^2 + 1.147P + 0.109 \qquad \text{(I-4)}$$

Stainless Steel

The analysis outlined in Section 4.4 was repeated for a delta-phase Pu sphere surrounded by stainless steel. The ^{240}Pu content for varying thicknesses of stainless steel, surrounding a delta-phase Pu sphere, was calculated using Equation E-1. The results in Table I-5 show the differences between the calculated ^{240}Pu content and the actual value of 5.96%, and the equation to adjust for the presence of stainless steel is given in Equation I-5.

Table I-5. Estimation of ^{240}Pu content for various stainless steel thicknesses surrounding a delta-phase Pu sphere.

Shielding Thickness (cm)	Counts/ second	Actual ^{240}Pu content (%)	Calculated ^{240}Pu content (%)	Difference (%)
0.0	455	5.96	5.85	0.11
0.5	433	5.96	5.54	0.42
1.0	400	5.96	5.09	0.87
1.5	371	5.96	4.69	1.27
2.0	334	5.96	4.20	1.76
2.5	307	5.96	3.84	2.12

$$\textit{Stainless Steel Correction (\%)} = -0.0689S^3 + 0.2876S^2 + 0.5177S + 0.1083 \qquad \text{(I-5)}$$

APPENDIX J. METHOD DEVELOPMENT FOR VARIOUS THRESHOLDS

Simulations were completed to analyze the changes in peak counts of the time correlated distributions for various energy thresholds. Threshold values were varied from 1.0 -2.0 MeV in increments of 0.1 MeV. Equations J-1 and J-2 shows the equations for changes in threshold for delta- and alpha-phase Pu spherical shells respectively, while Equations J-3 and J-4 are for delta- and alpha-phase Pu spheres respectively.

$$C = 42.86E^2 - 252.6E + 282.3 \quad \text{(J-1)}$$

$$C = -30.22E^3 + 199.7E^2 - 539.3E + 461.6 \quad \text{(J-2)}$$

$$C = -136.4E^3 + 932.7E^2 - 2399E + 1961 \quad \text{(J-3)}$$

$$C = -252.5E^3 + 1689E^2 - 4385E + 3630 \quad \text{(J-4)}$$

APPENDIX K. ^{240}PU CONTENT CALCULATOR

```
% 240Pu estimation method to determine the plutonium 240 content in a
Pu metal assembly
% Detects the presence of WGPu

% User Defined Options
data = 1;       % measurement: data = 0; simulation: data = 1
Pu = 0;         % delta phase: Pu = 1; alpha phase: Pu = 0
time = 60;     % measurement time in seconds
E = 1.5;       % energy threshold in MeV
W = 100000;      % total counts calculated by finding the area of the
5ns peak width centered on 0 ns
I = 0;    % inner radius of the plutonium sample in cm. Solid sphere I=0
O = 4.5;  % outer radius of the plutonium sample in cm

% Shielding Materials
S = 0.0;        % thickness of stainless steel shield in cm. S=0 if no
stainless steel shield is present
A = 0.0;        % thickness of aluminum shield in cm. A=0 if no aluminum
shield is present
L = 3.5;        % thickness of lead shield in cm. L=0 if no lead shield
is present
P = 0.0;        % thickness of polyethylene (non borated) shield in cm.
P=0 if no polyethylene shield is present
D = 0.0;        % thickness of depleted uranium shield in cm. D=0 if no
depleted uranium shield is present

% Reflector Materials
B = 0.0;        % thickness of beryllium reflector in cm. B=0 if no
beryllium reflector is present
G = 0.0;        % thickness of graphite reflector in cm. G=0 if no
graphite reflector is present

%% Calculations
if data == 0   %data from NMIS measurement
   W = W*3.7223;
else W = W;
end

C = W/time;

%% bare Pu metal assemblies

if (I>0) && (Pu==1) %bare delta-phase Pu shell
    T = O-I;
    CSHD = C+42.86*E^2-252.6*E+282.3;
    CSHD=abs(CSHD);
    shd =((CSHD-2.89)/75.35)+0.2617*T^6-2.28*T^5+7.949*T^4-
14.44*T^3+13.85*T^2-7.236*T+1.671+0.00107*O^3-0.05649*O^2-
0.009526*O+1.839;
```

```
    ushd_p=(1/75.35)*0.56;
    ushd_t=0.01;
    ushd_s=0.01;
    ushd=sqrt(ushd_p^2+ushd_t^2+ushd_s^2);
    sha = 0;
    usha = 0;
else if (I>0) && (Pu==0) %bare alpha-phase Pu shell
    T = O-I;
    CSHA = C-30.22*E^3+199.7*E^2-539.3*E+461.6;
    shd = 0;
    ushd=0;
    sha = ((-88.96+sqrt(88.96^2+(0.9376*(0.7408-CSHA))))/(-0.4688))-
0.9731*T^4+2.655*T^3-3.393*T^2+0.5772*T+0.5392+0.001051*O^3-
0.05488*O^2-0.01153*O+1.799;
    usha_p=(1/sqrt(7914.58 - 0.9376*C))*0.4;
    usha_t=0.07;
    usha_s=0.01;
    usha=sqrt(usha_p^2+usha_t^2+usha_s^2);
else sha = 0;
     usha = 0;
     shd = 0;
     ushd = 0;
    end
end

if (I==0) && (Pu==1) %bare delta-phase Pu sphere
    CSPD = C-136.4*E^3+932.7*E^2-2399*E+1961;
    %CSPD = abs(CSPD);
    spd = (-79.97+sqrt(79.97^2+(2.6076*(1.812-CSPD))))/(-1.3038)-
0.07218*O^6+1.103*O^5-6.895*O^4+22.11*O^3-38.34*O^2+33.36*O-5.441;
    uspd_p=(1/sqrt(6399.93 - 2.6076*CSPD))*0.74;
    uspd_s=0.05;
    uspd=sqrt(uspd_p^2+uspd_s^2);
    spa = 0;
    uspa = 0;
else if (I==0) && (Pu==0) %bare alpha-phase Pu sphere
    CSPA = C-252.5*E^3+1689*E^2-4385*E+3630;
    CSPA=abs(CSPA);
    spd = 0;
    uspd = 0;
    spa = (-182.6+sqrt(182.6^2+9.924*(0.2083-CSPA)))/(-4.962)-
0.2973*O^6+4.314*O^5-25.4*O^4+76.94*O^3-125.9*O^2+104.7*O-28.49;
    uspa_p=(1/sqrt(33344.8 - 9.924*CSPA))*1.458;
    uspa_s=0.09;
    uspa=sqrt(uspa_p^2+uspa_s^2);
else spa = 0;
     uspa = 0;
     spd = 0;
     uspd = 0;
    end
end

%% assemblies surrounded by reflectors
```

```
if (I>0) && (Pu==1) && (B>0) %delta-phase Pu shell surrounded by Be
reflector
    shdbe = -0.006667*B^4+0.01111*B^3+0.045*B^2+0.00127*B+0.00119;
    ushdbe=0.02;
    shabe = 0;
    ushabe = 0;
else if (I>0) && (Pu==0) && (B>0) %alpha-phase Pu shell surrounded by
Be reflector
    shdbe = 0;
    ushdbe=0;
    shabe = -9.529E-17*B^4-0.0163*B^3+0.1011*B^2-0.1312*B-0.009603;
    ushabe=0.01;
else shabe = 0;
     ushabe = 0;
     shdbe = 0;
     ushdbe = 0;
    end
end

if (I==0) && (Pu==1) && (B>0) %delta-phase Pu sphere surrounded by Be
reflector
    spdbe = -0.06444*B^3+0.5081*B^2-1.248*B+0.111;
    uspdbe= 0.01;
    spabe = 0;
    uspabe = 0;
else if (I==0) && (Pu==0) && (B>0) %alpha-phase Pu sphere surrounded by
Be reflector
    spdbe = 0;
    uspdbe = 0;
    spabe = -0.1178*B^3+0.591*B^2-2.436*B-0.1205;
    uspabe=0.02;
else spabe = 0;
     uspabe = 0;
     spdbe = 0;
     uspdbe = 0;
    end
end

if (I>0) && (Pu==1) && (G>0) %delta-phase Pu shell surrounded by
graphite reflector
    shdg = 1.73E-17*G^4+0.004444*G^3-0.006667*G^2+0.09651*G+0.0004762;
    ushdg= 0.01;
    shag = 0;
    ushag=0;
else if (I>0) && (Pu==0) && (G>0) %alpha-phase Pu shell surrounded by
graphite reflector
    shdg = 0;
    ushdg=0;
    shag =  0.02*G^4-0.09852*G^3+0.1694*G^2-0.05593*G-0.01056;
    ushag= 0.01;
else shag = 0;
     ushag=0;
     shdg = 0;
     ushdg=0;
```

```
    end
end

if (I==0) && (Pu==1) && (G>0) %delta-phase Pu sphere surrounded by
graphite reflector
    spdg = 0.07*G^4-0.3863*G^3+0.8786*G^2-1.075*G+1.1086;
    uspdg= 0.02;
    spag = 0;
    uspag = 0;
else if (I==0) && (Pu==0) && (G>0) %alpha-phase Pu sphere surrounded by
graphite reflector
    spdg = 0;
    uspdg = 0;
    spag = 0.07*G^4-0.4204*G^3+1.086*G^2-1.946*G-0.12;
    uspag=0.001;
else spag = 0;
     uspag = 0;
     spdg = 0;
     uspdg = 0;
    end
end

%% assemblies surrounded by shielding

if (I>0) && (Pu==1) && (A>0) %delta-phase Pu shell surrounded by Al
shielding
    shdal = -0.01667*A^4+0.08556*A^3-0.1442*A^2+0.2742*A-0.000119;
    ushdal = 0.004;
    shaal = 0;
    ushaal = 0;
else if (I>0) && (Pu==0) && (A>0) %alpha-phase Pu shell surrounded by
Al shielding
    shdal = 0;
    ushdal=0;
    shaal = 0.008889*A^3-0.04048*A^2+0.218*A-0.009762;
    ushaal=0.01;
else shaal = 0;
     ushaal=0;
     shdal = 0;
     ushdal=0;
    end
end

if (I==0) && (Pu==1) && (A>0) %delta-phase Pu sphere surrounded by Al
shielding
    spdal = -0.01852*A^3+0.05016*A^2+0.3791*A+0.108;
    uspdal=0.01;
    spaal = 0;
    uspaal = 0;
else if (I==0) && (Pu==0) && (A>0) %alpha-phase Pu sphere surrounded by
Al shielding
    spdal = 0;
    uspdal = 0;
    spaal = 0.1467*A^4-0.8815*A^3+1.819*A^2-1.168*A-0.1216;
```

```
    uspaal= 0.03;
else spaal = 0;
     uspaal = 0;
     spdal = 0;
     uspdal = 0;
    end
end

if (I>0) && (Pu==1) && (D>0) %delta-phase Pu shell surrounded by DU
shielding
    shddu = -0.09667*D^4+0.6989*D^3-1.934*D^2+2.617*D+0.0005952;
    ushddu=0.01;
    shadu = 0;
    ushadu=0;
else if (I>0) && (Pu==0) && (D>0) %alpha-phase Pu shell surrounded by
DU shielding
    shddu = 0;
    ushddu=0;
    shadu = -0.07667*D^4+0.5633*D^3-1.596*D^2+2.262*D-0.009643;
    ushadu=0.01;
else shadu = 0;
     ushadu=0;
     shddu = 0;
     ushddu=0;
    end
end

if (I==0) && (Pu==1) && (D>0) %delta-phase Pu sphere surrounded by by
DU shielding
    spddu = 0.08*D^3-0.6986*D^2+2.686*D+0.1079;
    uspddu=0.01;
    spadu = 0;
    uspadu = 0;
else if (I==0) && (Pu==0) && (D>0) %alpha-phase Pu sphere surrounded by
DU shielding
    spddu = 0;
    uspddu = 0;
    spadu = 0.09333*D^4-0.6089*D^3+1.11*D^2+0.7341*D-0.1224;
    uspadu=0.04;
else spadu = 0;
     uspadu = 0;
     spddu = 0;
     uspddu = 0;
    end
end

if (I>0) && (Pu==1) && (L>0) %delta-phase Pu shell surrounded by Pb
shielding
    shdpb = -0.02333*L^4+0.1826*L^3-0.6714*L^2+1.478*L-0.0004365;
    ushdpb=0.01;
    shapb = 0;
    ushapb=0;
else if (I>0) && (Pu==0) && (L>0) %alpha-phase Pu shell surrounded by
Pb shielding
```

```
    shdpb = 0;
    ushdpb=0;
    shapb = 0.07185*L^3-0.4759*L^2+1.269*L-0.01087;
    ushapb=0.01;
else shapb = 0;
     ushapb=0;
     shdpb = 0;
     ushdpb=0;
    end
end

if (I==0) && (Pu==1) && (L>0) %delta-phase Pu sphere surrounded by Pb
shielding
    spdpb = 0.04815*L^3-0.4327*L^2+1.921*L+0.108;
    uspdpb= 0.01;
    spapb = 0;
    uspapb = 0;
else if (I==0) && (Pu==0) && (L>0) %alpha-phase Pu sphere surrounded by
Pb shielding
    spdpb = 0;
    uspdpb = 0;
    spapb = 0.1467*L^4-0.877*L^3+1.632*L^2-0.06185*L-0.1211;
    uspapb=0.02;
else spapb = 0;
     uspapb = 0;
     spdpb = 0;
     uspdpb = 0;
    end
end

if (I>0) && (Pu==1) && (P>0) %delta-phase Pu shell surrounded by
polyethylene shielding
    shdpo = 0.01667*P^4-0.08259*P^3+0.1031*P^2+0.1704*P-0.0002778;
    ushdpo=0.004;
    shapo = 0;
    ushapo=0;
else if (I>0) && (Pu==0) && (P>0) %alpha-phase Pu shell surrounded by
polyethylene shielding
    shdpo = 0;
    ushdpo = 0;
    shapo = 0.007407*P^3-0.04778*P^2+0.2611*P-0.009921;
    ushapo=0.004;
else shapo = 0;
     ushapo = 0;
     shdpo = 0;
     ushdpo = 0;
    end
end

if (I==0) && (Pu==1) && (P>0) %delta-phase Pu sphere surrounded by
polyethylene shielding
    spdpo = -0.02222*P^3-0.03238*P^2+1.147*P+0.109;
    uspdpo=0.01;
    spapo = 0;
```

```
    uspapo = 0;
else if (I==0) && (Pu==0) && (P>0) %alpha-phase Pu sphere surrounded by
polyethylene shielding
    spdpo = 0;
    uspdpo = 0;
    spapo = 0.1133*P^4-0.6911*P^3+1.368*P^2-0.07127*P-0.1212;
    uspapo=0.02;
else spapo = 0;
     uspapo = 0;
     spdpo = 0;
     uspdpo = 0;
    end
end

if (I>0) && (Pu==1) && (S>0) %delta-phase Pu shell surrounded by
stainless steel shielding
    shdss = 0.006667*S^4-0.03481*S^3+0.003889*S^2+0.5393*S+0.0005556;
    ushdss=0.01;
    shass = 0;
    ushass = 0;
else if (I>0) && (Pu==0) && (S>0) %alpha-phase Pu shell surrounded by
stainless steel shielding
    shdss = 0;
    ushdss = 0;
    shass = 0.01333*S^4-0.07407*S^3+0.08444*S^2+0.4356*S-0.01008;
    ushass=0.004;
else shass = 0;
     ushass = 0;
     shdss = 0;
     ushdss = 0;
    end
end

if (I==0) && (Pu==1) && (S>0) %delta-phase Pu sphere surrounded by
stainless steel shielding
    spdss = -0.06889*S^3+0.2876*S^2+0.5177*S+0.1083;
    uspdss=0.031;
    spass = 0;
    uspass = 0;
else if (I==0) && (Pu==0) && (S>0) %alpha-phase Pu sphere surrounded by
stainless steel shielding
    spdss = 0;
    uspdss = 0;
    spass = 0.1267*S^4-0.8156*S^3+1.852*S^2-0.9978*S-0.1217;
    uspass=0.03;
else spass = 0;
     uspass = 0;
     spdss = 0;
     uspdss = 0;
    end
end

%%Plutonium-240 Content
```

```
correction =
sha+shd+spa+spd+shabe+shdbe+spabe+spdbe+shag+shdg+spag+spdg+shaal+shdal
+spaal+spdal+shadu+shddu+spadu+spddu+shapb+shdpb+spapb+spdpb+shapo+shdp
o+spapo+spdpo+shass+shdss+spass+spdss;
content = abs(correction);
uncertainty =
sqrt(usha^2+ushd^2+uspa^2+uspd^2+ushabe^2+ushdbe^2+uspabe^2+uspdbe^2+us
hag^2+ushdg^2+uspag^2+uspdg^2+ushaal^2+ushdal^2+uspaal^2+uspdal^2+ushad
u^2+ushddu^2+uspadu^2+uspddu^2+ushapb^2+ushdpb^2+uspapb^2+uspdpb^2+usha
po^2+ushdpo^2+uspapo^2+uspdpo^2+ushass^2+ushdss^2+uspass^2+uspdss^2);

formatSpec = 'Plutonium-240 Content = %4.2f+/-%.2f%%\n';
fprintf(formatSpec,content,uncertainty)

if content<=7.00 %if Pu sample is WGPu
   disp('This assembly contains weapons-grade plutonium.')
else
   disp('This assembly does not contain weapons-grade plutonium.')
end
```

VITA

Tracey-Ann Wellington was born in Kingston, Jamaica to Albert and Erica Wellington. She is the eldest of three children, Andrew and Terry. She earned a Bachelor of Science in Mathematical Physics from Randolph College and a Master of Science in Materials Science and Engineering from Texas A&M University. Currently, Tracey is a graduate research assistant in the Bredesen Center for Interdisciplinary Research and Graduate Education, working on a PhD in Energy Science and Engineering. After graduation, Tracey will be participating in the year-long National Nuclear Security Administration (NNSA) Graduate Fellowship Program (NGFP).